REVIEW PAPER

Check for
updates

Propagation characteristics of coronal mass ejections (CMEs) in the corona and interplanetary space

Fang Shen[1,2] · Chenglong Shen[3] · Mengjiao Xu[3] · Yousheng Liu[1,2] · Xueshang Feng[1] · Yuming Wang[3]

Abstract

Coronal mass ejections (CMEs) play an important role in space weather. The propagation characteristics of CMEs in the Corona and interplanetary space determine whether, when and how the CME will hit the Earth. To this end, a lot of progress has been made both on observational and numerical studies of CMEs. With the development of the advanced observational, theoretical and numerical methods, there emerges more and more research on the morphology, the kinematic evolution, the prediction of the arrival at 1 AU and the acceleration/deceleration processes of CMEs. Moreover, many direct observations and simulations have revealed that the CMEs may not propagate along a straight trajectory both in the corona and interplanetary space. Both observational and numerical studies have shown that, when two or more CMEs collide with each other, their kinematic characteristics may change significantly. Here, we present a review of the recent progress associated with the different aspects of CMEs, including their interplanetary counterparts ICMEs, especially focusing on the initiation of the CME, the CMEs' propagation characteristics, interaction with the background solar wind structures, the deflection of the CMEs, the interaction between successive CMEs, the particle acceleration associated with successive CMEs' interaction, and the effect of compound events on Earth's magnetosphere.

✉ Fang Shen
fshen@spaceweather.ac.cn

✉ Chenglong Shen
clshen@ustc.edu.cn

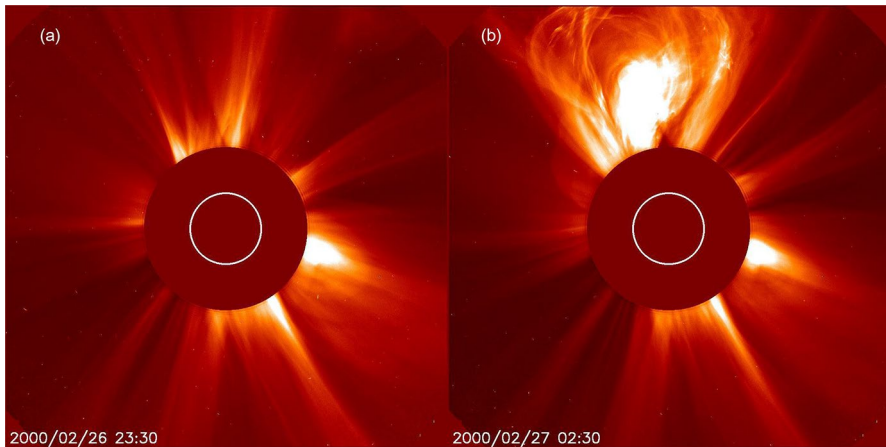Extended author information available on the last page of the article

(a)

(b)

2000/02/26 23:30

2000/02/27 02:30

Fig. 1 Observation of a typical CME on 27 February 2000 by SOHO/LASCO/C2 (**a** and **b** before and after eruption)

1 Introduction

CMEs are large-scale structures containing mass, kinetic energy, and magnetic flux that are expelled from the Sun into the heliosphere. They are responsible for many space weather events in the heliosphere, especially at Earth, such as geomagnetic storms, aurora and solar energetic particle events (SEPs). The observational study of CMEs began with a CME event recorded by the white light coronagraph onboard NASA's Seventh Orbiting Solar Observatory (OSO-7) on 14 December 1971 (Tousey 1973). However, the studies related to CMEs began much earlier. For example, geomagnetic storms discovered in the 1700s, solar flares discovered in the 1800s, and SEP events discovered in the 1900s are all now found to be closely related to CMEs (Gopalswamy 2016). Since then, people have gradually carried out studies on CMEs with the help of more advanced coronagraphs, such as Apollo Telescope Mount on Skylab (MacQueen et al. 1974), Solwind coronagraph onboard P78-1 satellite (Sheeley et al. 1980), Coronagraph Polarimeter on Solar Maximum Mission (SMM) (MacQueen et al. 1980), etc. These coronagraphs observed CMEs at different heights from 1.6 to 10 solar radii. The launch of the Solar and Heliospheric Observatory (SOHO) (Domingo et al. 1995) in 1995 greatly improved people's understanding of CMEs. The Large Angle Spectrometric Coronagraph (LASCO) (Brueckner et al. 1995) onboard SOHO is a set of three coronagraphs with high temporal and spatial resolution that image the solar corona from 1.1 to 32 solar radii, while C1 was lost rather early in the mission. CMEs may show many morphologies, the most typical of which is a three-part structure: a bright leading loop enclosing a dark low-density cavity, which contains a high-density core (Hundhausen 1993; Schwenn et al. 2006). Figure 1 shows an excellent example of CME's coronagraph image. Accurate determination of CME kinematics is feasible with the launch of the Solar Terrestrial Relations Observatory (STEREO) (Kaiser et al. 2008), which provided us with the opportunity to track CMEs continuously between

the Sun and Earth from multiple viewpoints. STEREO consists two spacecraft (STEREO A and STEREO B). Each spacecraft carries an identical imaging suite, the Sun Earth Connection Coronal and Heliospheric Investigation (SECCHI) (Howard et al. 2008), which image the solar corona from the solar disk to beyond 1 AU. The recently launched Wide-field Imager for Solar PRobe (WISPR) (Vourlidas et al. 2016) on board Parker Solar Probe and SoloHI (Howard et al. 2020) on board Solar Orbiter can further provide observations at different heights and latitudes.

With the development of coronagraph and advanced observation methods, the research on the morphology, structure and kinematic model of CME is more and more detailed. As observed in Thomson-scattered white light, CMEs are manifested as large-scale expulsions of plasma magnetically driven from the corona in the most energetic eruptions from the Sun (Manchester et al. 2017 and references therein). Chen (2011) provided a comprehensive overview of theoretical models and their observational basis of CMEs. The review of Webb and Howard (2012) mainly described the observational aspects of CMEs. Recently, reviews were made focusing on magnetic structures of solar eruptions, from the perspective of magnetic flux rope (Cheng et al. 2017) and modeling of magnetic field (Guo et al. 2017). Chen (2017) made a review on the physics of erupting solar flux ropes in the aspects of both theory and observation. A recent review by Temmer (2021) also gives the space weather perspective about CMEs and relation to flares.

As a CME is launched from the Sun, it propagates continuously outward through the heliosphere interacting with the ambient solar wind and impacting planets along its path. Their counterpart in the heliosphere are called interplanetary CMEs (ICMEs), which are characterized by the enhanced magnetic field strength, large and smooth rotation of the magnetic field vector, gradually decreasing solar wind speed, low plasma temperature and β, obvious counter-streaming electrons as well as abnormal element abundances and ion charge states (Chi et al. 2016; Zurbuchen and Richardson 2006; Richardson et al. 2010). ICMEs that strictly meet the magnetic field criteria are called magnetic clouds (MCs) (Burlaga et al. 1981). The others are called non-MCs, or simply magnetic ejecta (see Rouillard 2011). Although not all ICMEs are MCs, flux rope structures exist in nearly all ICMEs (Marubashi et al. 2015). When a flux rope is traversed by a spacecraft, the rotation angle of the observed fields depends on the distance between the flux rope axis and the spacecraft trajectory. Therefore, if the flux rope is passed through the center, it will show the characteristics of the MC, and if it is traversed from the edge, it will show the characteristics of the non-MC (e.g., Gopalswamy 2006). The poloidal flux of the flux rope in ICMEs approximately equals the reconnected flux during an eruption (Qiu et al. 2007; Hu et al. 2014). Therefore, Gopalswamy et al. (2018a) put forward a technique to construct a flux rope from the eruption data and coronagraph observations. This technique can be used by various models to predict the magnetic properties of ICMEs at Earth and other destination in the heliosphere (Gopalswamy et al. 2018b). The review by Rouillard (2011) gives a more modern view on the nomenclature of CMEs and ICMEs, in which an ICME is defined as the entire solar wind region altered by a solar transient, including the shock, sheath, solar wind pile-up, compression regions, driver gas, ejecta wake and/or the legs of magnetic loops; and a white light CME is defined broadly as any brightness variation associated with the

eruption and propagation of a solar transient. Howard and Tappin (2009) reviewed the theory of ICMEs observed in the heliosphere. The physical processes of CME/ICME evolution are reviewed in Manchester et al. (2017). Recently, Vourlidas et al. (2019) made an overview of predicting the geoeffectiveness properties of CMEs. The review by Kilpua et al. (2019) focused on the forecasting of magnetic structure and orientation of CMEs. For a comprehensive review on ICMEs, we refer to Luhmann et al. (2020), Temmer (2021) and Zhang et al. (2021).

The estimation of the magnetic flux carried out by a CME were made before by, e.g., Dasso et al. (2005), Owens (2008) and Dasso et al. (2009). In Dasso et al. (2005), for example, eight well-defined MCs were investigated and it was found that the axial flux was around 0.4×10^{21} Mx. As studied by Owens (2008), the magnetic flux carried out by a CME was usually 10^{20} to 10^{22} Mx for the axial flux and 10^{21} to 10^{22} Mx for the poloidal flux. By using a cylindrical force-free flux rope model, Wang et al. (2015) estimated that the total magnetic flux, which included axial flux and poloidal flux, was on the order of 10^{21} Mx with the median value of about 4.1×10^{21} Mx. The CME's mass ranges between 10^{11} and 4×10^{13} kg with an average of 3×10^{12} kg (Vourlidas et al. 2002). The CME speed has a wide limit, for example, over the coronagraphic field of view, CME fronts reveal radial speeds in the range of 300–500 km s^{-1} with maximum values observed up to 3000 km s^{-1}, accelerations of the order of 0.1–10 km s^{-2} and angular widths of about 30°–65° (Temmer 2021). Moreover, the ratio in density between the CME body and surrounding solar wind decreases from about 11 at a distance of 15 R_s to ~ 6 at 30 R_s (Temmer et al. 2021). Fast CMEs will drive shocks because their speed above the solar wind speed exceeds the fast mode MHD speed. The occurrence rate of the CME follows the solar cycle variance. In solar maximum, the rate of the CME can be as high as 3.5 CMEs per day (Yashiro et al. 2004). Therefore, the interaction between successive CMEs occurs frequently. The interaction of two or more CMEs can form the well-known multiple ICME or magnetic cloud structure. As compared to isolated CME events, CME–CME interaction always results in different interplanetary signatures as well as different geoeffectiveness, and often leads to complex phenomena, including magnetic reconnection, momentum exchange, energy transfer, the propagation of a fast magnetosonic shock through a magnetic ejecta, and so on (e.g., Lugaz et al. 2017; Shen et al. 2017b).

CMEs may not propagate along a straight trajectory both in the corona and interplanetary space. A promising explanation is that CMEs may be deflected during their propagation in the corona and/or in interplanetary space. CME–CME interaction may lead to the CME deflection (e.g., Wang et al. 2011; Shen et al. 2012b; Lugaz et al. 2012b). Moreover, both observations and simulations imply that even if there was only one CME, it could be deflected by the background solar wind structure and magnetic field. The deflection of isolated CMEs in corona and heliosphere has been studied by many researchers (e.g., Gopalswamy et al. 2003b, 2004, 2009b; Cremades and Bothmer 2004; Cremades et al. 2006; Wang et al. 2011, 2014; Lugaz et al. 2012b; Kahler et al. 2012; Zuccarello et al. 2012; Yang et al. 2012; DeForest et al. 2013; Zhou and Feng 2013; Möstl et al. 2015; Chi et al. 2018).

Magnetohydrodynamic (MHD) simulation is one of the important tools to study the evolution of the CMEs/ICMEs in both corona and interplanetary space. The

numerical results can be used to analyze the initiation, propagation characteristics observed by ground-based and space-based instruments (e.g., Chen 2011; Webb and Howard 2012; Cheng et al. 2017; Guo et al. 2017; Toriumi and Wang 2019). In the past years, a few featured review papers and book were concerned with MHD simulation. Lugaz and Roussev (2011) gave a detailed review and discussion on the efforts to use numerical simulations to study the magnetic topology, density structure, energetics and kinematics of ICMEs in the interplanetary space. Feng (2020) provided a recent in-depth review of the field focusing primarily on the current status of MHD simulation for space weather.

In this paper, we present a review of the propagation characteristics of CMEs from the Sun to 1 AU, including the morphology, the kinematic evolution and the prediction of the arrival at 1 AU of CMEs, the deflection and interaction of CMEs. In Sect. 2, we will give a brief overview of the morphology of the CME, including three-dimensional CME reconstruction commonly used in coronagraph observation and CME models in numerical simulation. The kinematic evolution and the prediction of the arrival at 1 AU of CMEs will be introduced in Sect. 3, where the acceleration/deceleration processes of CMEs and the numerical simulation on CME propagation are also presented. In Sect. 4, we summarize the studies of CME deflections in both corona and interplanetary space. In Sect. 5, we introduce the studies about the rotation, expansion, deformation and erosion of the CME. The interaction of CMEs are described in Sect. 6, focusing on the effects of CME interaction on the change of CME properties and severe space weather events. In the last section, we give a brief summary.

2 The morphology of CMEs

With the development of coronagraph observation, various CME models have emerged accordingly. As mentioned by Jacobs and Poedts (2011), there is no CME model sufficiently well developed to fully explain all of the observed features of solar eruptions and related phenomena (dimming regions, ribbons, post-eruption arcades, EUV waves, solar energetic particles, etc.). In addition, the basic pre-eruption configuration and the topological changes in the magnetic field that result in the conversion of a large fraction of the magnetic energy into kinetic energy are still not well understood. The main purpose of most of the existing CME models is to mimic the morphology near the Sun, to reproduce the plasma parameters comparable with 1 AU observations, and even to make real-time space weather forecasting simulations. Presently, significant progress has been made towards improving the performance of the existing CME initialization models.

2.1 Three-dimensional reconstruction of CMEs based on coronagraph observations

The leading edges of the CMEs normally leave bright traces in the images of visible light, inspiring a lot of techniques to investigate the three-dimensional (3-D)

geometrical and kinematic information of CMEs. Based on the observational characteristics of CMEs, the researchers assumed that the 3-D shape of the CME was a cone, and developed a cone model to fit the 3-D parameters of the CME (Howard et al. 1982; Michalek et al. 2003; Zhao et al. 2002; Xie et al. 2004). Xue et al. (2005a) improved the cone model to an ice cream cone model which is composed of a cone at the bottom and a partial sphere at the top. As suggested by a few investigations (e.g., Dal Lago et al. 2003; Schwenn et al. 2005; Gopalswamy et al. 2009a; Mäkelä et al. 2016), the ice cream cone model of the CME describes the relationship between radial and expansion speeds quite well, especially useful in CME arrival predictions. Wood et al. (2009) developed a 3-D density model for CMEs that was also successfully applied on STEREO data (Wood et al. 2017). Thernisien et al. (2006, 2009) further presented the graduated cylindrical shell (GCS) model employing a croissant-like empirical flux-rope structure to describe the morphology of the CME near the Sun. Besides, the GCS model has been extended to include the shock dome, so the true morphology of shock-driving CMEs can be modeled by using the GCS model (Olmedo et al. 2013; Hess and Zhang 2014; Xie et al. 2017; Gopalswamy et al. 2018c). The upper panel of Fig. 2 shows the configuration of GCS model. In the lower panel of Fig. 2, GCS model was operated on three continuous CMEs in the early days of 2017 September based on the observations of SOHO/LASCO and STEREO/COR2-A. Seen from these images, the GCS model can well represent the topology of these CMEs. Precise reconstruction results can be achieved by applying GCS fitting to multi-perspective observations of the same CME event. In addition, Many trace-fitting methods including the point-p, fixed-ϕ, harmonic mean, and self-similar expansion fitting methods have also been proposed (Sheeley et al. 1999; Howard et al. 2006; Davies et al. 2012; Möstl and Davies 2013). These trace-fitting methods depend on CME geometry, and are applied on elongation-time data extracted from STEREO/HI remote sensing images. They primarily represent a conversion method from time-elongation tracks into time-distance tracks. This is the basis to derive kinematical profile of CMEs and to study their propagation.

The above methods are called forward modeling technique. Apart from that, researchers have also developed methods to directly estimate 3-D information of the CME using multi-point observations (Maloney et al. 2009; Liewer et al. 2010). Stereoscopic analysis of a time series of CME coronagraph image pairs allows us to overcome projection effects (Howard and Tappin 2008; Temmer et al. 2009). Based on coordinated STEREO stereoscopic images, Liu et al. (2010) developed a geometric triangulation technique to track CMEs with no free parameters. Byrne et al. (2010) used a elliptical tie-pointing technique to reconstruct a full CME front in 3D. Feng et al. (2012a) developed mask fitting reconstruction method using coronagraph images from three viewpoints to obtain the 3-D shape of a CME without assuming a predefined family of shape functions (Feng et al. 2012a).

More recently, Li et al. (2020) developed a new method called correlation-aided reconstruction (CORAR) to recognize and locate CMEs based on two simultaneous STEREO-A/B HI1 (Heliospheric Imager 1: 15–84 R_s, or 4°−24° in elongation angle) images (Li et al. 2020). This method does not presume any morphology of transients and can be run in an automated way. Through the application of the CORAR method on the simulated CMEs, they found that within a large region of
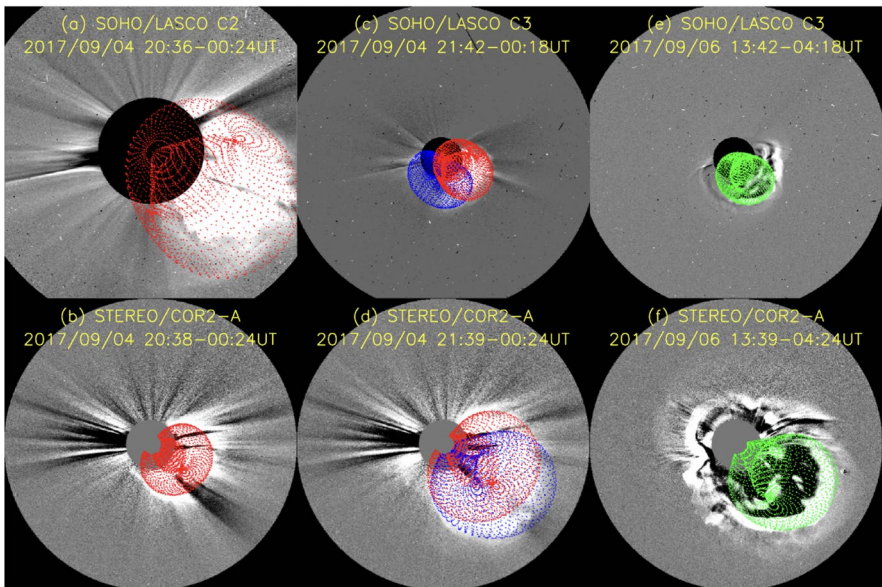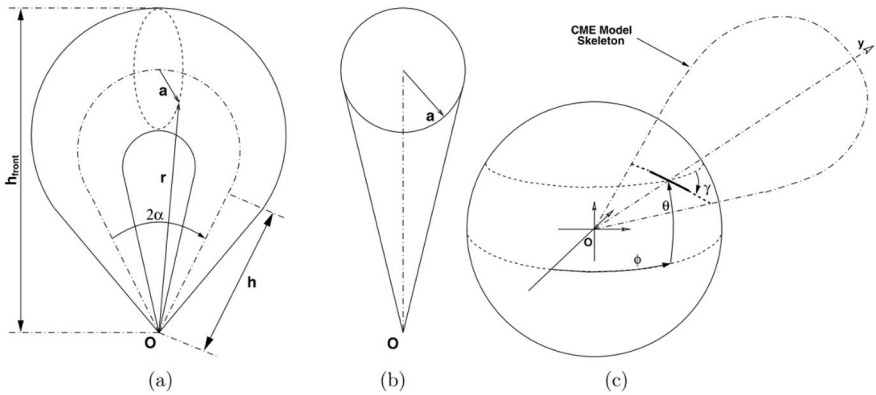
Fig. 2 Upper: Representations of the Graduated Cylindrical Shell (GCS) model **a** face-on and **b** edge-on. The dash-dotted line is the axis through the center of the shell. The solid line represents a planar cut through the cylindrical shell and the origin. *O* corresponds to the center of the Sun. **c** Positioning parameters. The loop represents the axis through the center of the shell, ϕ and θ are the longitude and latitude, respectively, and γ is the tilt angle around the axis of symmetry of the model. From Thernisien et al. (2009). Lower: An example of GCS reconstruction. The coronagraph images of three CMEs with GCS wire frames overlaid on top. At the moment shown by panel **c** and **d**, there are two interacting CMEs, which are reconstructed by red and blue wire frames. Adapted from Shen et al. (2018a)

the common field of view of the two HI1 cameras (particularly below the distance of 60 R_s), the CMEs can be recognized and located accurately. They further test the CORAR method with the HI1 image data on 3–4 April 2010 and retrieve the 3-D positional and geometrical information of a CME (Fig. 3). In Li et al. (2021), they developed a technique called maximum correlation-coefficient localization and
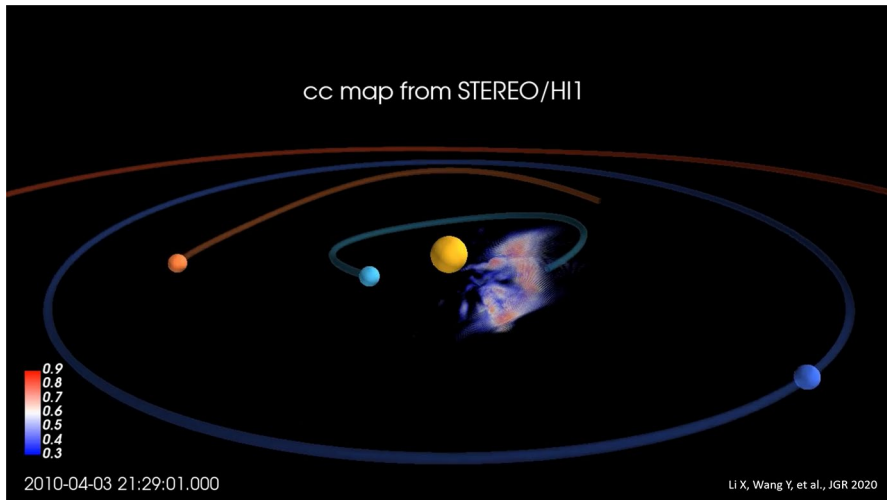
Fig. 3 3-D reconstruction result of the CME on 3 April 2010 by CORAR method. High-cc regions (red regions) shows the most possible position of the CME. The yellow ball represents the Sun. The light blue, orange, blue balls represent the Mercury, Venus and Earth, respectively. From Li et al. (2020)

cross-correlation tracking (MCT) to reconstruct the radial velocity map of CMEs in 3-D space based on 2-D white-light images, as shown in Fig. 4, and used it to estimate the expansion rate as well as some kinematic properties (Li et al. 2021).

2.2 CME models in numerical simulation

The cone model (Zhao et al. 2002; Xie et al. 2004) is one of the popular CME initiation models because of its simplicity and relatively good match with the observations of CME arrival time and arrival speed. In this model, the initial parameters of input size, speed and location are always determined from coronal observations, while it does not have internal magnetic field.

Flux rope model is another kind of widely used CME initialization model. This kind of model can reproduce many observed properties of CMEs, including the three-part density structure (Manchester et al. 2017). Different with the cone model, the flux rope model not only has the initial speed, density, temperature, but also has internal magnetic field and may therefore reproduce the plasma parameters including the arrival time, the CME speed, and the magnetic field components when a CME impacts Earth. The flux rope model was first implemented in 3D MHD simulations by Roussev et al. (2003).

Besides, the spherical plasmoid model and the magnetized plasma blob are also popular CME initialization models used in the recent years, such as in the models of EUHFORIA (Verbeke et al. 2019b), SUSANOO (Kataoka et al. 2009; Shiota and Kataoka 2016), CESE (Zhou et al. 2012, 2014; Zhou and Feng 2013), COIN-TVD (Shen et al. 2011b, c, 2012b, 2013b, 2014) and other models (e.g., Chané et al.
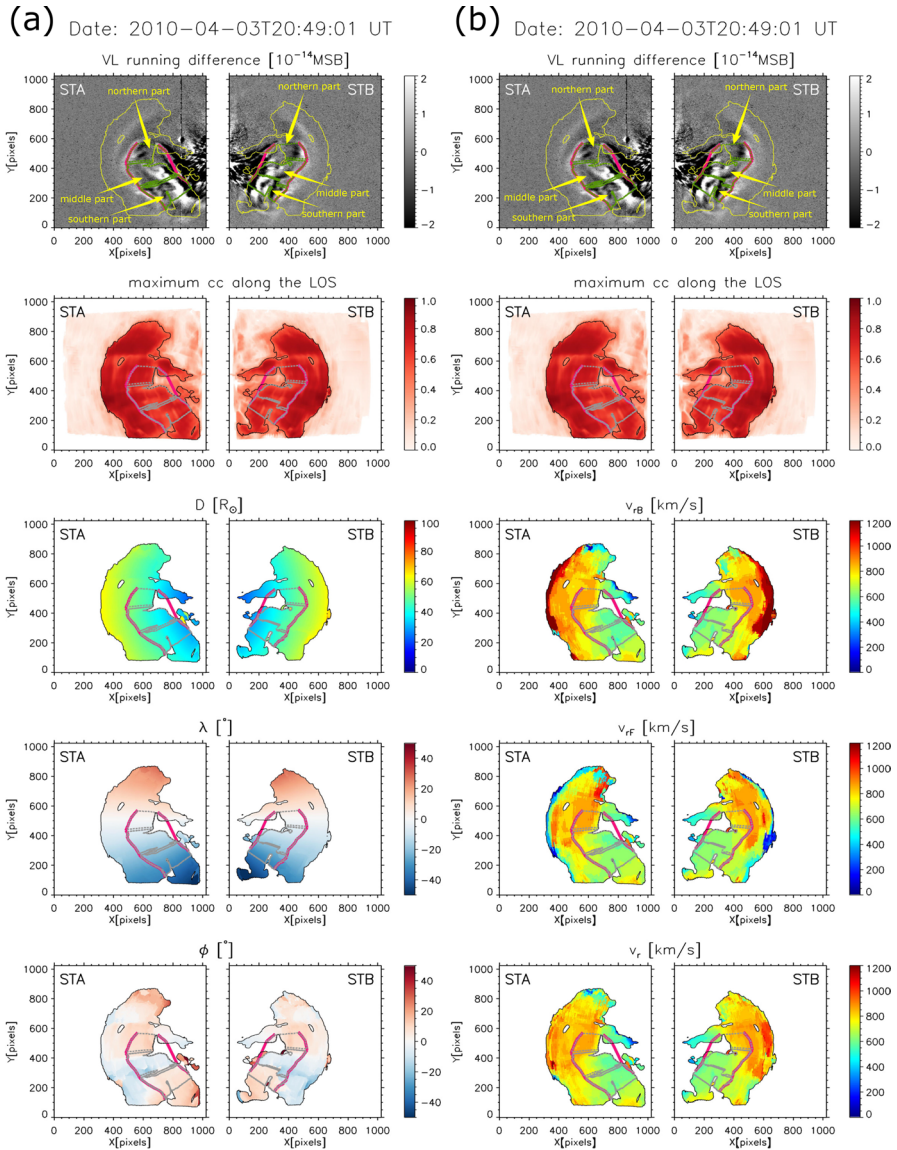
Fig. 4 Panel **a** 3D pp map of the CME at 20:49 UT on 3 April 2010 from the perspective of STEREO-A/B. Left and right columns in each panel: results from the STEREO-A and STEREO-B. Five rows from the top to the bottom: visible light (VL) running difference images, maximum cc along the LOS, the distance from the solar center (D), the latitude (λ), and the longitude (ϕ) of the solar wind transients in HEE coordinates. The solid yellow lines in the top row and the solid black lines in the other rows denote the high-cc regions. The leading edge and rear part of the ejecta are marked with thick solid purple curves, and the northern part ($-5° < \lambda < 5°$), middle part ($-20° < \lambda < -5°$), and southern part ($-35° < \lambda < -20°$) of the ejecta between the leading edge and the rear part are circled with dashed green curves in row 1 and dashed gray curves in rows 2–5 from the top to the bottom. Panel **b** Radial velocity map of the transients from the perspective of STEREO-A/B. From top to bottom: Each panel shows the VL running difference images, maximum cc along the LOS, backward radial velocity (v_{rB}), forward radial velocity (v_{rF}) and the final radial velocity ($v_r = (v_{rB} + v_{rF})/2$). The others are same as panel **a**. Adapted from Li et al. (2021)

2006). Similar to the flux rope models, these kinds of CME initialization models incorporate internal magnetic field and require the associated parameters.

3 The CMEs' kinematic evolution and the prediction of the arrival at 1 AU of ICMEs

Prediction of the arrival of interplanetary coronal mass ejections (ICMEs) at the Earth is one of the primary task for space-weather forecasting. Thus, the research on the kinematic evolution of CMEs is essential. In the past years, the successive launches of spacecraft including SOHO, STEREO, PSP, VEX, MESSENGER, MAVEN, and others as well as the constructions of various models have provided unprecedented opportunities to study the kinematic behavior of CMEs from the Sun to the different locations in the Heliosphere.

3.1 Acceleration/deceleration processes of CMEs

CMEs can be divided into fast CMEs and slow CMEs with a critical velocity of ~ 400 km s^{-1}. Slow CMEs are accelerated and fast CMEs are decelerated through the interaction with the background solar wind. Fastest CMEs face the greatest deceleration and the slowest CMEs undergo the maximum acceleration (Fig. 6c, d). The CME kinematical behavior and propagation velocity is depending on the acceleration processes when the CME explosively leaves the Sun and further on the interaction with the ambient solar wind. Both strongly affect the time when a CME reaches Earth. The question of whether fast and slow CMEs have different origination has been a hot topic in CME research (Gosling et al. 1976; St Cyr et al. 1999; Sheeley et al. 1999; Moon et al. 2002). Sheeley et al. (1999) indicated that CMEs can be divided into two principal types based on the accelerating and decelerating features, which are gradual CMEs and impulsive CMEs, through constructing continuous height/time maps of coronal ejecta as they move outward through the 2–30 R_s field of view of LASCO. Gradual CMEs are formed when prominences and their cavities rise up from below coronal streamers, while impulsive CMEs are often associated with flares and Moreton waves on the visible disk. This was further supported by Moon et al. (2002), which surveyed the speed and acceleration distributions of CMEs observed by SOHO/LASCO in 1996–2000, finding that CMEs associated with flares have a higher median speed than those associated with eruptive filaments. However, in recent years, more and more evidence have shown that there is no distinct difference between filament-associated CMEs and flare-associated CMEs (Vršnak et al. 2005; Yurchyshyn et al. 2005; Török and Kliem 2007). The theory of two types of CMEs was further dismantled by Feynman and Ruzmaikin (2004) by presenting a CME associated with both a solar flare and an erupting filament.

Generally speaking, the kinematic evolution of CMEs undergo three phases, namely: a gradual evolution, a fast acceleration, and a propagation phase, as indicated by Zhang et al. (2001). In gradual evolution phase, the CME front first forms and then slowly expands. The fast acceleration phase lasts from a few minutes to an

hour, with accelerations ranging from less than 100 m s^{-2} to about 7000 m s^{-2}, and in the later studies (Gopalswamy et al. 2018d; Veronig et al. 2019), the upper limit to the acceleration has been increased to about 10 km s^{-2}. In this phase, CMEs travel from less than one solar radius to several solar radii. The major acceleration process happens at low coronal heights. Following the fast acceleration phase, CMEs travel at a nearly constant speed or gradually accelerate/decelerate in interplanetary space due to the interaction with the background solar wind.

Using the observation of SOHO/LASCO, Zhang (2004) showed the kinematic properties of three CMEs, indicating that the acceleration phase could be impulsive, intermediate, or gradual. Figure 5 shows the kinematic plots of the three CMEs. The authors pointed out that the final velocity of a CME is determined by the magnitude
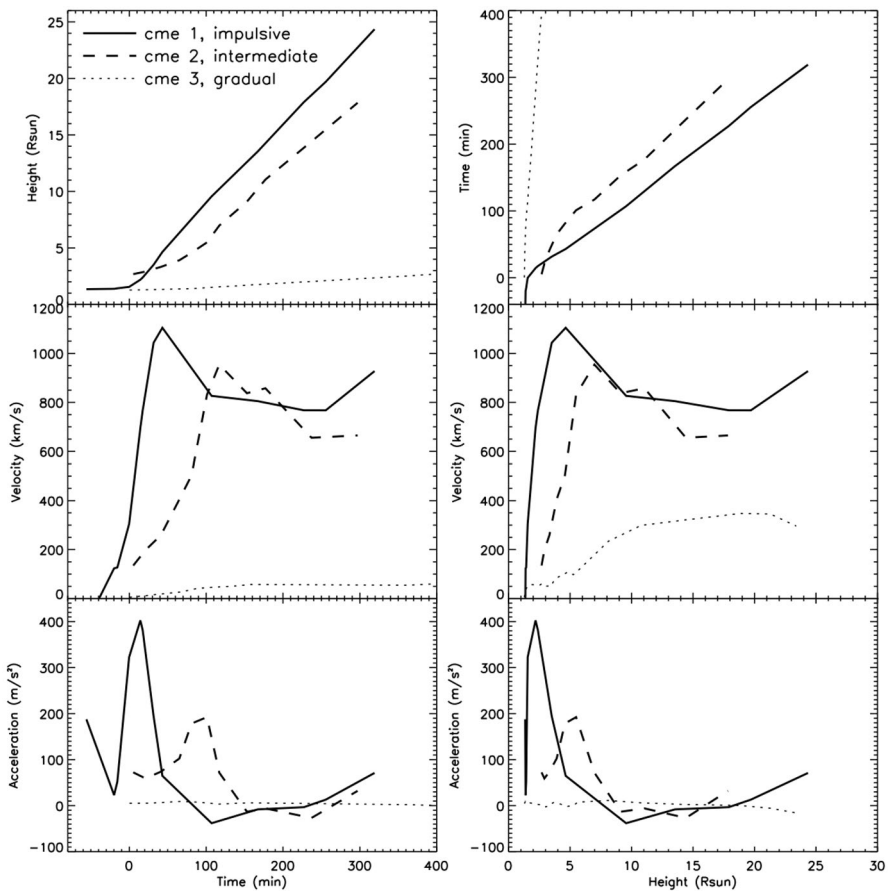

Fig. 5 Composite kinematic plots for three CMEs: impulsive (solid line), intermediate (dashed line), and gradual (dotted line). The left three panels show kinematic evolution versus time: height-time (top), velocity-time (middle), and acceleration-time (bottom). The right three panels show kinematic evolution versus height: time-height (top), velocity-height (middle), and acceleration-height (bottom). From Zhang (2004)

and duration of acceleration, which vary greatly from event to event. This was further supported by Vršnak et al. (2007) and Bein et al. (2011).

Bein et al. (2011) found that the peak acceleration values and acceleration duration of CMEs are widely distributed and inversely correlated. In addition, the acceleration of CMEs from compact sources are more impulsive, and they can achieve higher peak accelerations at smaller altitudes. These findings could be explained by the Lorentz force. Assuming the Lorentz force is the main accelerator of the CME, the acceleration can be calculated by the following function:

$$a < \frac{B^2}{2\mu_0 \rho L} = \frac{V_A^2}{2L} \tag{1}$$

with B the magnetic field strength within the CME body, μ_0 the magnetic permeability in vacuum, V_A the Alfven velocity, ρ the plasma density, V the CME velocity and L the characteristic length scale over which the magnetic field varies. It shows that the acceleration is not only controlled by the Alfven velocity but also depend on the size of the erupting structure, and the initially compact CMEs (small L, large V_A) will get higher accelerations.

In the inner corona, the coronal magnetic field is strong, while the solar wind has not yet fully developed, the force that dominates the CME kinematic is mainly the Lorentz force, which will accelerate CMEs as mentioned above. When CMEs travel outwards into the outer corona and the interplanetary space, the CME kinematic is turned to be controlled by the drag force of the solar wind due to the weakening of the magnetic field strength and the gradual enhancement of the solar wind (Borgazzi et al. 2009; Vršnak and Gopalswamy 2002; Vršnak and Zic 2007). Byrne et al. (2010) indicated that, beyond 7 R_s, the motion of the CME is determined by an aerodynamic drag in the solar wind. Sachdeva et al. (2015) studied a sample of 8 events to find out where the drag force starts to dominate and found different ranges for slow and fast CMEs. They found that the drag force is enough to explain the dynamics of the fastest CME. For the slower CMEs, solar wind drag is not the dominant effect on CME trajectories until 15–50 R_s. Moreover, Temmer et al. (2011) simulated the background solar wind and compared it with the speed evolution of three CMEs, showing that the CME might be still driven up to a distance of more than about 100 R_s by the induced Lorentz force due to ongoing magnetic reconnection.

Gopalswamy et al. (2000b) studied the velocities of a set of 23 ICME/corresponding source CME pairs, finding that CME speeds range over an order of magnitude while the ICME speeds lie in a relatively narrow range from 320 to 650 km s^{-1}, as shown in Fig. 6a, b. CMEs can be divided into fast CMEs and slow CMEs with a critical velocity of ~ 400 km s^{-1}. Slow CMEs are accelerated and fast CMEs are decelerated through the interaction with the background solar wind.

3.2 Prediction of the arrival of ICMEs at 1 AU

Predicting the arrival of ICMEs at 1 AU is one of the main tasks of space-weather forecasting (e.g., Feng and Zhao 2006; Feng et al. 2009; Zhao and Feng 2014; Zhao and Dryer 2014). The statistical relationships between the ICME transit time and
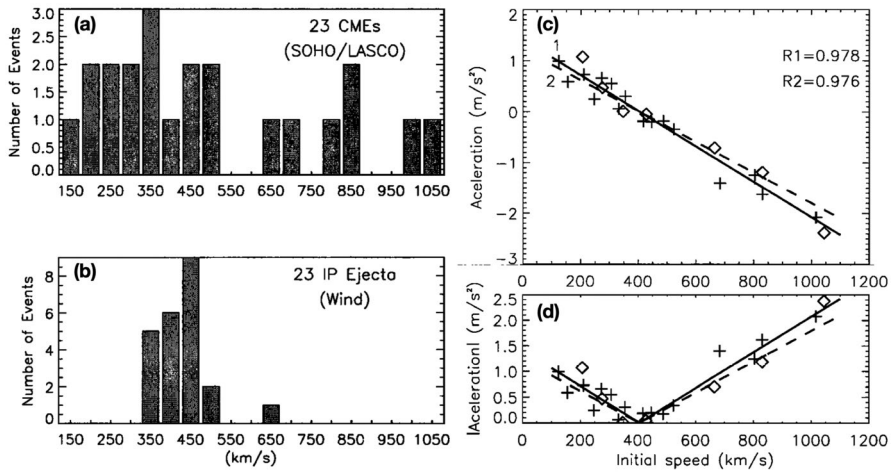
Fig. 6 Left: Histogram plots showing the velocity distribution of CMEs detected by SOHO/LASCO coronagraphs (**a**) and IP ejecta as detected by the Wind spacecraft (**b**). Right: Scatter plots of the acceleration (**c**)/the mean values of the acceleration (**d**) and the initial speed of the CME. Adapted from Gopalswamy et al. (2000b)

CME velocity achieved from coronagraph observations are widely used to predict the ICME arrival time (Gopalswamy et al. 2001a; Michalek et al. 2004; Manoharan 2006; Vršnak and Zic 2007). For example, Fig. 7 clearly indicates that the ICME transit time is dependent not only on the CME speed, but also on the solar wind speed. In addition, there exists a linear relation between the values of CME acceleration and CME speed. Many models have been developed over the years to estimate the time of travel, or arrival time, of the CME.

In addition to empirical models, there are also analytical models, like the drag-based models, based on the assumption that the aerodynamic drag is a dominant force governing the CME propagation in the interplanetary space. Vršnak et al. (2013, 2010) developed a Drag-Based Model (DBM) to describe the dynamics/kinematics of the heliospheric propagation of CMEs. Figure 8 presents several examples of the ICME kinematics calculated by DBM. It is clear from the figure that ICMEs tend to adjust to the solar-wind speed. In addition, most of the acceleration/deceleration occurs near the Sun. As we know that the DBM is a 2D analytical model for heliospheric propagation of CMEs in ecliptic plane predicting the CME arrival time and speed at Earth or any other given target in the solar system, and the Drag-Based Ensemble Model (DBEM; Dumbović et al. 2018) takes into account the variability of model input parameters by making an ensemble of n different input parameters to calculate the distribution and significance of the DBM results. Since DBEM has the advantage to be a very fast, reliable and simple model, it is suited for fast real-time space-weather forecasting. Čalogović et al. (2021) described in detail a new DBEMv3 version which converts the input from GCS into the cross-section to calculate the drag force. They evaluated the model for the first time determining the DBEMv3 performance and errors by using various CME-ICME lists and it was
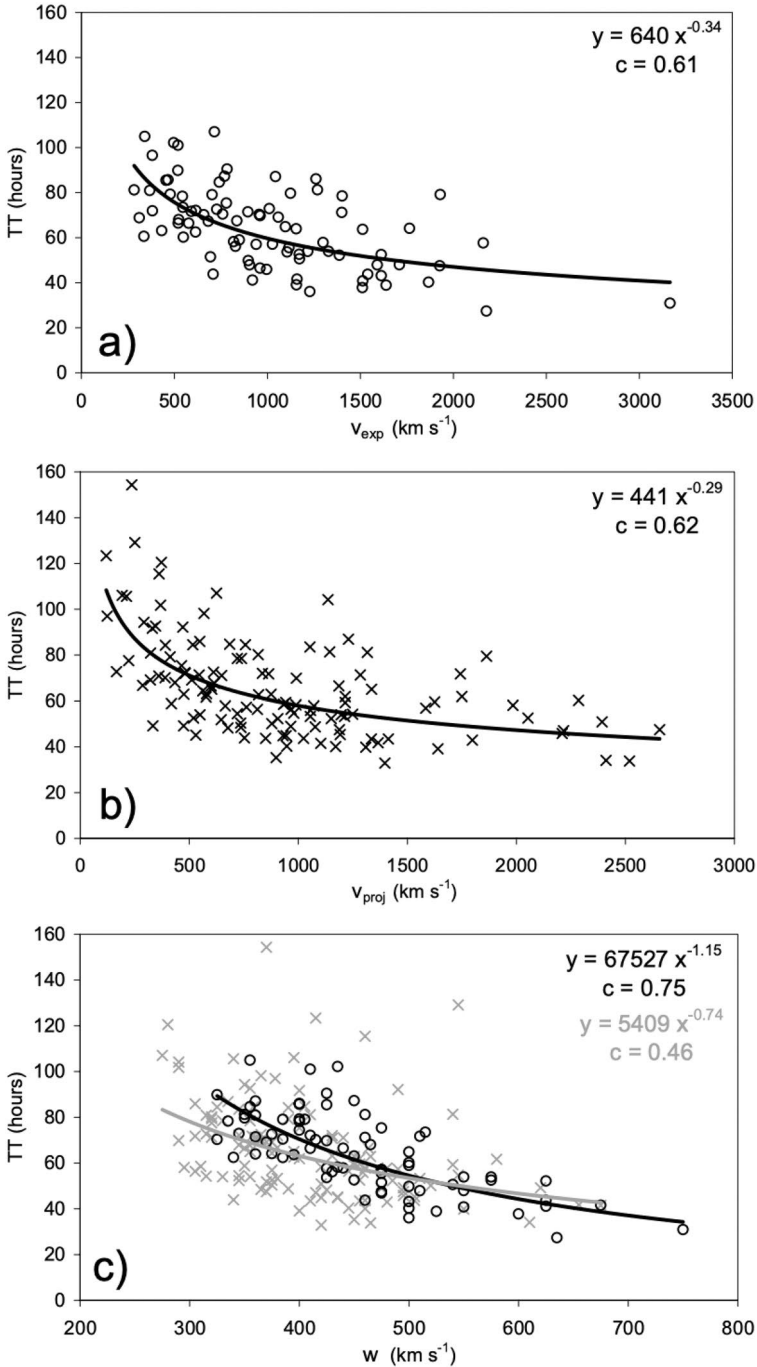
Fig. 7 ICME transit times shown as a function of CME initial speed (**a**) and (**b**), and solar wind velocity (**c**). The power-law least-square fit parameters are given in the insets, together with the correlation coefficient c. From Vršnak and Žic (2007)
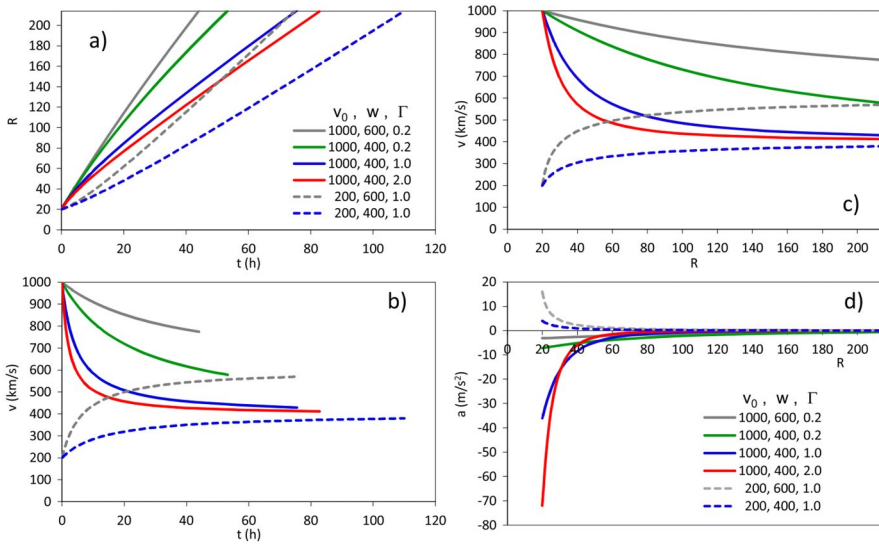
Fig. 8 Examples of ICME kinematics based on DBM; the initial heliocentric distance is set to 20 R_s. **a** Heliocentric distance versus time; **b** ICME speed versus time; **c** ICME speed versus distance; **d** ICME acceleration versus distance. In panels **a** and **d**, v_0 and w are the initial speed of CME and the speed of ambient solar wind with unit of km s^{-1}, respectively; $\Gamma = \gamma \times 10^7$ km^{-1}, where γ is the drag parameter. From Vršnak et al. (2013)

compared with previous DBEM versions. Their results showed that DBEMv3 had slight improvement in the performance for all calculated output parameters compared to the previous DBEM versions.

Riley et al. (2018) summarized the current CME forecasting models which have been used to predict the CME arrival times and shock arrival times during the interval from 2013 through late 2017 in the Community Coordinated Modeling Center (CCMC) scoreboard. The CCMC scoreboard is a platform provided to scientists to compare their forecasts with each other in real-time. In general, these models can be classified as CME-shock arrival forecasts or CME arrival forecasts. In the former category, the shock time of arrival (STOA; Dryer et al. 2004) and WSA-ENLIL+Cone (WEC) Model (Odstrcil et al. 2004a) are two examples; and in the latter category, the WEC Model also plays an important role, while the DBM (Vršnak et al. 2013) serves to illustrate a complementary approach to the problem. Riley et al. (2018) found that the CME shock arrival times for all models combined are predicted on average within 10 h but with standard deviations of sometimes more than 20 h.

Some models make use of HI images, which require techniques to convert the measured elongation into radial distance. Braga et al. (2020) investigated the prediction of arrival time of CMEs using observations solely from heliospheric imager HI-1 onboard the twin STEREO spacecraft. They used co-temporal HI-1 observations from two viewpoints to construct an elliptical model of the CME fronts and hence estimated their locations in the solar corona. Beyond the HI-1 FOV, they applied a drag force model to propagate the CME up to 1 au. Then they compared

the CME arrival time errors computed with this approach to those calculated using mainly observations from SECCHI coronagraphs, and their results, similar with e.g., the Colaninno et al. (2013), Hess and Zhang (2014), Möstl et al. (2014) and Rollett et al. (2016) results, suggested that the estimation of the arrival time using HI-1 measurements could result in a more accurate estimation (i.e., smaller error) than in those cases based on coronagraph observations, at least for fast CME events. However, using HI observations can reduce the advanced warning time compared to coronagraph observations. More sophisticated models combine both the drag-based approach and HI observations, e.g., the Ellipse Evolution model based on HI observations (ELEvoHI; Rollett et al. 2016), which assumes that the CME frontal shape within the ecliptic plane is an ellipse, and allows the CME to adjust to the ambient solar wind speed based on DBM (Žic et al. 2015). By using ELEvoHI, Hinterreiter et al. (2021) carried out a comparison of CME arrival time and speed predictions from two vantage points. They found a mean arrival time difference of 6.5 h between predictions from the two different viewpoints, which could reach up to 9.5 h for individual CMEs, while the mean arrival speed difference is 63 km s^{-1}. They also pointed out that an ambient solar wind with a large speed variance could lead to larger differences in the STEREO-A and STEREO-B CME arrival time predictions. Amerstorfer et al. (2021) studied 18 different combinations of inputs to run the HI-based ensemble CME arrival prediction model, ELEvoHI, to ascertain the set-up leading to the most accurate arrival time and speed predictions. Their results found that the accurate modeling of the ambient solar wind was of particular importance to improve CME predictions. Shanmugaraju and Vršnak (2014) also investigated the transit Time of CMEs under different ambient solar wind conditions by using DBM, and their research obtained more details on the dependence of the CME Sun–Earth transit time on the CME speed and the ambient solar wind speed.

Paouris and Mavromichalaki (2017) developed an effective acceleration model (EAM), which was based on the assumption that the ambient solar wind interacted with the ICME resulting in constant acceleration or deceleration, for predicting the arrival time of the shock that preceded a CME. Recently, Paouris et al. (2021) made a Comparison of the improved EAM model, which was called as EAMv3, with the WSA-ENLIL+Cone ensemble models and the DBEM Models. They selected a sample of 16 CMEs/ICMEs, in 2013–2014, for the comparison. Basic performance metrics such as the mean absolute error (MAE), mean error (ME) and root mean squared error (RMSE) between observed and predicted values of arrival time were presented. Their results showed that both of the MAE and ME for EAM model were smaller than that for DBEM and ENLIL. Zhuang et al. (2017) also developed an integrated CME-arrival forecasting (iCAF) system, assembling the modules of CME detection, three-dimensional (3D) parameter derivation, and trajectory reconstruction to automatically predict whether or not a CME arrives at Earth.

Recently, Verbeke et al. (2019a) summarized the progress made by the CME Arrival and Impact working team since April 2017, and the models they overviewed include the DBM/DBEM model, EAMv2, ElEvoHI and a few current active MHD models. And they described a community-driven benchmarking effort to adopt specific metrics, skill-scores, events and datasets to improve ICME arrival time predictions.

3.3 Numerical simulation on CME propagation

The propagation and kinematics of CMEs are also widely studied in numerical simulation. By using cone model as CME initialization, Odstrcil et al. (2005) applied the 3-D MHD simulation to the 12 May 1997 interplanetary event to analyze possible interactions of the ICME propagating in various steady state and evolving configurations of the background solar wind. By using the WSA-ENLIL+Cone ensemble model, which is the combination of the WSA-ENLIL model and the cone model, Taktakishvili et al. (2011) simulated a series of selected well-observed halo CME events. Their simulation results showed that this WSA-ENLIL+Cone ensemble model with the observations from coronagraph as input could give reasonably good results for the CMEs' arrival times for the selected "geoeffective" CME events. Bain et al. (2016) also use the WSA-ENLIL+Cone heliospheric model to study shock connectivity during the SEP-rich periods in the August 2010 and July 2012, and their simulation results demonstrated that much SEP activity can be understood by using such model and especially from knowing about both remote and local shock source connections. The WSA-ENLIL+Cone ensemble model is also known as one of the effective CME arrival prediction tools. Dewey et al. (2015) used this ensemble model to study the CME-related solar wind perturbations on the Mercury system. Their simulation results revealed that the modeled results could be compared with the observations by the spacecraft of MErcury Surface, Space ENvironment, GEochemistry and Ranging (MESSENGER) from March 2011 to December 2012. Pomoell and Poedts (2018) integrated the cone model into EUHFORIA model to simulate the CME events in the inner heliosphere during 17–29 July 2015. Also by combining the cone model and the EUHFORIA model, Scolini et al. (2018) tested the effect of different CME shapes on the simulation results, and their results showed that all the parameters specifying the CME shape in the model significantly affect simulation results at 1 AU, and the predicted CME geoeffectiveness. By using the cone model, Riley and Ben-Nun (2021) also pointed out the main sources of uncertainties in predicting a CME's arrival time at Earth, which were the initial properties of the ejecta, including its speed, mass, and direction of propagation and the properties of the ambient solar wind into which it propagated.

Lionello et al. (2013) inserted an out-of-equilibrium flux rope in the coronal model of the MAS-ENLIL model as CME initiation model, and they simulated the propagation of an interplanetary CME (ICME) from 18 R_s to 1.1 AU. Their simulation results showed this model could reproduce the propagation process of the CME precisely. By using the MAS/MAS-H model combined the modified Titov–Démoulin (TD) model (Titov et al. 2014), Török et al. (2018) inserted a magnetically stable flux rope to generate a CME close to the observed properties of the 2000 July 14 "Bastille Day" eruption. By using MHD simulation, they analyzed the properties of the CME propagation from it's eruption near the Sun, to propagating to the Earth. Figure 9a showed the initial flux-rope field lines, Fig. 9b depicted the field lines of the flux-rope core at $t = 164.10$, shortly after eruption onset, Fig. 9c, d demonstrated the interplanetary magnetic field and ICME flux rope at $t = 256$, shortly before it reached 1 AU. Here, the unit of time is Alfvén time, and 1 Alfvén time is about 24 min. Jin et al. (2013) also used the TD flux-rope model to initiate the CME, and
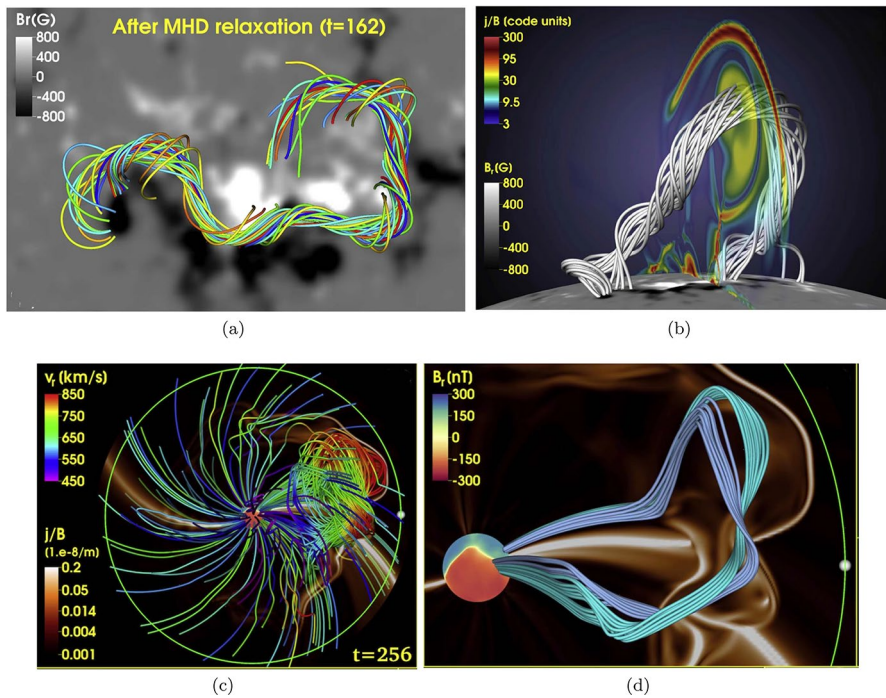
Fig. 9 **a** Initial flux-rope field lines with zero-β relaxation; **b** field lines of the flux-rope core at $t = 164.10$; **c** interplanetary magnetic field and ICME flux rope at $t = 256$; **d** close-up view on **c**, showing two flux bundles at the core of the flux rope. From Török et al. (2018)

simulated a fast CME erupted from active region NOAA AR 11164 during CR2107. They compared the propagation of this fast CME and the thermodynamics of CME-driven shocks in both the 1T (one-temperature) and 2T (two-temperature: coupled electron and proton) CME simulations. Their simulation results revealed that, to produce the CME structures and CME-driven shocks more physically correct, it is important to connect the electron heat conduction with proton shock heating.

Moreover, Jin et al. (2016) inserted the analytical Gibson–Low (GL) flux rope model (Gibson and Low 1998) with different parameters into the solar wind background which was constructed by AWSoM SC model (van der Holst et al. 2014), to simulate the CME event occurred at 00:04 UT on 15 February 2011. Their simulation results showed that a CME's impact on the surrounding solar wind structures would be affected by many factors, such as, the magnetic strength of these structures, the distance from the erupting flux rope to the source region of the background fields, and the interaction between the CME with the large-scale magnetic field. Jin et al. (2017a) developed a new data-driven tool called Eruptive Event Generator Gibson-Low (EEGGL) to automatically determine the GL flux rope parameters, based on the synoptic magnetogram data from GONG and the observations of SOHO/LASCO. By combining the EEGGL model and the AWSoM solar wind model (Oran et al. 2013; van der Holst et al. 2014), Jin et al. (2017b) performed a MHD simulation to study the CME propagation on the 7 March 2011 from the

chromosphere to 1 AU, and their results could reproduce many of the observed features both near the Sun and in the heliosphere. Figure 10a depicted the initial GL flux rope configuration for 7 March 2011 CME event with central plane showing the radial velocity, and Fig. 10b compared EUV waves in the simulation and in the SDO/AIA observation.

Wu et al. (2016) combined a data-driven flux rope model for the CME initiation and a global coronal-heliosphere MHD model to simulate the propagation of the CME event on 6 September 2011, based on an observed eruptive twisted flux rope deduced from solar vector magnetograms. And their simulation results suggested that the flux rope evolution model could reproduced the physical properties of the CME, and the morphology resembled the observations by STEREO/COR-1.

By combining the 3D SIP-CESE MHD model (Feng et al. 2007, 2010, 2012b, 2015) with the spherical plasmoid mimicking CME initiation model, Zhou et al. (2012, 2014) and Zhou and Feng (2013) investigated the CME propagation process of a few Sun–Earth connection CME events, such as 4 November 1997, 12 May 1997, and 2010 April 3 CME events. And their simulated results provided a relatively satisfactory comparison with the Wind spacecraft observations, such as the southward interplanetary magnetic field and large-scale smooth rotation of the magnetic field associated with the CME for the 1997 November 4 event (Zhou et al. 2012); and shock arrival time at Earth with ~2 hours error for the 2010 April 3 CME events (Zhou et al. 2014).

By using the 3D COIN-TVD MHD model with the magnetized plasma blob as CME initialization model, Shen et al. (2011c) and Shen et al. (2014) simulated the single CME propagation events and the interaction of two CMEs events, such as 4 April 2000, 12 July 2012 CME events, and 28 March 2001 CME–CME interaction event. Figure 11 shows the relative density($(\rho - \rho_0)/\rho_0$) distribution and the magnetic field lines at $t = 0.5, 10, 20$, and 30 h. Their simulation could reproduce the real 3D nature of the CME in morphology and their evolution from the Sun to the Earth relatively well.

A spheromak-type magnetic flux rope was also taken as the magnetic field structure of the initial CME model by, e.g., Kataoka et al. (2009) and Shiota and Kataoka (2016), to simulate the propagation of the CME by using the SUSANOO model. Figure 12a–c show the Magnetic field structures on the meridional plane at 2003.10.29 03:00UT, 2003.10.30 00:00UT, 2003.10.30 15:01UT; Fig. 12d shows the three-dimensional view of CME 11 at the same timing as Fig. 12b in HGI coordinate. In recent years, the spheromak model was included in EUFHORIA (Verbeke et al. 2019b) and shown to have relative good comparison with in situ measurements for some Sun-to-Earth propagation of CME events (e.g., see Scolini et al. 2019; Palmerio et al. 2019). An et al. (2019) used a spheromak-shaped ICME model to define observation constrained parameters representing ICME properties, and performed a series of MHD simulations by changing these parameters to investigate the relation between ICME properties and space weather disturbances at the Earth. Their simulations showed that the injection speed, mass, longitude of the source region, and magnetic field strength rather affected the onset time of space-weather disturbances at the Earth. Singh et al. (2020) proposed a modified spheromak model and demonstrated its applicability to CME simulation in the inner heliosphere. Through a
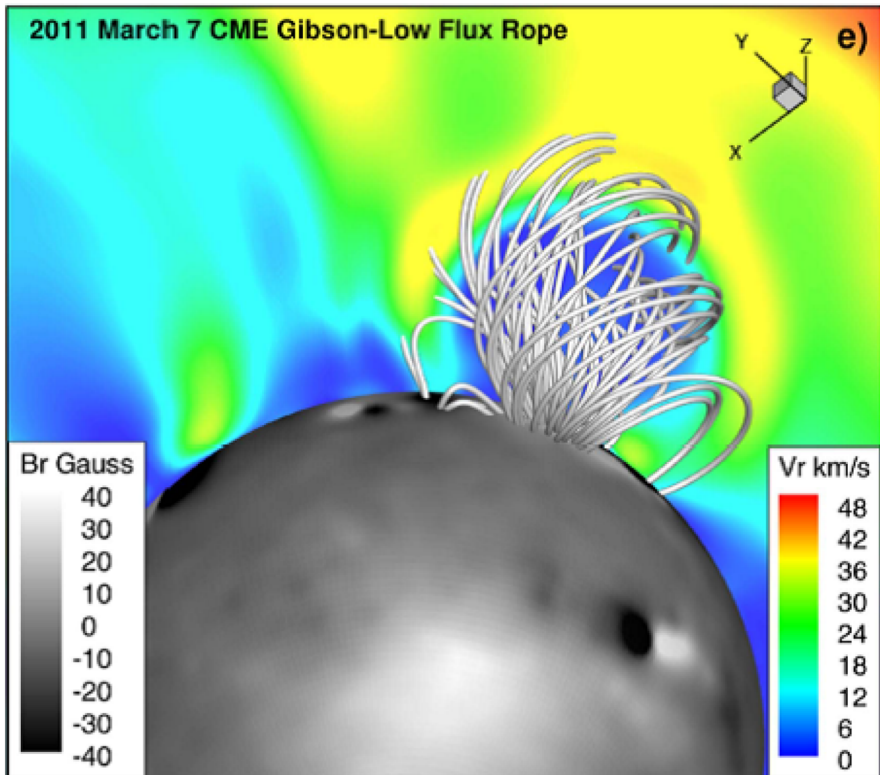
(a)
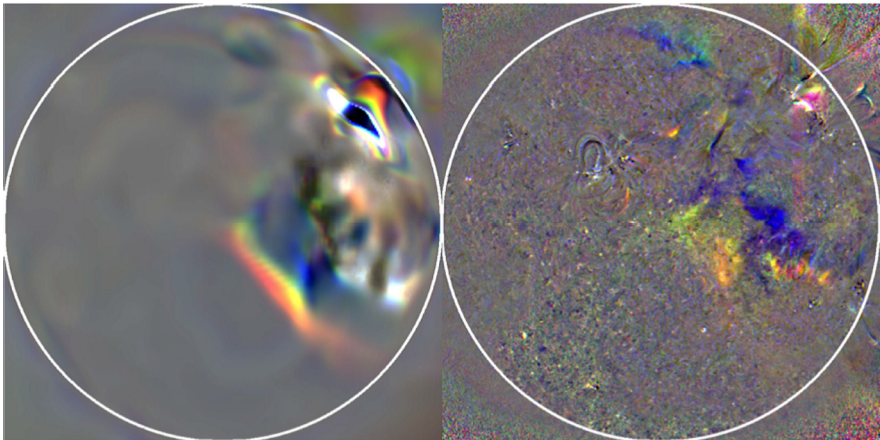
(b)

Fig. 10 a Initial GL flux rope configuration for 7 March 2011 CME; **b** EUV waves in the simulation (left) and in the SDO/AIA observation (right). From Jin et al. (2017b)
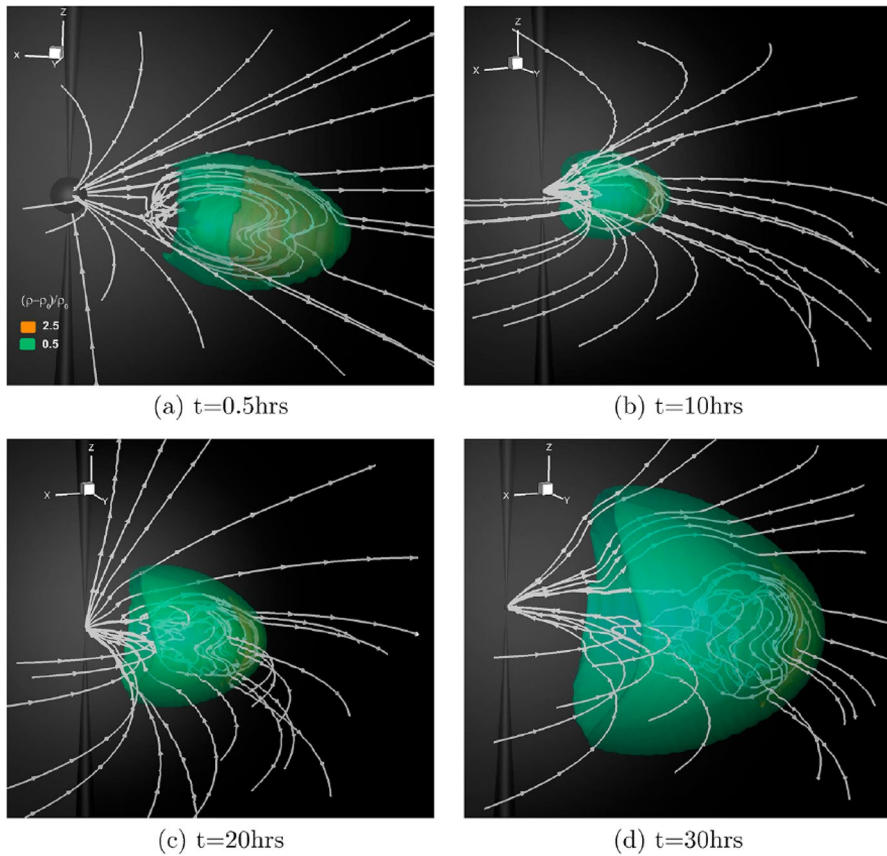
Fig. 11 Three-dimensional view of the relative density $((\rho - \rho_0)/\rho_0)$ distribution at $t = 0.5, 10, 20$ and 30 h. The color code in the panels represents the two levels of isosurfaces of the relative density. The magnetic field topology is represented by the white magnetic field lines. From Shen et al. (2014)

parametric study, they found that the speed of a CME was much more dependent on its poloidal flux than on the toroidal flux. They also used this model to simulate the 2012 July 12 CME event and compared the plasma properties at 1 AU with observations, and the predicted CME properties agreed reasonably with observational data. Iwai et al. (2021) used 3D MHD simulations based on interplanetary scintillation (IPS) observations, and spheromak-shape CME models with various initial speeds to investigate the accuracy of CME arrival times at the Earth. Their results suggested that the assimilation of IPS data into MHD simulations could improve the accuracy of CME arrival time forecasts, and the magnetic field included in the spheromak model, the CME size, the background solar wind structure all could influence the predicted arrival time.

With input based on actual solar observations, the HAFv.2 and 3D MHD model was used to simulate a variety of CME events, such as the interplanetary evolution of the observed geoeffective CME during 1–4 August 2010 (Wu et al. 2011), and the
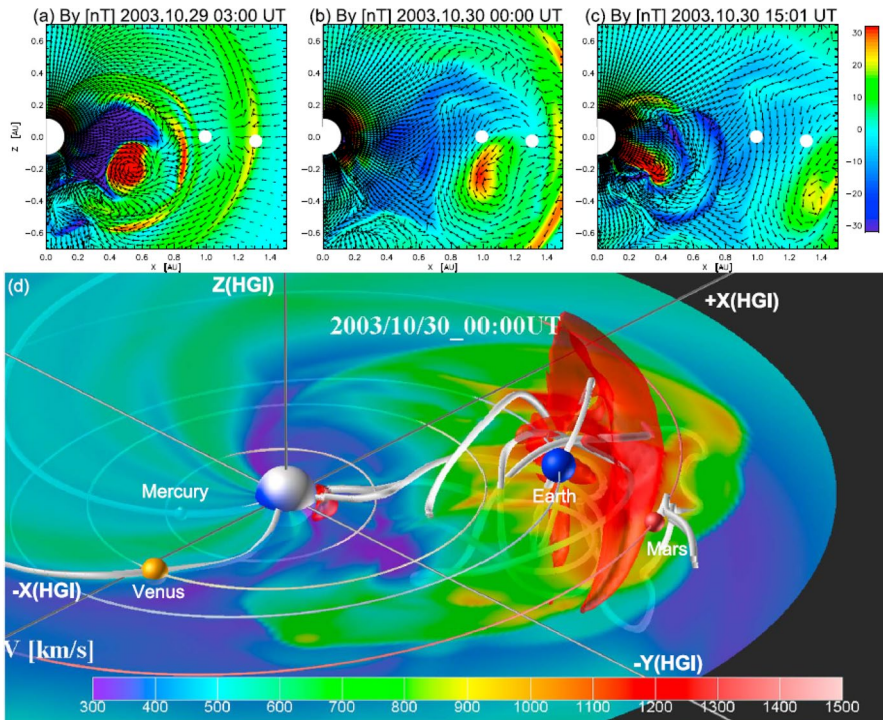
Fig. 12 a–c Magnetic field structures on the meridional plane of the HEE coordinate where Earth located. The color shows distribution of the toroidal component (By in HEE), and the arrows show magnetic field direction of poloidal component. **d** Three-dimensional view of CME 11 at the same timing as **b** in HGI coordinate. The red surface shows high stream area whose speed exceeds 1200 km s^{-1}. Background colors on the transparent XY plane in HGI (the solar equatorial plane) show solar wind velocity distribution. The thick tubes are magnetic field lines that connected around the positions of planets (shown with colored spheres associated with their orbits). From Shiota and Kataoka (2016)

effects of coronal hole on CME/shock morphology in the inner heliosphere with 7 March 2011 solar events (Wood et al. 2012a). Liou et al. (2014) also employed this model to investigate the propagation of the extremely fast backside CME event on 23 July 2012 and the modeled results were in agreement with the in-situ measurement from STEREO-A. Specially, Wu et al. (2017) investigated the CME encountered by the Wind spacecraft on 9 September 2011 in detail and verified the association of the short-duration (~ 35 min) extremely dense pulse (with a peak of ~ 94 cm^{-3}) with the heliospheric plasma sheet compressed by the interplanetary shock.

Combining the 3D IN-TVD-MHD model (Shen et al. 2018b), Liu et al. (2019) established a CME flux rope model based on the graduated cylindrical shell (GCS) model and applied it into the numerical simulation on the propagation and deflection of the fast CMEs in the interplanetary space from 0.1 AU to 1 AU. Recently, Shen et al. (2021a) numerically investigated the effect of the initial parameters of the GCS-based CME Flux-rope Model, including the initial density, the thickness of CME flux tube, initial mass, and initial magnetic field, on the simulation results

at the observers located in the directions aligned with the initial propagating direction of the CME. The simulation results showed that when the initial density and geometric size of the CME changed at the same time, both of them affected the propagation of the CME; when the initial density and geometric size of the CME changed but the total mass remained approximately the same, the propagation of the CME was not affected much. We also found that when the initial magnetic field strength increased, both the peak value of the total magnetic field and the duration time of the prominence of B_{total} and B_z increased obviously. Furthermore, Shen et al. (2021b) extended the previous work to study the influence of the different CME initial parameters on the simulation results at locations with different longitudes and latitudes. The results indicated that as long as the initial mass of the CME remained unchanged, the initial geometric thickness had different influence at latitudinal and longitudinal directions, and the deflection of the CMEs always occurred in both latitudinal and longitudinal directions.

As stated in the recent review paper (Zhang et al. 2021), in the recent years, there are many developments in the number of 3D MHD models that have been successfully used to simulate the Sun-to-Earth propagation of CMEs. For example, by means of out-of-equilibrium flux ropes, the CME initialization process becomes quicker and easier to perform in coronal codes; interplanetary models (always starting at 0.1 AU) have been used with spheromak and/or flux rope CMEs, which bridges the gap between computationally intensive Sun-to-Earth simulations and interplanetary simulations with MHD models. However, the number of Sun-to-Earth simulations of CMEs initiated at the solar surface with a realistic model is still relatively low. Furthermore, initiating CMEs by using magnetofrictional or flux emergence or other self-consistent models based on more and more abundant solar observations may lead to a better physical understanding of CMEs. In addition, a more accurate background solar wind modeling might lead to a clear improvement of CME propagation. Further improvements towards this coupling are expected in the next few years.

4 The deflection of CMEs

Based on remote sensing and in-situ observations near the Earth, the researchers found that not all Earth-directed CMEs would eventually reach the Earth, while some CME events originating at the edge of the Sun could arrive (Wang et al. 2002; Gopalswamy et al. 2009b; Wang et al. 2011, 2014). This interesting phenomenon stems from the CME deflection which is the departure from a radial trajectory that commonly occurs with significant in-course changes in direction. Understanding the deflection of CMEs is of great interest to the space weather community because of their implications for improving the prediction of CME. CME's geoeffectiveness is to a large extent affected by CME deflection. There are a lot of CMEs that are not originated in solar disk center, but due to the deflection, they reached the Earth and trigger large geomagnetic storms. On the other hand, the CME on 2014 January 7 originated in an active region near disk center, and hence, a significant geomagnetic

impact was forecasted. However, due to the non-radial motion, no geomagnetic storm occurred (Möstl et al. 2015).

Many studies about the CME coronagraph observations revealed the latitudinal deflections and the longitudinal deflections have been further measured by reconstructing the 3-D CME trajectory using coronagraph or heliospheric imager observations from multiple viewpoints (e.g., Liu et al. 2010; Byrne et al. 2010; Lugaz et al. 2010; Bosman et al. 2012; Nieves-Chinchilla et al. 2013; Cécere et al. 2020). Both the corotating interaction region (CIR) and heliospheric current sheet (HCS) structures of the background solar wind could play a substantial role in the propagation of CMEs and their geoeffectiveness (e.g., Odstrcil et al. 1996, 2004b; Zhao et al. 2007). Therefore, as the CME interacts with the solar wind structure (e.g., CIR, HCS), it may deflect during its propagation. The studies on the CME deflection are the important aspects in the CME research, and have achieved a lot of progress in recent years.

To measure the deflection of CMEs from the Sun to 1 AU, Isavnin et al. (2013) separately estimated the CME orientation in the close vicinity of the Sun using the forward modeling technique and near 1 AU using the Grad–Shafranov reconstruction. According to their statistical study, the longitudinal deflection of the CME was small, less than 6°. The latitudinal deflection was clearly larger than the longitudinal, exceeding 10° for the majority of events with the largest deflection of 35°. Wood et al. (2017) compared the CME propagation directions with the locations of associated solar activity, finding that the angular discrepancy has a mean and standard deviation of 19.3° ± 9.6°.

It should also be mentioned that CME deflection can manifest as the deflection of its components. The prominence at the core of the CME was found to be deflected, suggesting that the CME deflected as a whole (Gopalswamy and Thompson 2000; Gopalswamy et al. 2000a; Gopalswamy 2015). The CME deflection can also be represented by the reflection of shocks surrounding CMEs. The extreme ultraviolet (EUV) waves, which are associated with CMEs, are found to be reflected by coronal holes (Gopalswamy et al. 2009d; Olmedo et al. 2012). Wood et al. (2012b) found that in the 2011 March 7 CME event, the CME body was deflected away by an adjacent coronal hole, but the shock readily expands into the fast outflow from the coronal hole, resulting in the CME with ejecta not well centered within the shock surrounding it. The deflection of CMEs also triggered many driverless shocks that were not followed by drivers (Gopalswamy et al. 2009c, 2010a). Such driverless shocks were mostly observed during the declining phase of solar cycle 23, consistent with the abundance of low-latitude coronal holes in this phase.

CMEs can be deflected in the corona, where the magnetic field dominates the dynamic process. It has been proven and widely studied that the asymmetry of magnetic field structure can make the CME deflect (e.g.,Gopalswamy et al. 2003a; Cremades et al. 2006; Gui et al. 2011; Shen et al. 2011a; Wang et al. 2011; Zhou and Feng 2013; Kilpua et al. 2009; Kay et al. 2015, 2016). Gopalswamy et al. (2009c) showed that the trajectory of CMEs was greatly affected when there are adjacent coronal holes. The coronal hole acts as a magnetic wall that constrains the CME propagation. Furthermore, Gopalswamy and Mäkelä (2014) indicated that coronal holes were the major source of deflection in the rise and declining phases of

solar cycles. In the maximum phase, deflection by large-scale streamers or pseudo streamers seems to be important. Another kind of possible deflection occurs in the interplanetary when the CME interacts with other structures. A typical example is the effect of other CMEs (Gopalswamy et al. 2001a; Lugaz et al. 2012b; Shen et al. 2012a). Moreover, a single CME in interplanetary space may also be deflected due to the influence of the background solar wind (e.g., Wang et al. 2004, 2014). And this kind of kinetic model for CME deflection in the interplanetary space (DIPS) was put forward by the study of Wang et al. (2004), which suggested that a fast CME would always be blocked by the background solar wind and deflected to the east, while a slow one would be pushed and deflected to the west when propagating in the interplanetary space freely. The background mass and magnetic field will accumulate at the leading flow, which makes the total pressure rise in the west front of CME and finally causes the deflection. Manchester et al. (2017) mentioned both the CME deflection in the corona and in the heliosphere, and attributed this to two primary causes: magnetic forces produced by the background corona and the background solar wind flow pattern.

4.1 CME deflection in the corona

In the corona, the deflection of CMEs are mainly controlled by the magnetic field structures. Therefore, the latitudinal deflection of the CME is very common and evident due to the effect of the background magnetic field of the Sun. Quantitative analysis suggest that CMEs always have higher deflection rates in the inner corona, generally below 4 R_s (Gui et al. 2011). The CME deflection is always equatorward near solar minimum, while deflections to higher latitudes are also frequent during solar maximum (Cremades et al. 2006). Besides, the longitudinal deflection also exist in the corona due to the effect of the neighbouring magnetic field structures.

Shen et al. (2011a) argued that CMEs tend to deflect toward the region of the lower magnetic energy density by the combined effect of the magnetic pressure and tension forces, as shown by Fig. 13. It is a sketch of the CME-perturbed background magnetic field. The associated restoring force acting on the upper part of the CME points downward and is roughly given by $f_U \approx \omega_U \Delta V_U / L_U$, where ω_U is the average energy density in the upper part, L_U is the characteristic length of the part. Similarly, there is a restoring force acting on the lower part, which points in the opposite direction. Comparing the two forces, we can estimate the direction toward which the CME will propagate. Based on this theoretical method, Gui et al. (2011) carried out a statistical analysis about the CME deflection in the corona, confirming that the deflections are consistent with the gradient of the magnetic energy density. Figure 14 is the analysis of the CME on November 16, 2007. They also noticed that the gradient of the magnetic energy density decreases rapidly with increasing height. Such a weak gradient is not enough to deflect a CME significantly as it travels through interplanetary space. This is consistent with Isavnin et al. (2014), which demonstrated that about 62% and 58% of the total latitude and longitude deflection happened in the corona.
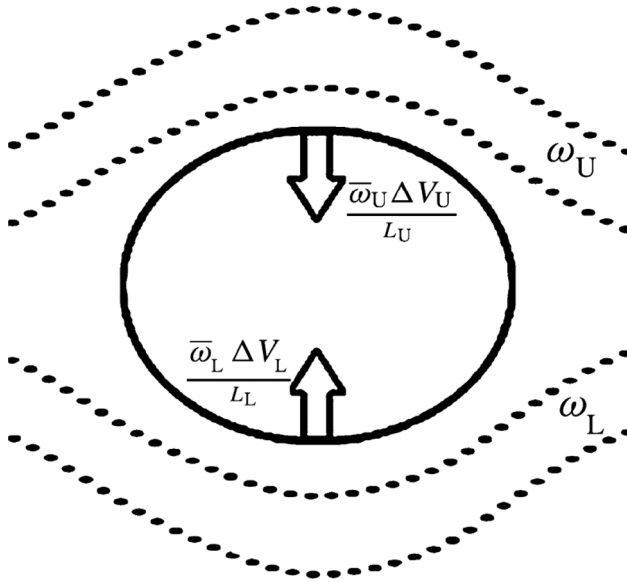
Fig. 13 Sketch of the CME-perturbed background magnetic field. The solid ellipse and dashed lines represent the CME and background magnetic field, respectively. The arrows mark the restoring forces acting on the upper and lower part of the CME. From Shen et al. (2011a)
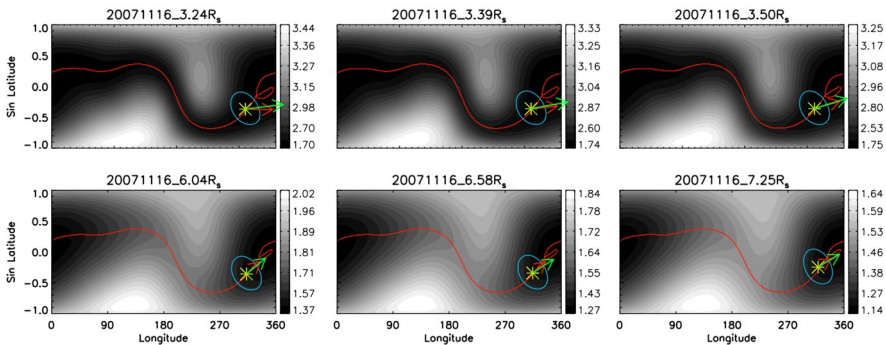

Fig. 14 The comparison between the gradient of the magnetic energy density and the deflection of the CME. The magnetic field energy density in gray scale in each panel is calculated based on the extrapolated coronal magnetic field at the corresponding altitude. The projected leading edge of the CME is indicated on the Carrington map by the yellow asterisk. The deflection and the gradient are represented by the green and red arrows, respectively. The lengths of the green and red arrows indicate the deflection rate and the relative strength of the gradient, respectively. The red curves indicate the heliospheric current sheet. From Gui et al. (2011)

Kay et al. (2013) developed a model, ForeCAT (Forecasting a CME's Altered Trajectory), of CME deflection due to magnetic forces. Figure 15 shows ForeCAT results for CMEs with various masses and final propagation velocities initiated at different locations. Kay et al. (2015) pointed out that the magnitude and direction of
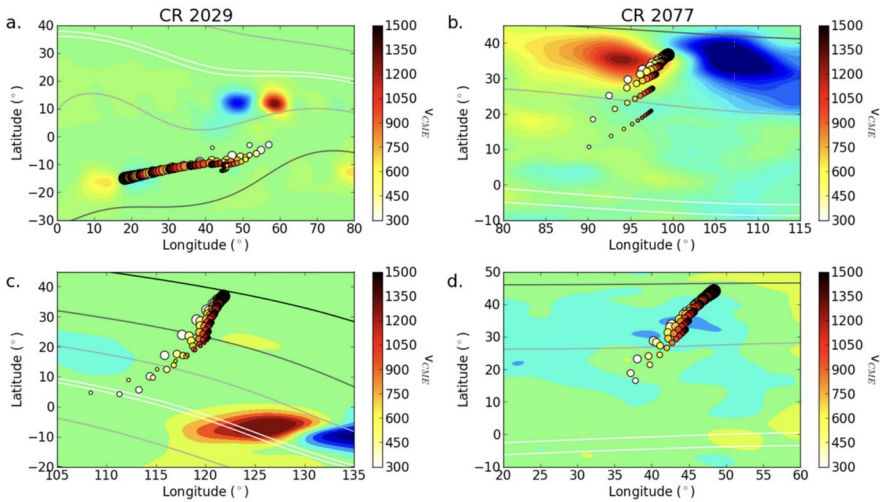
Fig. 15 Each panel shows the latitude and longitude at 10 R_s of 100 individual ForeCAT CMEs with varying masses and final propagation velocities. The circle size represents the CME mass (larger being more massive), and the color fill represents the CME velocity. The background color contours show the radial magnetic field at $1.05R_s$, showing the location of the ARs, and the line contours show the total magnetic field strength at the source surface height, 2.5 R_s, which indicates the location of the HCS. From Kay et al. (2015)

the deflection is determined, by CME parameters such as the mass and velocity, as well as the solar magnetic field and magnetic gradients. Both global gradients and local gradients, related to active regions or other small-scale structures, can contribute to the total deflection. Wide, slow, low-mass CMEs in backgrounds with large magnetic fields and magnetic gradients have the largest deflection.

Gopalswamy et al. (2014b) analyzed the non-radial motion of the CME on 2014 January 7. The CME had a poor latitudinal connectivity to Earth, but it caused a large solar energetic particle event. They showed that the non-radial motion of this CME seemed to be caused by a combination of a large coronal hole and the large arcade in the active region that did not participate in the eruption. This event has also been analyzed by Möstl et al. (2015). The observations demonstrated that this CME was strongly channelled into a non-radial direction by the effects of its locally surrounding magnetic field.

Heinemann et al. (2019) performed a comprehensive analysis for the CME-HSS event on 2011 June 22, by using multi-viewpoint data and combined modeling efforts (nonlinear force-free field modeling, GCS CME modeling, and the ForeCAT model). The results indicated that the major interaction between the CME and the HSS started at a height of 1.3 R_s up to 3 R_s. Over that distance range, the CME underwent a strong north-eastward deflection of at least 30° due to the open magnetic field configuration of the coronal hole. Cécere et al. (2020) analyzed the influence of the magnetic environment on the early development of a particular CME event on 2011 January 24 by using the GCS model. They found that the deflection amounts to 42° in latitude and 20° in longitude and that most of it occurs at altitudes

below $4R_s$. And the magnetic field environment suggested that field lines from the southern coronal hole acted as a magnetic wall that produced the large latitudinal deflection; while a nearby pseudostreamer and a northward extension of the southern coronal hole may be responsible for the eastward deflection of the CME. By using 2.5D version of VAC MHD model, Zuccarello et al. (2012) and Bemporad et al. (2012) numerically studied the importance of the coronal streamers in the deflection of CMEs. Their results showed that because of the imbalance in the magnetic pressure and tension forces, the CME deflected toward the current sheet of the larger northern helmet streamer and finally gets into the streamer. As pointed out by Zuccarello et al. (2012), during solar minima, sunspots (and hence active region of CMEs) originate at higher latitudes, and the polar coronal holes are extensive, indicative of strong polar field that deflects the CMEs. Therefore, even CMEs originating from high latitude could be easily deflected toward the HCS, eventually resulting in geoeffective events, and that this latitudinal migration depended on both the strength of the large-scale coronal magnetic field and the magnetic flux of the erupting filament.

4.2 CME deflection in the interplanetary space

Gosling et al. (1987) analyzed 19 fast CMEs, finding that 17 of them showed eastward deflections of the ejection plasma. They suggested that this is a consequence of solar rotation and the spiral geometry of the ambient solar wind. Wang et al. (2002) found that the longitude distribution of the Earth-encountered front side halo CMEs (EFHCMEs) has not only an east–west (E–W) asymmetry, but also depends on the EFHCMEs' transit speeds from the Sun to 1 AU. The faster the EFHCMEs are, the more westward does their distribution shift, and as a whole, the distribution shifts to the west. They believed that such E–W asymmetry appearing in the source longitude distribution is due to the deflection of CMEs' propagation in the
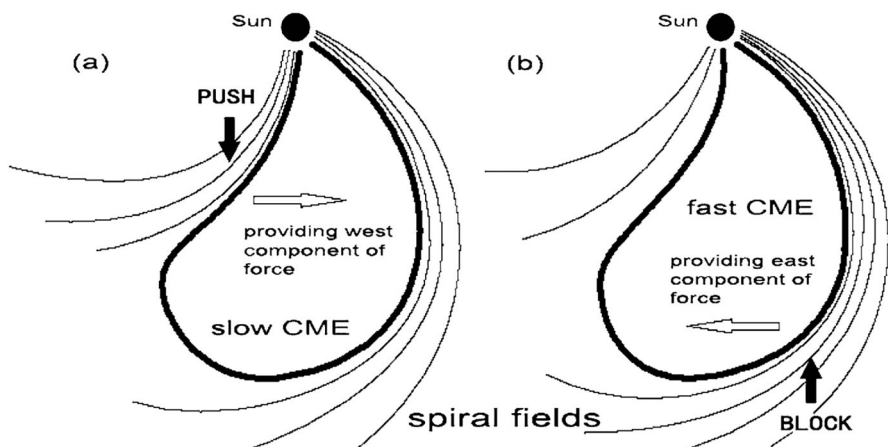

Fig. 16 A sketch map of the DIPS model. From Wang et al. (2004)

interplanetary medium. Based on the statistical result, Wang et al. (2004, 2014) put forward a deflection model (CME Deflection in the InterPlanetary Space, DIPS) to study the deflection propagation of CME in the ecliptic plane. Figure 16 is the schematic pictures of the DIPS model which shows that a fast CME will be blocked by the background solar wind ahead and deflected to the east, whereas a slow CME will be pushed by the following background solar wind and deflected to the west.

The DIPS model assumes that the background solar wind and interplanetary magnetic field (IMF) are dominant and the CME is a fluid parcel so that the CME in the ecliptic plane tends to move along IMF lines. The Parker spiral IMF is given by:

$$r_0 = v_{sw}t \tag{2}$$

$$\varphi_0 = \varphi_i - \Omega t \tag{3}$$

where v_{sw} is the solar wind speed, ω is the solar rotation, ϕ is the initial longitude, and t is the time since the plasma element left the Sun. Assuming that the CME is a plasma parcel with a radial speed of v_r, the magnetic field line drawn by the CME is given by:

$$r = v_r t \tag{4}$$

$$\varphi = \varphi_i - \Omega t + \Delta\phi(t) \tag{5}$$

since the CME is frozen-in in the interplanetary magnetic field, there are:

$$\frac{r_0}{\varphi_0 - \varphi_i} = \frac{r}{\varphi - \varphi_i}. \tag{6}$$

Here $\Delta\phi$ is the time-dependent or distance-dependent deflection angle of the CME. Then, it is easy to derive that:

$$\Delta\phi(t) = \frac{v_{sw} - v_r}{v_{sw}}\Omega t. \tag{7}$$

When v_r equals v_{sw}, $\Delta\phi$ will be zero, indicating a radial propagation of the CME. While if v_r is larger (smaller) than v_{sw}, $\Delta\phi$ will be smaller (larger) than zero, resulting in the eastward (westward) deflection of the CME.

To study the CME deflection more effectively and gain more useful information, MHD modeling can be used as a feasible and efficient method. By using the 3D SIP-CESE MHD model, Zhou and Feng (2017) simulated the propagation characteristics of CMEs launched at different positions in a realistic structured ambient solar wind and indicated the CME deflection caused by the influence of heliospheric current sheet (HCS). The initial CMEs were initiated at different solar latitudes with respect to the HCS and the Earth in the same ambient solar wind. Figure 17 (top and middle row) shows the 3-D evolutionary structures of CMEs for the four cases with different launch positions at 30 h after their launches; Fig. 17 (bottom row) shows the corresponding Sun–Earth meridional slice for the four cases. Their research suggests that CMEs tend to deflect to the
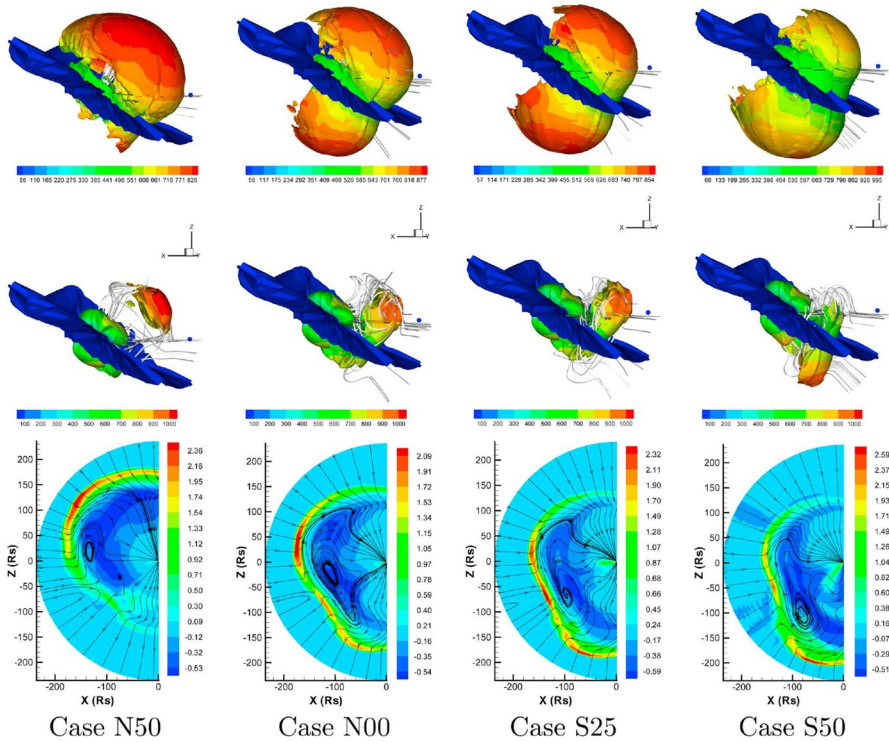
Fig. 17 Three-dimensional representations of the CMEs 30 h after the initiation of the four cases. Three-dimensional isosurfaces of (top row) $\rho = 1.5\rho_{wind}$ and (middle row) magnetic field strength $|B| = 15$ nT are drawn. The position of the Earth is marked by the blue sphere. (bottom row) The contour plots of the relative density distribution on the solar-terrestrial meridian plane after 30 h for the four cases. From Zhou and Feng (2017)

HCS in the latitudinal direction near the Sun and then propagate almost parallel to the HCS in the interplanetary space. One of the earliest reports on CME deflection towards the HCS can be found in Gopalswamy and Thompson (2000). Besides, the statistical results by Zhao et al. (2007) also indicated that the shocks associated flares are located on the same side of the HCS as the Earth have a greater chance of reaching the Earth than those shocks on the opposite side.

By using a 2.5D MHD model, Zhuang et al. (2019) simulated the deflection of CMEs with different speeds in the interplanetary space. Their simulation confirmed the existence of the CME deflection in the interplanetary space, which was related to the difference between the CME speed and the solar wind speed. Figure 18 shows the deflection of CMEs with different initial velocity V_{m0} in the interplanetary solar wind medium. They revealed that the CME with smaller or larger speed than the ambient solar wind, would be deflected to the west or east, and the deflection angle is directly proportional to the speed difference between the CME and the ambient solar wind.
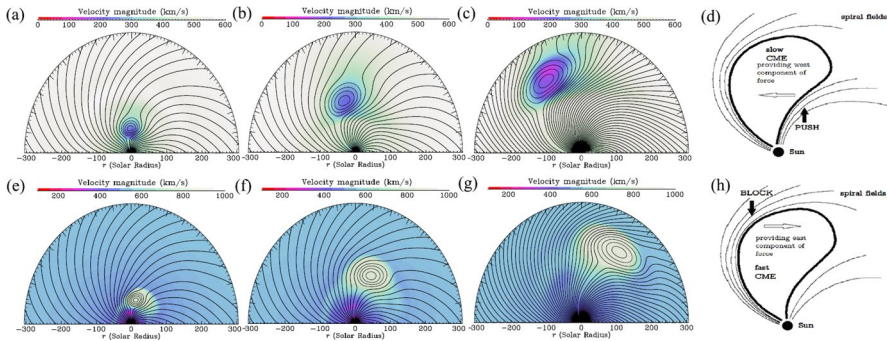
Fig. 18 Westward and eastward deflection of the flux rope in the laboratory frame with $V_{m0} = 300$ and $V_{m0} = 1500$ km s^{-1} in panels **a–c** and **e–g**, respectively. The closed lines plot the flux rope structure, and the open lines show the background magnetic field. The false color shows the flow velocity magnitude. Panels **d** and **h** give the same schematic pictures of slow and fast CME propagation in the interplanetary medium in Wang et al. (2004). From Zhuang et al. (2019)

By using the 3D IN-TVD-MHD model and the GCS-based flux rope CME initialization model, Liu et al. (2019) simulated the propagation and deflection of the fast CMEs in the interplanetary space, and analysed the influence of the CIR structure on the deflection. Figure 19a, c show the deflection angles and trajectories of the CME when interacting with the CIR; (b) and (d) show the situation without interaction. Their simulation results demonstrated that when the fast CME hit the CIR on its west side, it would deflect eastward, and the deflection angle would increase compared with the situation without CIR.

5 The rotation, expansion, deformation and erosion of CMEs

It was found that many CMEs rotate significantly around the direction of propagation, changing the axial orientation of the magnetic flux rope in the ICME, thus altering the strength and duration of the southward magnetic field, and ultimately affecting the geoeffectiveness of the ICME. There is substantial observational evidence for the CME rotation (Yurchyshyn et al. 2007; Vourlidas et al. 2011; Thompson et al. 2012; Liu et al. 2018). Vourlidas et al. (2011) presented the direct detection of a rotating CME in the middle corona. The rotation rate of the CME is as high as 60° per day. Thompson et al. (2012) found that the CME happened on April 9, 2008 had rotated 115° at the height of 2.5 R_s

Green et al. (2007) found that the direction of the CME rotation is determined by the sign of helicity of the source region. For positive (negative) helicity, the magnetic flux rope of the CME rotates clockwise (counterclockwise). This implies that the conversion of twist into writhe in a kink-unstable magnetic flux rope is a possible mechanism for the rotation. Many numerical simulations have been done to analyze the mechanism of the CME rotation (Török and Kliem 2003; Fan and Gibson 2004; Lynch et al. 2009; Kliem et al. 2012). Lynch et al. (2009) showed that, in sheared arcade magnetic breakout eruptions, the resulting flux ropes created by
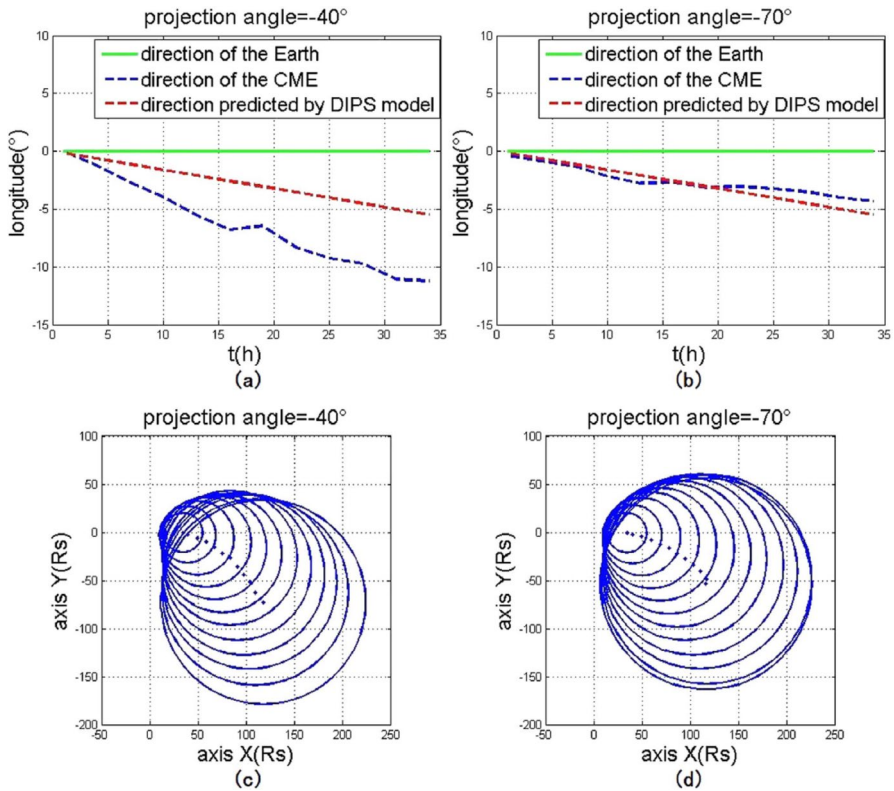
Fig. 19 **a**, **c** Temporal images of the CME's deflection angles and the trajectories of the CME, respectively, for the case when the CME interacts with the CIR. **b**, **d** Images for the case when the CME does not interact with the CIR. **a** and **b** are shown in the heliocentric Earth ecliptic coordinate system, while **c** and **d** are in rotating coordinates. The green line is the longitude of the Earth; the blue dashed line is the CME direction of our simulation; the red dashed line is the CME direction predicted by DIPS model (Wang et al. 2004). The time interval for each CME circle in **c** and **d** is 3 h. From Liu et al. (2019)

the flare reconnection undergo significant rotation during their propagation through approximately 2 R_s of the closed field corona. Kliem et al. (2012) pointed out that the Lorentz force due to the external shear field component and the relaxation of tension in the twisted field are the major contributors to the CME rotation.

During propagation, CMEs expand due to the imbalance between internal and external pressures. In the early days, researchers believed that CMEs expand self-similarly (Chen et al. 2000, 2009). In addition, using multi-perspective observations, many researchers have also found that CMEs exhibit self-similar expansion (Poomvises et al. 2010). However, there are also some studies showing that CME expansion is not always self-similar. The expansion in the radial direction weakens with heliocentric distance, and CMEs undergo a phase of lateral overexpansion in the corona (Patsourakos et al. 2010a, b). Thus, as the CME moves into interplanetary space, its cross section flattens in the direction of propagation (see
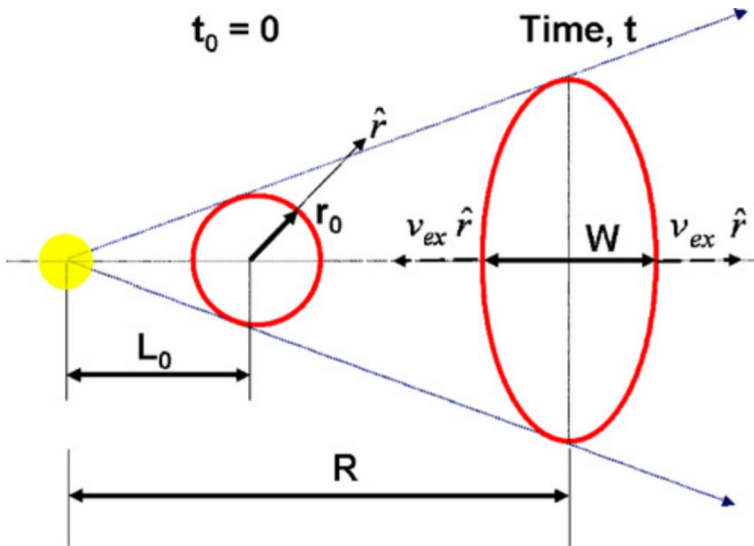
Fig. 20 Schematic to display the geometry of a CME propagating into the heliosphere. The aspect ratio of a CME is shown to be affected by CME expansion. From Savani et al. (2011)

Fig. 20). Riley and Crooker (2004) presented a kinematic study of the evolution of CMEs in the solar wind, showing that the cross section of the CME would evolve into a convex-outward pancake shape. This phenomenon is known as the "pancaking effect" (Vršnak et al. 2019; Liu et al. 2006; Owens et al. 2006).

Gopalswamy et al. (2014a) indicated that CMEs in solar cycle 24 showed excess expansion than those in solar cycle 23. Such anomalous expansion is caused by the reduced total pressure in the heliosphere. The anomalous expansion of CMEs seems to be responsible for the mild space weather during solar cycle 24 (Gopalswamy et al. 2015a). The anomalous expansion results in the dilution of the magnetic contents of CMEs, so the geomagnetic storms are generally weak. CME-driven shocks propagating through the weak heliospheric field are less efficient in accelerating energetic particles, so the particles do not attain high energies. Given the prediction of weak solar cycle 25, CME expansion is an important topic in CME studies.

As CMEs propagate away from the Sun, they may undergo magnetic reconnection with the ambient interplanetary magnetic field. It was found that the magnetic reconnection would peel off substantial amounts of magnetic flux from the CME (Dasso et al. 2006, 2007; Ruffenach et al. 2012). This process is called the CME erosion. Locally, this process is observed as a region bounded by two current sheets, and so that the changes of B and V are correlated at one boundary but anticorrelated at the other. Through a statistical study, Ruffenach et al. (2015) pointed out that CMEs may be eroded at the front or at rear and in similar proportions, with a significant average erosion of about 40% of the total azimuthal magnetic flux. Some previous works also indicated that CME erosion may give birth to some small-scale flux ropes (Feng and Wu 2009; Tian et al. 2010; Xu et al. 2020)

6 The interaction of CMEs

If a slow CME and a fast CME erupt continuously from the adjacent positions, then the fast CME will approach and interact with the slow CME during propagation. CMEs' interaction was first reported by Gopalswamy et al. (2001b) based on the SOHO/LASCO observations (Fig. 21). In recent years, using the large field of view observations from STEREO/SECCHI, theoretical analysis and numerical simulation, extensive efforts further confirm the result that interaction may change the kinematic parameters of CMEs greatly, and also have influence on CME magnetic field and on particle acceleration (Lugaz et al. 2009, 2012a; Temmer et al. 2012, 2014; Mishra et al. 2014, 2015a).

Near the Earth, complex structures caused by multiple CME interactions are frequently observed in a variety of forms, including complex ejecta(Burlaga et al. 2002), multi-magnetic clouds (multi-MC) (Wang et al. 2003a), and shock-interplanetary coronal mass ejections (S-ICMEs) (Wang et al. 2003b; Lugaz et al. 2015a). The observational signatures of multi-magnetic clouds include: (1) the presence of several magnetic clouds and interacting regions between them; (2) each subcloud in multi-MC primarily meets the criteria of isolated magnetic cloud, except that the proton temperature is not as low as that in typical magnetic cloud due to the compression between the subclouds; and (3) the speed of solar wind at the rear part of the front subcloud does not continuously decrease,(4) in the interaction region between the subclouds, the magnetic field becomes less regular and weaker, and the temperature and plasma-beta increase. Figure 22 gives an example of a multi-MC. Multi-magnetic clouds are caused by the magnetic reconnection between CMEs. Through magnetic reconnection, magnetic energy is converted into particle energy and the magnetic field topology is changed. Many observations of reconnection exhaust in CME interaction regions are reported, which are characterized by the accelerated ion flow within magnetic field reversal regions (Gosling et al. 2005; Xu et al. 2011; Raghav and
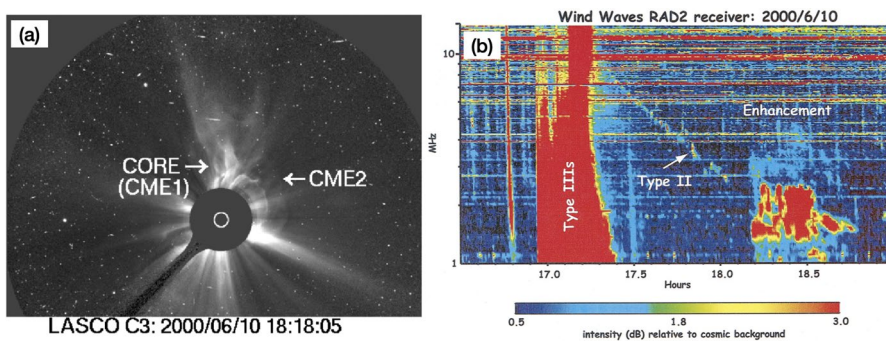

Fig. 21 Observations of CME–CME interaction. **a** LASCO/C3 image at 18:18 UT obtained at the time of the radio enhancement. **b** Radio enhancement due to the interaction between CMEs. Adapted from Gopalswamy et al. (2001b)
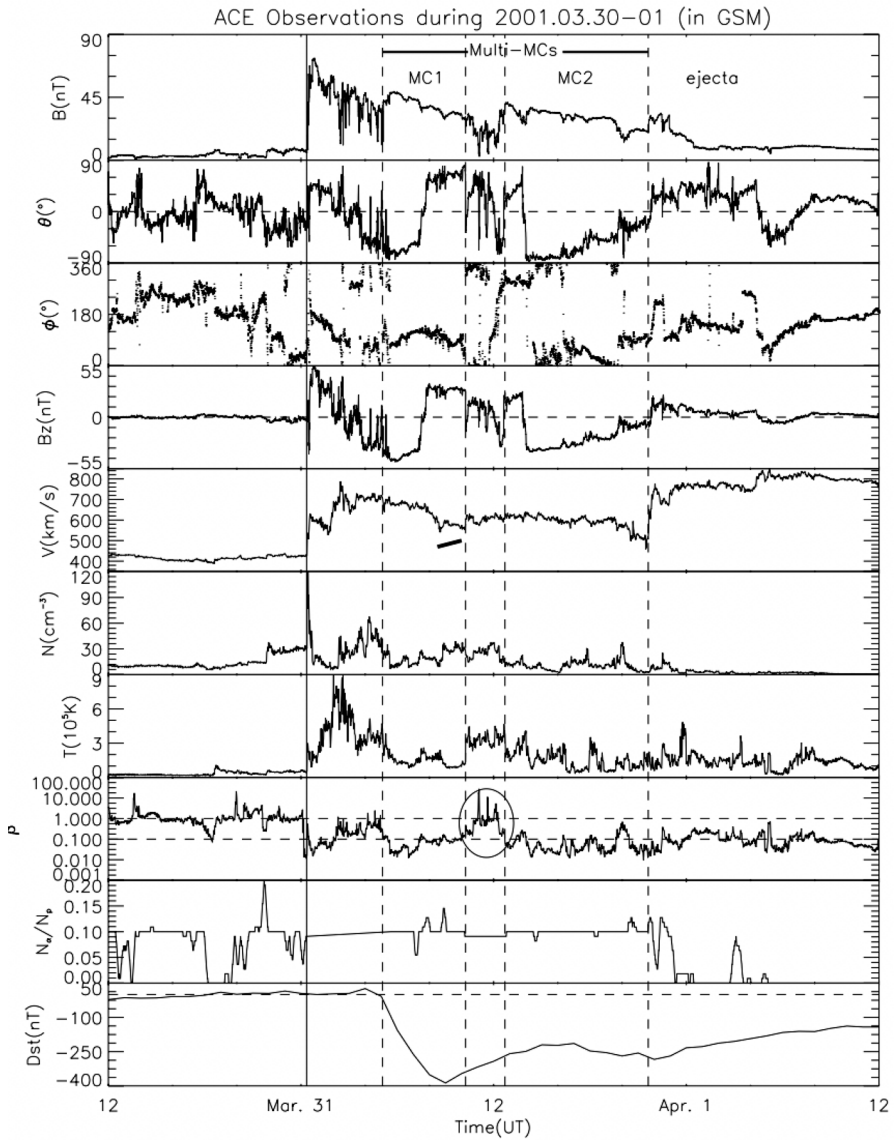
Fig. 22 An example of multi-magnetic cloud. From Wang et al. (2003a)
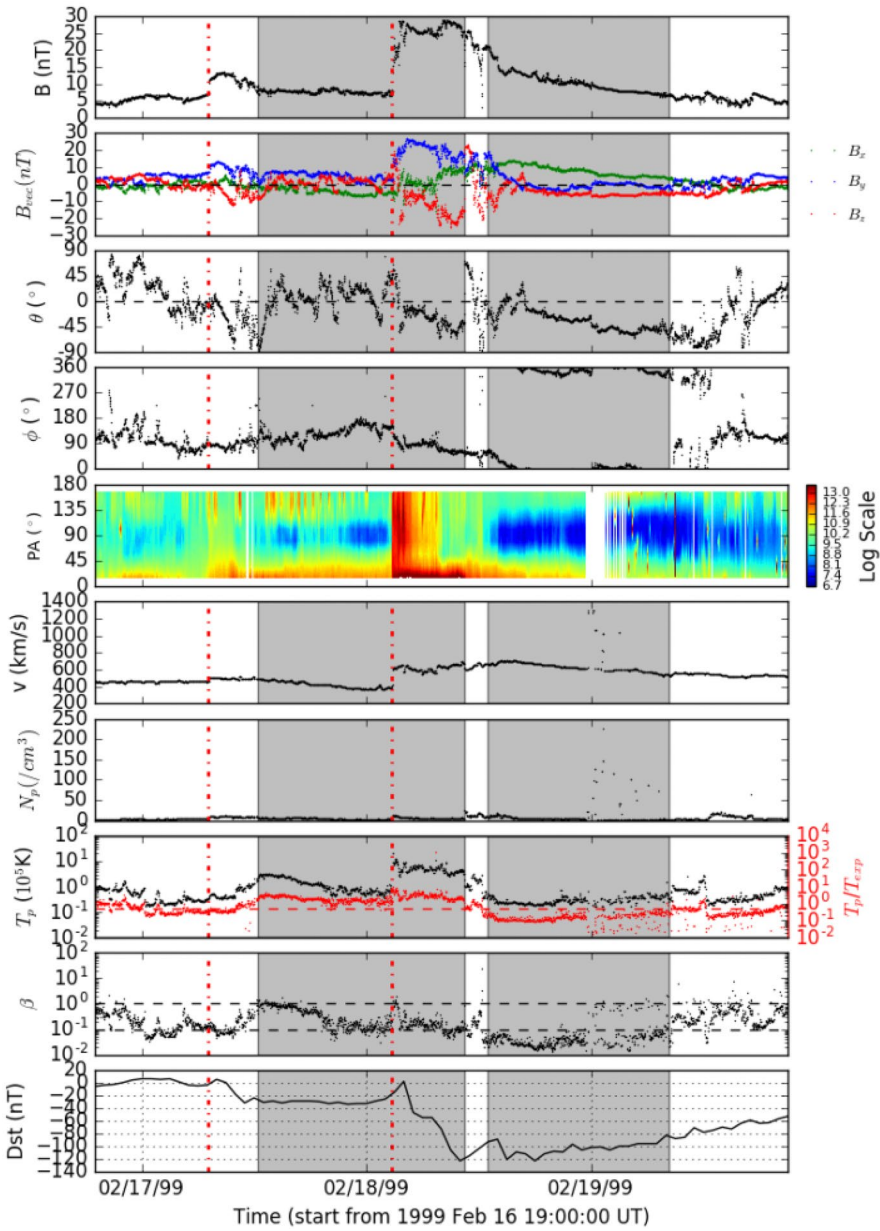
Fig. 23 An example of S-ICME

Kule 2018).In S-ICME, a shock driven by a following fast CME catches up and then propagates into the previous slow CME, as shown in Fig. 23.

6.1 Effects of CME–CME interaction on CME propagation

Many numerical simulations have investigated the formation and propagation of the interactional CMEs (Lugaz et al. 2005; Xiong et al. 2006, 2007; Shen et al. 2012b, 2013b, 2016). The CME interaction leads to a speed balance between the interacting CMEs. Wang et al. (2005b) analyzed the interaction of two successive CMEs using a 2.5-D MHD simulation. This simulation illustrates the process of the formation and propagation of two identical CMEs, which are ejected with speeds of 400 km s^{-1} and 600 km s^{-1} respectively and initially separated by 12 h. In this case, neither CME drove a shock. The simulation result showed that the fast cloud is slowed down significantly because of the blocking by the preceding slow one, implying that the final speed of the Multi-CME structure is dominated by the preceding slow one.
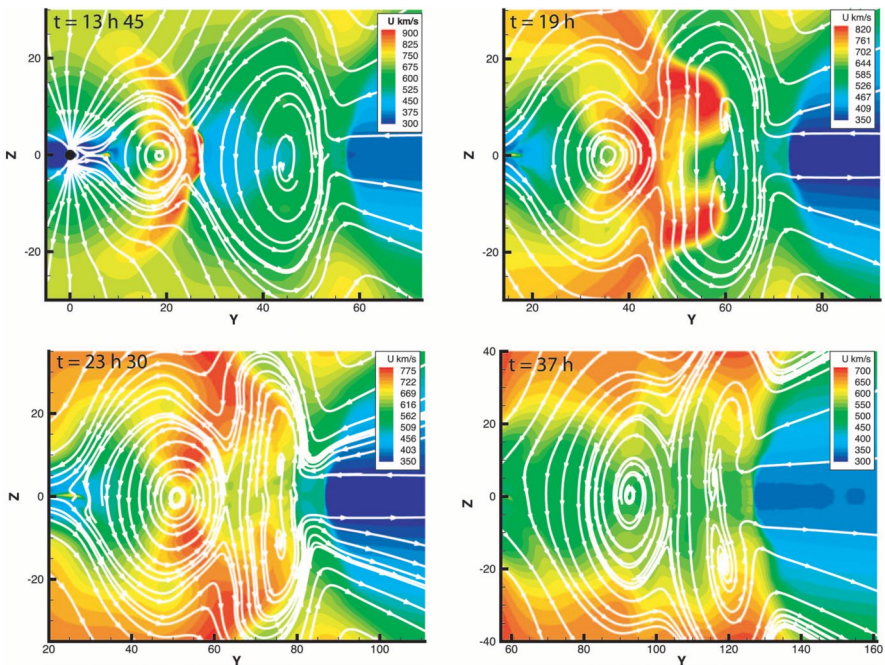

Fig. 24 Plasma speed in the *y–z* plane at four different times during the interaction of the two CMEs. "Streamlines" drawn in white illustrate the direction of the magnetic field in the plane. Top left: $t = 13.75$ h, as the trailing shock enters the first cloud. Top right: $t = 19$ h, as the trailing shock has just passed the center of the first cloud. Bottom left: $t = 23.5$ h, as the trailing shock enters the dense sheath of plasma associated with the leading shock. Bottom right: $t = 37$ h; note the uniformization of the speed in the two clouds at this time. Also note the change in scales between the different panels. From Lugaz et al. (2005)
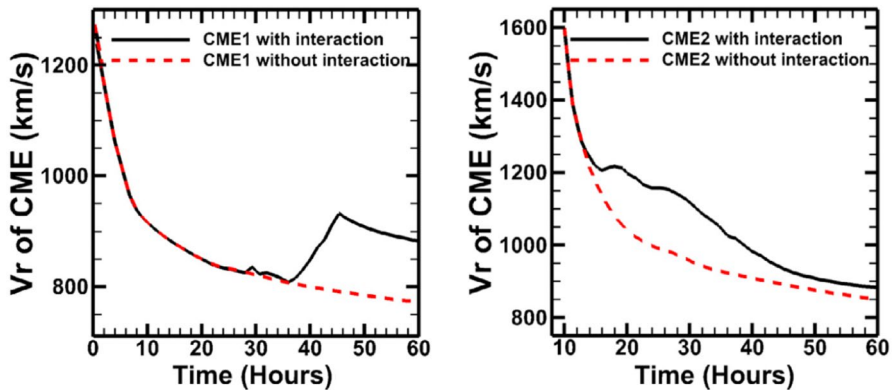
Fig. 25 The speed-time profile of the two CMEs with and without interaction. Adapted from Shen et al. (2012b)

Meanwhile, Lugaz et al. (2005) presented a 3-D compressible MHD model of the interaction of two CMEs with shocks. Seen from Fig. 24, the tailing shock gradually catches up the first CME, then propagates in it, and finally it merges with the leading shock. They showed that the propagation of the tailing shock in the first CME was crucial to homogenize the velocity. Similar results have been achieved by Shen et al. (2012b), which employed a 3-D MHD simulation for the evolution of two interacting CMEs in a realistic ambient solar wind during the period 28–31 March 2001 event. Figure 25 shows the simulation result of the velocity and acceleration evolution. There is a significant momentum exchange between the two interacting CMEs, which leads to the acceleration and deceleration of the CME. By the way, in addition to changes in velocity, CME–CME interaction may result in the deflection of one CME by another (Xiong et al. 2009; Shen et al. 2012a).

Shen et al. (2011b, 2012b) also simulated the interaction of two CMEs using the COIN-TVD MHD model, analyzed variations of different forces acting on the CMEs during interaction, and revealed that the momentum exchange during the interaction of two CMEs was very important for the deceleration and acceleration of the CMEs.

Scolini et al. (2019) studied two Earth-directed CME–CME interaction events occurring on 14 July 2012 and 13–14 June 2012 using the EUHFORIA model. For each event, they simulated the CMEs using both the cone model and the spheromak model. Their analysis indicated that the use of a spheromak model constrained with observations-based CME input parameters significantly improved the prediction of the ICME internal magnetic field intensity and orientation at the Earth. The prediction of the CME arrival time at the Earth was found to be highly dependent on the CME model and CME input parameters used.

Shen et al. (2012a) present a comprehensive picture of a unique collision between two CMEs which occurred on November 2, 2008 and November 3, 2008. Their analysis showed that the two magnetized plasmas collided as if they were solid. The total kinetic energy of the plasmoid system increased by 6.6%, which has a significant effect on its dynamics. Figure 26 shows the STEREO/SECCHI images of
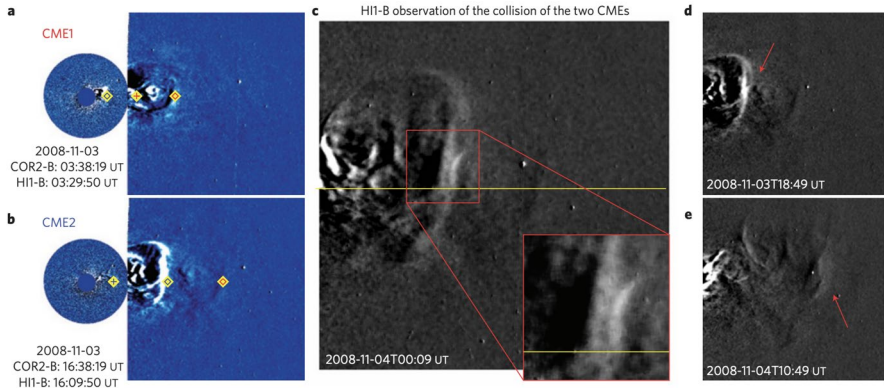
Fig. 26 The STEREO/SECCHI images of the two CMEs and their collision in the heliosphere. **a, b** Running-difference images showing CME1 and CME2. The red diamond and plus symbols mark the front and rear edges of CME1, respectively, and the blue symbols are for CME2. **c** The running-difference image of HI1-B showing the collision of the two CMEs. **d, e** The beginning and end of the collision; the red arrows indicate the collision region. From Shen et al. (2012a)
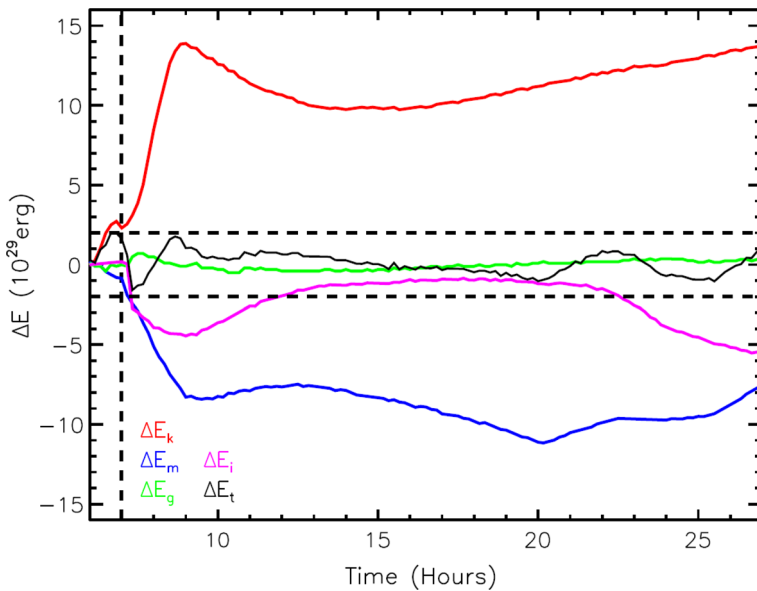
Fig. 27 Energy difference between the case of collision (case 1) and the case of non-collision (case 2). A positive value means that the energy in case 1 is larger than that in case 2. The vertical dashed line marks the beginning of the collision, and the horizontal dashed lines indicate the level of numerical error. From Shen et al. (2013b)

the two CMEs and their collision in the heliosphere. This finding suggests that the CMEs' magnetic energy and thermal energy could be converted into kinetic energy through a more efficient way. The 3D COIN-TVD model was also used to study the

super-elastic collisions of CMEs (Shen et al. 2013b). Figure 27 shows the energy variations for the case of collision (case 1) and the case of non-collision (case 2). Their simulation results showed that the collision led to extra kinetic energy gain by 3−4% of the initial kinetic energy of the two CMEs, which suggested that the collision of CMEs could be superelastic. Besides these studies, a series relevant researches have been performed (Lugaz et al. 2012b; Temmer et al. 2012; Liu et al. 2014; Mishra et al. 2015a, b; Shen et al. 2017b). Their results showed that CME collisions were not always super-elastic, it might also be inelastic or elastic. Shen et al. (2016) further confirmed the dependence of CMEs' collision type on the ratio of the CME's kinetic energy to the CME's total energy using MHD simulation.

MHD simulation was also used to model multiple CMEs (more than two CMEs) interaction. By employing the 3D MHD simulation, Shiota and Kataoka (2016) studied the propagation and interaction process of multiple CMEs associated with the complex active region NOAA 10486 from 30 R_s to 430 R_s in October to November 2003. In their CME model, a spheromak-type magnetic field configuration was used to form an internal magnetic flux rope. This CME model passed through the inner boundary and finally detached from the inner boundary after its passage. Their simulated results could provide reasonably good results for velocity and the profile of southward magnetic field component of the Halloween Event on 29 October 2003. The simulation also indicated that the propagation of the following CME could be significantly affected by the trails of the preceding CMEs.

Webb et al. (2013) tracked the propagation of multiple CMEs of late July to early August 2010 in the inner heliosphere by comparing the results from the ENLIL model, 3D reconstruction techniques based on a kinematic solar wind model, and in situ results from multiple spacecraft, and their simulation results could reproduce the 3D reconstructed densities of in situ density structures at five spacecraft spread over 150° in ecliptic longitude and from 0.4 to 1 AU in radial distance.

The September 2017 series of CME–CME interaction events have been studied using in-situ observations (Shen et al. 2018a) and by means of numerical simulations (Werner et al. 2019; Scolini et al. 2020). Werner et al. (2019) numerically modeled the multiple CMEs based on coronagraph image observations. Figure 28 shows the radial solar wind velocity on the ecliptic plane at 7 September 18:00 UTC, which contains all three CMEs.Their result suggested the preconditioning of the interplanetary medium should be taken into account when making forecasts of CMEs erupting in quick succession. That was because the predicted arrival time of the first interplanetary shock was drastically improved, while the background solar wind preconditioned by the passage of the first interplanetary shock likely caused the last CME to experience insignificant deceleration and led to the early arrival of the second interplanetary shock, and the similar conclusion was also made by Liu et al. (2014). Moreover, the opposite happens when the preceding CMEs are slow, and they increase the effective drag to a later fast CME (Gopalswamy et al. 2013).

Palmerio et al. (2019) analyzed the propagation and geoeffectiveness of four CMEs that erupted from the Sun during May 21–23, 2013, using multiwavelength and multipoint remote-sensing observations, also aided by 3D EUHFORIA model. All of the four CMEs could be considered to be "problematic"; however, all the CMEs that arrived at Earth caused a moderate geomagnetic disturbance. Their
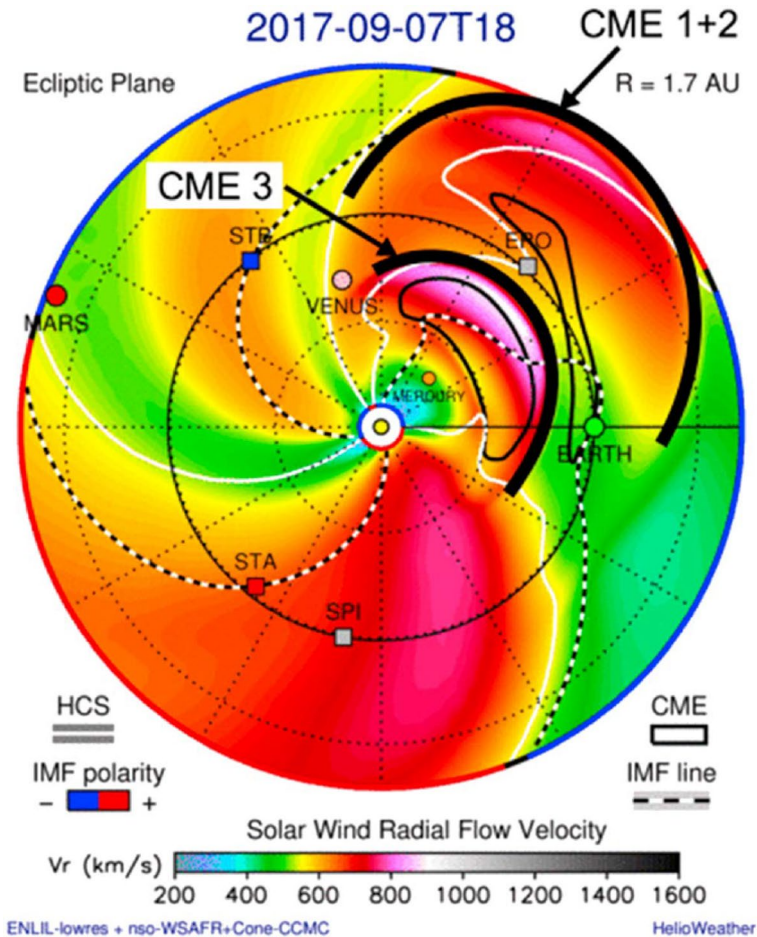
Fig. 28 The radial solar wind velocity output from the baseline run as shown on the ecliptic plane at 7 September 18:00 UTC. From Werner et al. (2019)

studies also demonstrated the benefits of combining a detailed EUV, white-light, and radio analysis as well as 3D heliospheric modeling.

6.2 Effects of CME–CME interaction on CME magnetic field

It is well-known that ICMEs and their complex structures are the major sources of geomagnetic storms (Gonzalez et al. 1994, 1999, 2007; Echer et al. 2008; Shen et al. 2017a). This is mainly because they often contain a long-lasting intense southward magnetic field component. By analyzing 88 strong geomagnetic storms from 1996 to 2005, Zhang et al. (2007b) found that 87% of strong geomagnetic storms were caused by ICMEs and their complex structures. This result was then confirmed by Shen et al. (2017a). In addition, the interplanetary causes of super-intense

geomagnetic storms ($Dst_{min} \leq -250$ nT) that occurred during solar cycle 23 studied in Echer et al. (2008) indicated that only magnetic clouds (including both sheath regions and body parts) had fields intense enough and with long enough duration to cause superstorms.

As the compression between multiple ICMEs or the shock and ICME would enhance the magnetic field intensity in the interaction structures, such events are thought to be more geoeffective than individual ICMEs (Wang et al. 2003b, 2005a; Xue et al. 2005b; Zhang et al. 2007a; Lugaz et al. 2015a, b; Shen et al. 2017a). By analyzing the complex structure of the shock-magnetic cloud in October 2000 and November 2001, Wang et al. (2003b) reported for the first time that the intense geomagnetic storms could be caused by shock compression of the preceding ICMEs. Xue et al. (2005b) analyzed eight great geomagnetic storms with $Dst_{min} \leq -200$ nT from 2000 to 2001 and found that four of them were caused by the compression between multiple CMEs. Farrugia et al. (2006) indicated that interacting CMEs are important interplanetary sources of large double-dip geomagnetic storms. Lugaz et al. (2015b) statistically studied the S-ICMEs and found that 19 out of 49 S-ICMEs in their study were associated with intense geomagnetic storms ($Dst_{min} \leq -100$ nT) within 12 h of the shock arrival at the Earth. Shen et al. (2017a) showed that about 60% S-ICMEs were accompanied with intense geomagnetic storms, which demonstrated that S-ICMEs have a higher probability in causing geomagnetic storms, especially intense geomagnetic storms, than individual ICMEs or other types of ICME complex structure.

All these results indicate that the multiple ICMEs especially the shock-ICMEs events are important in causing geomagnetic storms. Compression of the magnetic field enhances the southward component, and also enhances the geoeffectiveness of S-ICMEs structures. In addition, S-ICMEs can lead to a new type of double-dip storm unlike the classical double-dip storm caused by different Bz structures in shock sheath and ICME. In such storms, both dips are due to the Bz structure in ICMEs, as indicated by Gopalswamy et al. (2015b). To quantitatively study the enhancement of the geomagnetic storm caused by shock-ICME interaction, Shen et al. (2018a) analyzed an intense geomagnetic storm triggered by an S-ICME in 2017 September (see Fig. 29). Through recovering the shocked part of the ICME back to the uncompressed states using the method put forward by Wang et al. (2018) and then substituting them into Dst prediction models, they quantitatively found that shock compression roughly doubled the intensity of the geomagnetic storm.

Using the same method, Xu et al. (2019b) further studied 18 moderate to intense geomagnetic storms caused by S-ICMEs. It was found that due to shock compression, the maximum southward magnetic field of the ICME doubles and the dawn-dusk electric field increases 2.2 times. On average, shock compression can increase the intensity of geomagnetic storms by 1.4 times. Furthermore, they showed that there is a significant correlation between the shock density compression ratio and the ability of shock to enhance geomagnetic storms. The larger the impact density compression ratio is, the more obvious the Dst index decreases.

Very few studies could quantify the geo-effectiveness amplification (e.g., B_z or other geomagnetic activity indices) by performing global Sun-to-Earth simulations of real multiple CMEs events. Scolini et al. (2020) used EUHFORIA
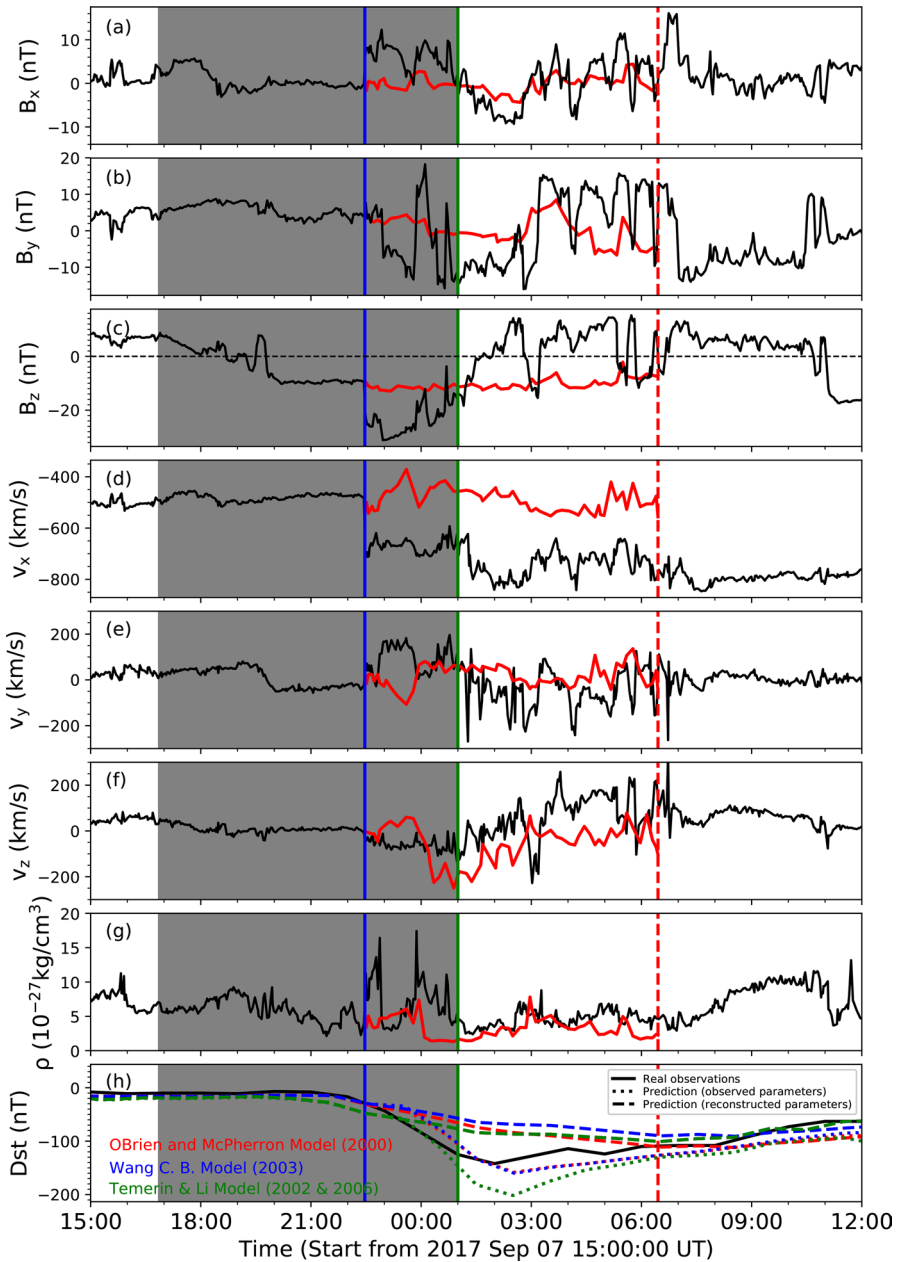
Fig. 29 The observational data and recovered uncompressed state of magnetic field, solar wind speed, total plasma density and Dst index from September 6, 2017 to September 8, 2017. The shade region shows the period of the ICME and the blue line shows the time of the shock arrival. The black lines in panel **a**–**h** between the first two vertical lines (blue and green vertical lines) show the original observations, and the red lines between the first and third vertical lines (blue and red vertical lines) represent the recovered parameters. Panel **h** shows the real data (black line) and the prediction results based on the observed (dashed lines) and recovered (dashed-dotted lines) parameters of Dst index. Different colors represent different prediction methods. From Shen et al. (2018a)
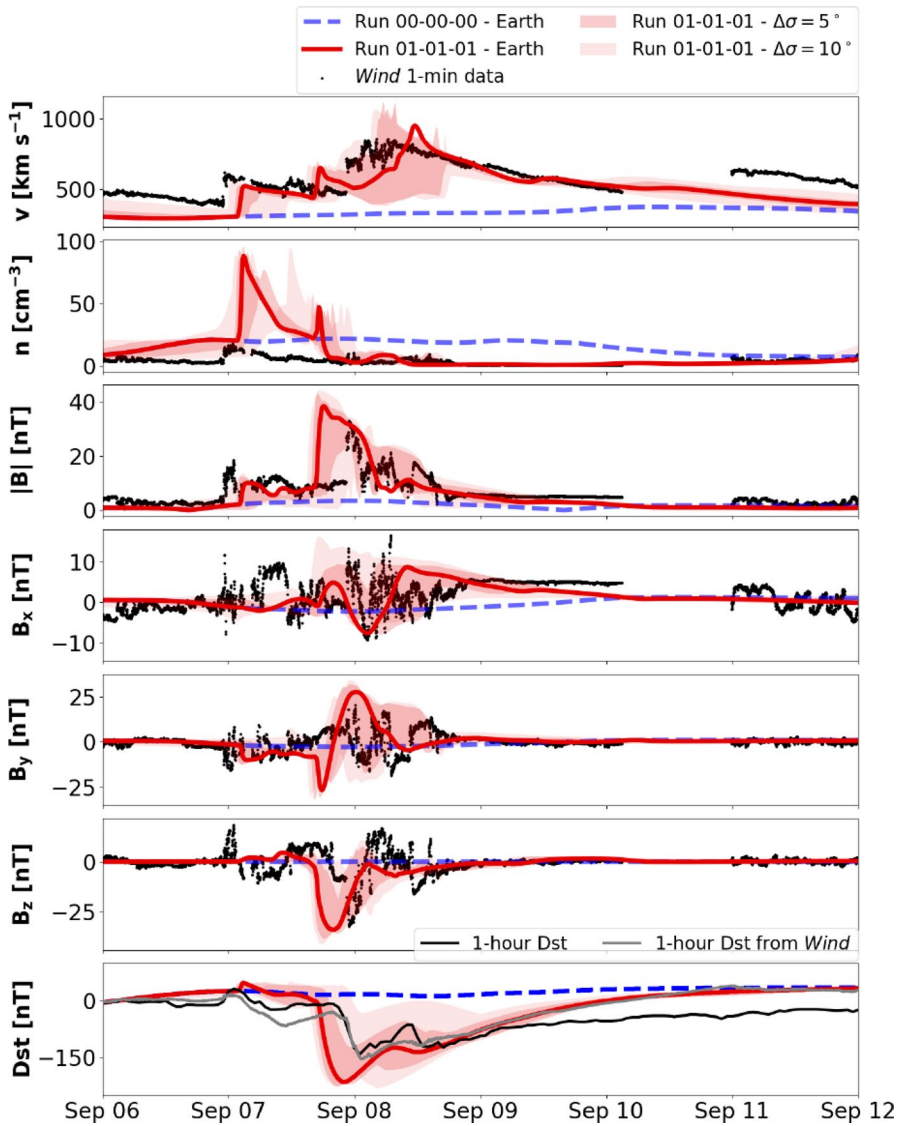
Fig. 30 Comparison of EUHFORIA time series (red and blue) with in-situ measurements from Wind (black) for the whole temporal computational domain (both in GSE coordinates). From Scolini et al. (2020)

model to study how complex interactions between multiple interacting CMEs on their way to the Earth may result in the geo-effectiveness of the September 2017 series of events. Figure 30 showed the comparison between the time series modeled from EUHFORIA at Earth and in-situ measurements from Wind. Their results showed that a key factor at the origin of the intense storm triggered by these September 2017 CMEs was their arrival at the Earth during the phase of

maximum B_z amplification, and the time interval between the interacting CME eruptions and their relative speeds may important to determine the resultant impact of complex CMEs at different heliocentric distances.

The CME–CME interaction event observed on 13–14 June 2012 has also been studied by both in-situ measurements (Srivastava et al. 2018; Kilpua et al. 2019) and numerical simulation (Scolini et al. 2019). As discussed by Srivastava et al. (2018), this event was composed of a sequence of two CMEs that were launched from NOAA AR 11504. The first CME erupted on 13 June 2012 and it was observed by LASCO/C2 at 13:25 UT to propagate with an average projected speed of 632 km s^{-1}. On the following day, a second CME, entered the C2 coronagraph at 14:12 UT, and propagated towards the Earth with an average projected speed of 987 km s^{-1}. The kinematics of these two interacting CMEs were estimated using the data from the Sun Earth Connection Coronal and Heliospheric Investigation (SECCHI) instrument onboard the Solar Terrestrial Relations Observatory (STEREO), and the results showed that the collision was inelastic in nature (Srivastava et al. 2018). Their study also found that this interaction event led to the strongest sudden storm commencement (SSC) (~ 150 nT) of solar cycle 24.

Kilpua et al. (2019) also examined the CME–CME interaction event on 13–14 June 2012 using in-situ observations from the almost radially aligned spacecraft at Venus and Earth, as well as using heliospheric modeling and observation. Their results showed that the June 14 CME reached the June 13 CME near the orbit of Venus and significant interaction occurred before they both reached the Earth. The shock driven by the June 14 CME propagated through the June 13 CME and then the two CMEs coalesced, forming the signatures of one large, coherent flux rope at L1. They also discussed the origin of the strong interplanetary magnetic fields related to this sequence of events, the complexity of interpreting solar wind observations in the case of multiple interacting CMEs, and the coherence of the flux ropes at different observation points.

Lugaz et al. (2013) simulated the influence of the relative orientation of the two interacting CMEs on their interaction and the resulting structure using the SWMF MHD model. Their simulations indicated that as a CME with a high inclination overtook one with a low inclination, the second CME only appeared as an extended "tail," and the usual multiple-magnetic-cloud event was found to be always associated with the interaction of two CMEs with the same orientation.

The Alfvén waves are speculated to be one of the major possible energy exchange/dissipation mechanism during the CME–CME interaction process, and the magnetic reconnection process is justified to be responsible for multiple CMEs merging. Based on in-situ observation, Raghav and Kule (2018) presented an unambiguous evidence of sunward torsional Alfvén waves in the interacting region after the collision of multiple CMEs. They revealed that Alfvén waves and magnetic reconnection were the possible energy exchange/dissipation mechanisms during large-scale CMEs interaction.

6.3 Effects of CME–CME interaction on particle acceleration

It is generally accepted that the large gradual SEP events are accelerated by CME-driven shocks (Kahler et al. 1984; Reames 2013). Those most energetic SEP events, that reach the neutral atmosphere of Earth and produce secondary neutrons , are called Ground level enhancement (GLE) events. GLEs are thought to be mainly accelerated by CME-driven shocks. Gopalswamy et al. (2010b) analyzed the sources of 16 GLE events in solar cycle 23, finding that all of them are associated with shock acceleration.

Due to the space weather concerns, a great deal of research has been done on the conditions under which GLE events may occur. It has been determined that GLE events depend on many different aspects of particle acceleration by shocks, including early shock evolution, preconditioning, magnetic connectivity and CME deflection, and the state of the heliosphere (Gopalswamy et al. 2014c; Nitta et al. 2012). Shocks with larger speeds and smaller formation heights are more likely to associated with GLE events (Cliver 2006; Gopalswamy et al. 2010b, 2017). Elevated seed population, like flare-accelerated particles, also plays an important role Tylka et al. (2005).

In recent years, the influence of CME interaction on solar energetic particle events, which leads to enhanced seed particles and background turbulence, has attracted people's attention (Gopalswamy et al. 2002, 2003b; Mäkelä et al. 2015; Gopalswamy et al. 2004; Li and Zank 2005; Li et al. 2012; Zhuang et al. 2020). Gopalswamy et al. (2002) first illustrated that the interaction between a fast primary CME and one or more preceding CME(s) was an important aspect of SEP production. They further studied the CMEs associated with SEP events of solar cycle 23, indicating that the majority of SEP producing CMEs propagate through the near-Sun interplanetary medium severely disturbed and distorted by the preceding CMEs. Furthermore, the preceding CMEs are faster and wider on the average, so they may provide seed particles for CME-driven shocks that follow (Gopalswamy et al. 2003b, 2004).

Li and Zank (2005) proposed that the shock driven by a preceding CME can leave a turbulent downstream wake where the enhanced SEP production will occur at the primary CME shock. Later, Li et al. (2012) proposed the "Twin-CME" scenario (see Fig. 31) in which CME–CME interaction leads to the enhancements of SEP events. The combined effect of the presence of the first shock and the existence of the reconnection between the open and close magnetic filed lines is that when the second CME erupts and drives a second shock, one finds both an excess of seed population and an enhanced turbulence level at the front of the second shock than the case of a single CME-driven shock. Ding et al. (2013) analyzed the large SEP events in solar cycle 23, indicating that large SEP events tend to be "twin-CME" events. Using observational data from multiple satellites, Shen et al. (2013a) found that the first GLE event of solar cycle 24 also stems from the interaction of two fast CMEs, in line with the "twin-CME" scenario.

Many studies have shown that the energetic particle intensities are usually depressed in ICMEs, particularly in those traveling in the ecliptic plane (Lario et al. 2005; Malandraki et al. 2005; Cane and Lario 2006). Richardson (1997) found
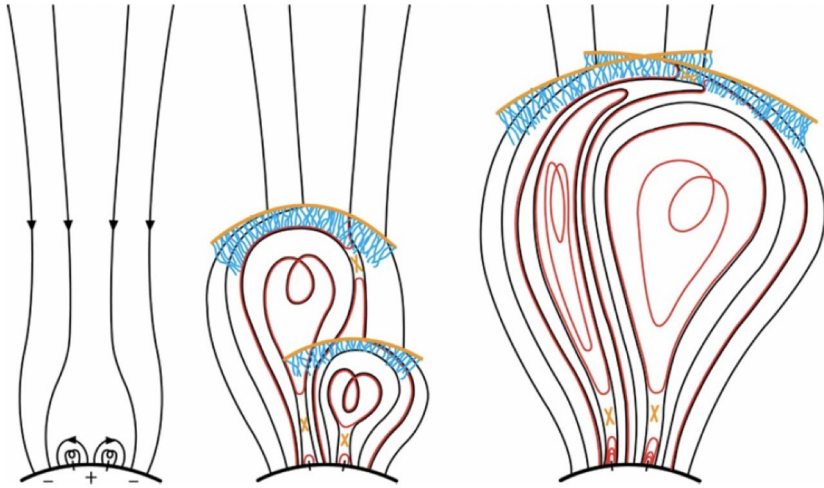
Fig. 31 The cartoons depicting our "twin-CME" scenario for the generation of an extreme SEP event. Two CMEs erupt from the same or nearby source active regions. Interchange reconnection between open magnetic field and that enclosing the first CME can release driver material of the first CME to the turbulence-enhanced downstream of the first CME shock. This material can be subsequently accelerated by the second CME shock. From Li et al. (2012)

that near the ecliptic, entry into and exit from an ICME is typically accompanied by a decrease and a recovery, respectively, in the particle density over a range of rigidities. For protons with energy smaller than 100 MeV, the intensity drop can be greater than 70%. They suggested that ejecta are predominantly closed magnetic structures, thus avoiding the easy access and exit of particles. Cane and Lario (2006) reported the energetic particle response to the passage of an fast ICME observed by the ACE spacecraft in September 1998. The shock might also act as a discontinuity which can reflect the energetic particles (Kirin et al. 2020). This fast ICME drove a strong interplanetary shock that locally accelerated ions to more than 60 MeV at its arrival at 1 AU. In this event, they found a sharp decrease of the low-energy ion intensities precisely in the ICME interval, which demonstrated that the penetration of shock accelerated particles into the ICME is restricted. In addition, Kallenrode (2001) studied the influence of the magnetic cloud on the propagation of the energetic particles with a numerical model. The simulation results showed that a magnetic cloud may act as a barrier for external energetic particles' propagation.

On the other hand, Shen et al. (2008) pointed out that in S-ICMEs, the behavior of energetic particles may be much different. In the S-ICME on November 5, 2001, an extraordinary energetic particle enhancements over the entire period of the S-ICME was identified. This enhancement might be due to the combined effects of the shock and the MC boundaries: the shock can accelerate particles within the ICME and the ICME boundaries prevent the leakage of these accelerated particles, as shown in Fig. 32. In addition to this event, energetic particle enhancements also occurred in the S-ICME on September 7, 2017 (Shen et al. 2018a). Using the protons with energies form ∼ 200 keV to ∼ 7 MeV observed by Wind/3dp as a measure,
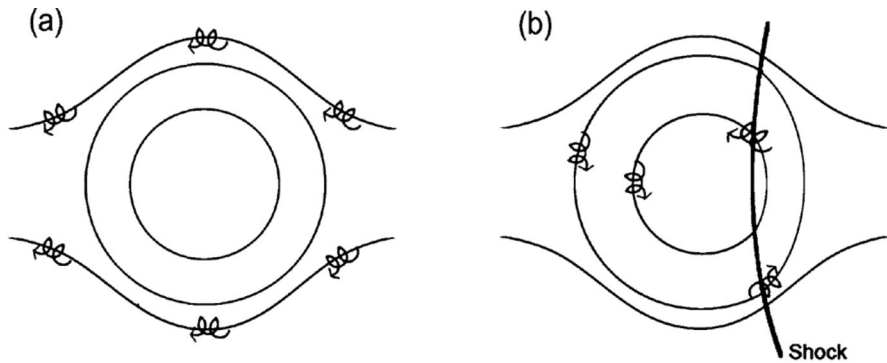
Fig. 32 A diagram of the cross-section of the isolated ICME (**a**) and the S-ICME (**b**). From Shen et al. (2008)

Xu et al. (2019a) check the proton intensity signatures of the 487 ICMEs between 1995 and 2017. A total of 12 ICMEs with extraordinary energetic particle enhancements have been found, 9 of which are S-ICMEs. Figure 33 shows an example of S-ICME with enhanced energetic particles. In addition, they also pointed out that shocks inside energetic particle enhanced S-ICMEs are relatively fast and strong. These results indicated that shock-ICME interaction may be an effective local acceleration mechanism, and will significantly enhance the SEP events.

7 Conclusions and future prospects

In this paper, the main developments in the investigation of the propagation, deflection and interaction of CMEs from the Sun to 1 AU in recent years, by mean of observational, theoretical and numerical methods have been reviewed.

During the propagation of the CMEs from the Sun, the leading edges of the CMEs normally leave bright traces in the images of visible light, which have inspired various techniques to investigate the 3-D geometrical and kinematic information of CMEs with the help of the coronagraph observations. From the previous observational studies and numerical simulations, the kinematic evolution of CMEs always undergo three phases, which are a gradual evolution, a fast acceleration, and a propagation phase. In the gradual evolution phase, the CME front is first formed and then undergoes a slow expansion. The fast acceleration phase always lasts from a few minutes to an hour. The main acceleration of CMEs occurs at low coronal heights (e.g., $\leq 2R_s$) and in this phase, CMEs are mainly accelerated by the Lorentz force. After the main impulsive acceleration phase the CME propagates with a gradual acceleration/deceleration due to the interaction with the ambient solar wind flow during propagation in the interplanetary space, mostly influenced by the drag force.

The propagation directions of CMEs may show departures from a radial trajectories, which is called CME deflection. The CME deflection can be approximately divided into two parts: the deflection in the corona due to the magnetic forces and
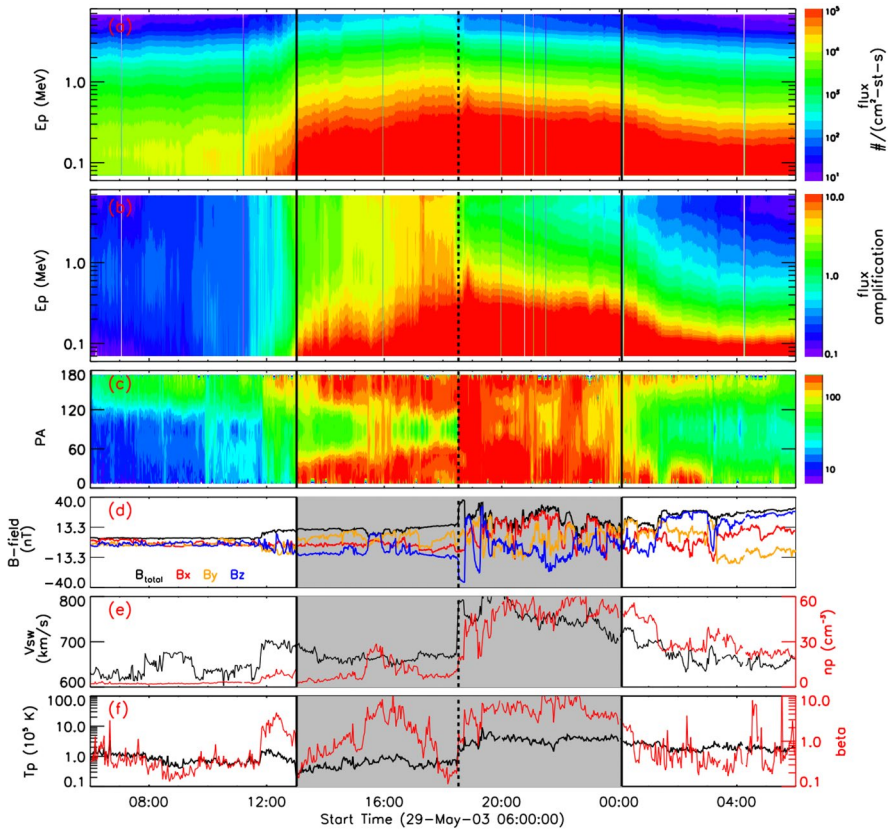
Fig. 33 Wind observations of an ICME on 29 May 2003. From top to the bottom, panels are the distribution of energetic proton intensities in 7 energy channels, the normalized energetic proton intensities, the suprathermal electron pitch-angle distribution, magnetic field strength (*B*) and three components of magnetic field vector in GSE coordinate, solar wind speed (*v*) and proton density (Np), proton temperature (Tp) and *β*. The shaded region shows the period of the ICME, and the vertical dashed black line inside represents the shock. From Xu et al. (2019a)

the deflection in the interplanetary space due to the interaction with the background solar wind. If a slow CME and a fast CME erupt continuously from the adjacent positions, then the fast CME will approach and interact with slow CMEs during propagation. Many observational studies and numerical simulations have investigated the formation and propagation of the interactional CMEs. The interaction of the CMEs can lead to the compression, reconnection and momentum transfer between the CMEs and may contribute to solar energetic particle events and geomagnetic storms.

This review has only concerned the major progress in observations, physical understanding and numerical simulations of CMEs achieved in the recent years. In future research, with the continuous collection of new observational data, e.g., from Parker Solar Probe and Solar Orbiter, more extensive studies on the CMEs can be

carried out. They observe the Sun's atmosphere up close, with high spatial resolution telescopes and compares these observations with measurements taken in the environment directly surrounding the spacecraft – together creating a one-of-a-kind picture of how the Sun can affect the space environment further out in the solar system. Therefore, we expect to have more frequent and better in situ measurements of CMEs in the innermost heliosphere. Besides, thanks to its unique and difficult to achieve orbit, the future NASA Solaris solar polar mission (Hassler et al. 2020) will also provide the first-ever pictures of the Sun's polar regions. In addition, The concept of the Solar Ring mission put forward by Wang et al. (2020) will be the first attempt to routinely monitor and study the Sun and inner heliosphere from a full 360-degree perspective in the ecliptic plane. The current preliminary design of the Solar Ring mission is to deploy six spacecraft, grouped in three pairs, on a sub-AU orbit around the Sun. The two spacecraft in each group are separated by about 30° and every two groups by about 120°. This configuration with necessary science payloads will allow us to establish the unprecedented capability of resolving the ICMEs at multiple longitudes, which therefore can lead to a better understanding of the evolution and space weather effect of CMEs.

References

T. Amerstorfer, J. Hinterreiter, M.A. Reiss, C. Möstl, J.A. Davies, R.L. Bailey, A.J. Weiss, M. Dumbović, M. Bauer, U.V. Amerstorfer, R.A. Harrison, Evaluation of CME arrival prediction using ensemble modeling based on heliospheric imaging observations. Space Weather **19**, e02553 (2021)

J. An, T. Magara, K. Hayashi, Y.J. Moon, Parametric study of ICME properties related to space weather disturbances via a series of three-dimensional MHD simulations. Sol. Phys. **294**, 143 (2019). https://doi.org/10.1007/s11207-019-1531-6

C.N. Arge, D. Odstrcil, V. Pizzo, L.R. Mayer, Improved method for specifying solar wind speed near the sun, in Proceedings of the Tenth International Solar Wind Conference, vol. 679, 190–193 (2003). https://doi.org/10.1063/1.1618574

H. Bain, M. Mays, J. Luhmann, Y. Li, L. Jian, D. Odstrcil, Shock connectivity in the 2010 August and 2012 July solar energetic particle events inferred from observations and ENLIL modeling. Astrophys. J. **825**, 1 (2016). https://doi.org/10.3847/0004-637X/825/1/1

B.M. Bein, S. Berkebile-Stoiser, A.M. Veronig, M. Temmer, N. Muhr, I. Kienreich, D. Utz, B. Vrsnak, Impulsive acceleration of coronal mass ejections. I. Statistics and coronal mass ejection source region characteristics. Astrophys. J. (2011). https://doi.org/10.1088/0004-637X/738/2/191

A. Bemporad, F. Zuccarello, C. Jacobs, M. Mierla, S. Poedts, Study of multiple coronal mass ejections at solar minimum conditions. Sol. Phys. (2012). https://doi.org/10.1007/s11207-012-9999-3

A. Borgazzi, A. Lara, E. Echer, M.V. Alves, Dynamics of coronal mass ejections in the interplanetary medium. Astron. Astrophys. **498**, 885–889 (2009)

E. Bosman, V. Bothmer, G. Nisticò, A. Vourlidas, R.A. Howard, J.A. Davies, Three-dimensional properties of coronal mass ejections from STEREO/SECCHI observations. Sol. Phys. **281**, 167–185 (2012). https://doi.org/10.1007/s11207-012-0123-5

C.R. Braga, A. Vourlidas, G. Stenborg, A. Dal Lago, R.R.S. de Mendonça, E. Echer, Predicting the time of arrival of coronal mass ejections at Earth from heliospheric imaging observations. J. Geophys. Res. (Space Phys.) **125**, e27885 (2020). https://doi.org/10.1029/2020JA027885

G.E. Brueckner, R.A. Howard, M.J. Koomen, C.M. Korendyke, C.J. Eyles, The large angle spectroscopic coronagraph (LASCO). Sol. Phys. **162**, 357–402 (1995)

L. Burlaga, E. Sittler, F. Mariani, R. Schwenn, Magnetic loop behind an interplanetary shock—Voyager, Helios, and IMP 8 observations. J. Geophys. Res. Space Phys. **86**, 6673–6684 (1981). https://doi.org/10.1029/JA086iA08p06673

L.F. Burlaga, S.P. Plunkett, O.C. St Cyr, Successive CMEs and complex ejecta. J. Geophys. Res. **107**, 1266 (2002)

J. Byrne, S. Maloney, J. Mcateer, J. Refojo, P. Gallagher, Propagation of an Earth-directed coronal mass ejection in three dimensions. Nat. Commun. **1**, 74 (2010). https://doi.org/10.1038/ncomms1077

J. Čalogović, M. Dumbović, D. Sudar, B. Vršnak, K. Martinić, M. Temmer, A. Veronig, Probabilistic drag-based ensemble model (DBEM) evaluation for heliospheric propagation of CMEs. Solar Physics **296**(114) (2021). https://doi.org/10.1007/s11207-021-01859-5

H. Cane, D. Lario, An introduction to CMEs and energetic particles. Space Sci. Rev. **123**, 45–56 (2006). https://doi.org/10.1007/s11214-006-9011-3

M. Cécere, M.V. Sieyra, H. Cremades, M. Mierla, A. Sahade, G. Stenborg, A. Costa, M.J. West, E. D'Huys, Large non-radial propagation of a coronal mass ejection on 2011 January 24. Adv. Space Res. **65**, 1654–1662 (2020). https://doi.org/10.1016/j.asr.2019.08.043

E. Chané, C. Jacobs, B. van der Holst, S. Poedts, D. Kimpe, On the effect of the initial magnetic polarity and of the background wind on the evolution of CME shocks. Astron. Astrophys. **432**(1), 331–339 (2005). https://doi.org/10.1051/0004-6361:20042005

E. Chané, B. van der Holst, C. Jacobs, S. Poedts, D. Kimpe, Inverse and normal coronal mass ejections: evolution up to 1 AU. Astron. Astrophys. **447**(2), 727–733 (2006). https://doi.org/10.1051/0004-6361:20053802

E. Chané, S. Poedts, B. van der Holst, On the combination of ace data with numerical simulations to determine the initial characteristics of a CME. Astron. Astrophys. **492**(2), L29–L32 (2008). https://doi.org/10.1051/0004-6361:200811022

P.F. Chen, Coronal mass ejections: models and their observational basis. Living Rev. Sol. Phys. **8**, 1 (2011). https://doi.org/10.12942/lrsp-2011-1

J. Chen, Physics of erupting solar flux ropes: coronal mass ejections (CMEs)—recent advances in theory and observation. Phys. Plasmas **24**, 090501 (2017). https://doi.org/10.1063/1.4993929

J. Chen, R.A. Santoro, J. Krall, R.A. Howard, A. Burkepile, Magnetic geometry and dynamics of the fast coronal mass ejection of 1997 September 9. Astrophys. J. **533**, 481 (2000)

J. Chen, R.A. Howard, G.E. Brueckner, R. Santoro, A. Simnett, Evidence of an erupting magnetic flux rope: LASCO coronal mass ejection of 1997 April 13. Astrophys. J. **490**, L191 (2009)

X. Cheng, Y. Guo, M. Ding, Origin and structures of solar eruptions I: magnetic flux rope. Sci. China Earth Sci. **60**, 1383–1407 (2017). https://doi.org/10.1007/s11430-017-9074-6

Y. Chi, C. Shen, Y. Wang, M. Xu, P. Ye, S. Wang, Statistical Study of the Interplanetary Coronal Mass Ejections from 1995 to 2015. Sol. Phys. **291**(8), 2419–2439 (2016). https://doi.org/10.1007/s11207-016-0971-5

Y. Chi, C. Shen, B. Luo, Y. Wang, M. Xu, Geoeffectiveness of stream interaction regions from 1995 to 2016. Space Weather **16**, 1960–1971 (2018). https://doi.org/10.1029/2018SW001894

E.W. Cliver, The unusual relativistic solar proton events of 1979 August 21 and 1981 May 10. Astrophys. J. **639**, 1206–1217 (2006). https://doi.org/10.1086/499765

R.C. Colaninno, A. Vourlidas, C.C. Wu, Quantitative comparison of methods for predicting the arrival of coronal mass ejections at Earth based on multiview imaging. J. Geophys. Res. (Space Phys.) **118**, 6866–6879 (2013). https://doi.org/10.1002/2013JA019205. arXiv:1310.6680

H. Cremades, V. Bothmer, On the three-dimensional configuration of coronal mass ejections. AAP **422**, 307–322 (2004). https://doi.org/10.1051/0004-6361:20035776

H. Cremades, V. Bothmer, D. Tripathi, Properties of structured coronal mass ejections in solar cycle 23. Adv. Space Res. **38**, 461–465 (2006). https://doi.org/10.1016/j.asr.2005.01.095

A. Dal Lago, R. Schwenn, W.D. Gonzalez, Relation between the radial speed and the expansion speed of coronal mass ejections. Adv. Space Res. **32**, 2637–2640 (2003). https://doi.org/10.1016/j.asr.2003.03.012

S. Dasso, C.H. Mandrini, P. Démoulin, M.L. Luoni, A.M. Gulisano, Large scale MHD properties of interplanetary magnetic clouds. Adv. Space Res. **35**, 711–724 (2005). https://doi.org/10.1016/j.asr.2005.02.096

S. Dasso, C.H. Mandrini, P. Démoulin, M.L. Luoni, A new model-independent method to compute magnetic helicity in magnetic clouds. Astron. Astrophys. **455(1)**, 349–359 (2006). https://doi.org/10.1051/0004-6361:20064806

S. Dasso, M.S. Nakwacki, P. Démoulin, C.H. Mandrini, Progressive transformation of a flux rope to an ICME. Comparative analysis using the direct and fitted expansion methods. Sol. Phys. **244**, 115–137 (2007). https://doi.org/10.1007/s11207-007-9034-2. arXiv:0706.2889

S. Dasso, C.H. Mandrini, B. Schmieder, H. Cremades, C. Cid, Y. Cerrato, E. Saiz, P. Démoulin, A.N. Zhukov, L. Rodriguez, A. Aran, M. Menvielle, S. Poedts, Linking two consecutive nonmerging magnetic clouds with their solar sources. J. Geophys. Res. (Space Phys.) **114**, A02109 (2009). https://doi.org/10.1029/2008JA013102

J.A. Davies, R.A. Harrison, C.H. Perry, C. Möstl, N. Lugaz, T. Rollett, C.J. Davis, S.R. Crothers, M. Temmer, C.J. Eyles, N.P. Savani, A self-similar expansion model for use in solar wind transient propagation studies. Astrophys. J. **750**, 23 (2012). https://doi.org/10.1088/0004-637X/750/1/23

C.E. DeForest, T.A. Howard, D.J. McComas, Tracking coronal features from the low corona to Earth: a quantitative analysis of the 2008 December 12 coronal mass ejection. ApJ **769**, 43 (2013). https://doi.org/10.1088/0004-637X/769/1/43

R. Dewey, D. Baker, B. Anderson, M. Benna, C. Johnson, D. Gershman, G. Ho, W. McClintock, D. Odstrcil, L. Philpott, J. Raines, D. Schriver, J. Slavin, S. Solomon, R. Winslow, T. Zurbuchen, Improving solar wind modeling at mercury: incorporating transient solar phenomena into the WSA-ENLIL model with the cone extension. J. Geophys. Res. Space Phys. (2015). https://doi.org/10.1002/2015JA021194

L. Ding, Y. Jiang, L. Zhao, G. Li, The "Twin-CME'' scenario and large solar energetic particle events in solar cycle 23. Astrophys. J. **763**, 30 (2013)

V. Domingo, B. Fleck, A.I. Poland, The SOHO mission: an overview. Sol. Phys. **162**, 1–37 (1995)

M. Dryer, Z. Smith, C.D. Fry, W. Sun, C.S. Deehr, S.I. Akasofu, Real-time shock arrival predictions during the "Halloween 2003 epoch''. Space Weather **2**, S09001 (2004). https://doi.org/10.1029/2004SW000087

M. Dumbović, J. Čalogović, B. Vršnak, M. Temmer, M.L. Mays, A. Veronig, I. Piantschitsch, The drag-based ensemble model (DBEM) for coronal mass ejection propagation. Astrophys. J. **854**, 180 (2018). https://doi.org/10.3847/1538-4357/aaaa66. arXiv:1801.07473

E. Echer, W.D. Gonzalez, B.T. Tsurutani, Interplanetary conditions leading to superintense geomagnetic storms (Dst ≤ -250 nT) during solar cycle 23. Geophys. Res. Lett. **35**, L06S03 (2008)

Y. Fan, S.E. Gibson, Numerical simulations of three-dimensional coronal magnetic fields resulting from the emergence of twisted magnetic flux tubes. Astrophys. J. **609**, 1123–1133 (2004). https://doi.org/10.1086/421238

C.J. Farrugia, V.K. Jordanova, M.F. Thomsen, G. Lu, S.W.H. Cowley, K.W. Ogilvie, A two-ejecta event associated with a two-step geomagnetic storm. J. Geophys. Res. Atmos. (2006). https://doi.org/10.1029/2006JA011893

X. Feng, *Magnetohydrodynamic Modeling of the Solar Corona and Heliosphere* (Springer, Singapore, 2020)

H.Q. Feng, D.J. Wu, Observations of a small interplanetary magnetic flux rope associated with a magnetic reconnection exhaust. Astrophys. J. **705**, 1385–1387 (2009). https://doi.org/10.1088/0004-637X/705/2/1385

X. Feng, X. Zhao, A new prediction method for the arrival time of interplanetary shocks. Sol. Phys. **238**, 167–186 (2006). https://doi.org/10.1007/s11207-006-0185-3

X. Feng, Y. Zhou, S.T. Wu, A novel numerical implementation for solar wind modeling by the modified conservation element/solution element method. ApJ **655**, 1110–1126 (2007). https://doi.org/10.1086/510121

X.S. Feng, Y. Zhang, W. Sun, M. Dryer, C.D. Fry, C.S. Deehr, A practical database method for predicting arrivals of "average'' interplanetary shocks at Earth. J. Geophys. Res. (Space Phys.) **114**, A01101 (2009). https://doi.org/10.1029/2008JA013499

X. Feng, L. Yang, C. Xiang, S.T. Wu, Y. Zhou, D. Zhong, Three-dimensional solar WIND modeling from the Sun to Earth by a SIP-CESE MHD model with a six-component grid. ApJ **723**, 300–319 (2010). https://doi.org/10.1088/0004-637X/723/1/300

L. Feng, B. Inhester, Y. Wei, W.Q. Gan, T.L. Zhang, M.Y. Wang, Morphological evolution of a three-dimensional coronal mass ejection cloud reconstructed from three viewpoints. Astrophys. J. **751**, 18 (2012a). https://doi.org/10.1088/0004-637X/751/1/18

X. Feng, C. Jiang, C. Xiang, X. Zhao, S.T. Wu, A data-driven model for the global coronal evolution. ApJ **758**, 62 (2012b). https://doi.org/10.1088/0004-637X/758/1/62

X. Feng, X. Ma, C. Xiang, Data-driven modeling of the solar wind from 1 R_s to 1 AU. J. Geophys. Res. (Space Phys.) **120**, 10159–10174 (2015). https://doi.org/10.1002/2015JA021911

J. Feynman, A. Ruzmaikin, A high-speed erupting-prominence CME: a bridge between types. Sol. Phys. (2004). https://doi.org/10.1023/B:SOLA.0000022996.53206.9d

S. Gibson, B.C. Low, A time-dependent three-dimensional magnetohydrodynamic model of the coronal mass ejection. Astrophys. J. **493**, 460 (1998). https://doi.org/10.1086/305107

W.D. Gonzalez, J.A. Joselyn, Y. Kamide, H.W. Kroehl, G. Rostoker, B.T. Tsurutani, V.M. Vasyliunas, What is a geomagnetic storm? J. Geophys. Res. **99**, 5771–5792 (1994)

W. Gonzalez, B. Tsurutani, A. de Gonzalez, Interplanetary origin of geomagnetic storms. Space Sci. Rev. **88**(3/4), 529–562 (1999). https://doi.org/10.1023/A:1005160129098

W.D. Gonzalez, E. Echer, A.L. Clua-Gonzalez, B.T. Tsurutani, Interplanetary origin of intense geomagnetic storms (Dst ≤ −100 nT) during solar cycle 23. Geophys. Res. Lett. **34**, L06101 (2007)

N. Gopalswamy, Properties of interplanetary coronal mass ejections. Space Sci. Rev. **124**, 145–168 (2006). https://doi.org/10.1007/s11214-006-9102-1

N. Gopalswamy, The dynamics of eruptive prominences, in *Solar Prominences* ed. by J.C. Vial, O. Engvold, p. 381 (2015). https://doi.org/10.1007/978-3-319-10416-4_15. arXiv:1407.2594

N. Gopalswamy, History and development of coronal mass ejections as a key player in solar terrestrial relationship. Geosci. Lett. **3**, 8 (2016). https://doi.org/10.1186/s40562-016-0039-2. arXiv:1602.03665

N. Gopalswamy, P. Mäkelä, Latitudinal connectivity of ground level enhancement events, in *Outstanding Problems in Heliophysics: From Coronal Heating to the Edge of the Heliosphere*, ed. by Q. Hu, G.P. Zank (San Francisco, CA: ASP), vol. 484, p. 63 (2014). arXiv:1310.8506

N. Gopalswamy, B.J. Thompson, Early life of coronal mass ejections. J. Atmos. Sol. Terr. Phys. **62**, 1457–1469 (2000). https://doi.org/10.1016/S1364-6826(00)00079-1

N. Gopalswamy, Y. Hanaoka, H. Hudson, Structure and dynamics of the corona surrounding an eruptive prominence. Adv. Space Res. **25**, 1851–1854 (2000a). https://www.sciencedirect.com/science/article/pii/S0273117799005979. https://doi.org/10.1016/S0273-1177(99)00597-9. Coronal structure and dynamics near solar activity minimum

N. Gopalswamy, A. Lara, R. Lepping, M. Kaiser, D. Berdichevsky, O. St Cyr, Interplanetary acceleration of coronal mass ejections. Geophys. Res. Lett. (2000b). https://doi.org/10.1029/1999GL003639

N. Gopalswamy, A. Lara, S. Yashiro, M. Kaiser, R. Howard, Predicting the 1-AU arrival times of coronal mass ejections. J. Geophys. Res. Space Phys. (2001a). https://doi.org/10.1029/2001JA000177

N. Gopalswamy, S. Yashiro, M.L. Kaiser, R.A. Howard, J.L. Bougeret, Radio signatures of coronal mass ejection interaction: coronal mass ejection cannibalism? Astrophys. J. **548**, L91–L94 (2001b)

N. Gopalswamy, S. Yashiro, G. Michałek, M.L. Kaiser, R.A. Howard, D.V. Reames, R. Leske, T. von Rosenvinge, Interacting coronal mass ejections and solar energetic particles. Astrophys. J. Lett. **572**, L103–L107 (2002). https://doi.org/10.1086/341601

N. Gopalswamy, M. Shimojo, W. Lu, S. Yashiro, K. Shibasaki, R.A. Howard, Prominence eruptions and coronal mass ejection: a statistical study using microwave observations. Astrophys. J. **586**, 562–578 (2003a). https://doi.org/10.1086/367614

N. Gopalswamy, S. Yashiro, A. Lara, M.L. Kaiser, B.J. Thompson, P.T. Gallagher, R.A. Howard, Large solar energetic particle events of cycle 23: a global view. Geophys. Res. Lett. 30 (2003b). https://agupubs.onlinelibrary.wiley.com/doi/abs/10.1029/2002GL016435. https://doi.org/10.1029/2002GL016435

N. Gopalswamy, S. Yashiro, S. Krucker, G. Stenborg, R.A. Howard, Intensity variation of large solar energetic particle events associated with coronal mass ejections. J. Geophys. Res. Space Phys. 109 (2004). https://agupubs.onlinelibrary.wiley.com/doi/abs/10.1029/2004JA010602. https://doi.org/10.1029/2004JA010602

N. Gopalswamy, A. Dal Lago, S. Yashiro, S. Akiyama, The expansion and radial speeds of coronal mass ejections. Cent. Eur. Astrophys. Bull. **33**, 115–124 (2009a)

N. Gopalswamy, P. Mäkelä, H. Xie, S. Akiyama, S. Yashiro, CME interactions with coronal holes and their interplanetary consequences. J. Geophys. Res. (Space Phys.) **114**, A00A22 (2009b). https://doi.org/10.1029/2008JA013686

N. Gopalswamy, P. Mäkelä, H. Xie, S. Akiyama, S. Yashiro, CME interactions with coronal holes and their interplanetary consequences. J. Geophys. Res. (Space Phys.) **114**, A00A22 (2009c). https://doi.org/10.1029/2008JA013686

N. Gopalswamy, S. Yashiro, M. Temmer, J. Davila, W.T. Thompson, S. Jones, R.T.J. McAteer, J.P. Wuelser, S. Freeland, R.A. Howard, EUV wave reflection from a coronal hole. Astrophys. J. Lett. **691**, L123–L127 (2009d). https://doi.org/10.1088/0004-637X/691/2/L123

N. Gopalswamy, P. Mäkelä, H. Xie, S. Akiyama, S. Yashiro, Solar sources of "driverless" interplanetary shocks, in *Twelfth International Solar Wind Conference*, ed. by M. Maksimovic, K. Issautier, N. Meyer-Vernet, M. Moncuquet, F. Pantellini (2010a), pp. 452–458. https://doi.org/10.1063/1.3395902

N. Gopalswamy, H. Xie, S. Yashiro, I. Usoskin, Ground level enhancement events of solar cycle 23. Indian J. Radio Space Phys. **39**, 5 (2010b)

N. Gopalswamy, P. Mäkelä, H. Xie, S. Yashiro, Testing the empirical shock arrival model using quadrature observations. Space Weather **11**, 661–669 (2013). https://doi.org/10.1002/2013SW000945. arXiv:1310.8510

N. Gopalswamy, S. Akiyama, S. Yashiro, H. Xie, P. Mäkelä, G. Michalek, Anomalous expansion of coronal mass ejections during solar cycle 24 and its space weather implications. Geophys. Res. Lett. (2014a). https://doi.org/10.1002/2014GL059858

N. Gopalswamy, H. Xie, S. Akiyama, P.A. Mäkelä, S. Yashiro, Major solar eruptions and high energy particle events during solar cycle 24. Earth Planets Space **66**, 104 (2014b)

N. Gopalswamy, H. Xie, S. Akiyama, P.A. Mäkelä, S. Yashiro, Major solar eruptions and high-energy particle events during solar cycle 24. Earth Planets Space **66**, 104 (2014c). https://doi.org/10.1186/1880-5981-66-104. arXiv:1408.3617

N. Gopalswamy, S. Akiyama, S. Yashiro, X. Hong, G. Michalek, The mild space weather in solar cycle 24. Physics **1500**, 14–19 (2015a)

N. Gopalswamy, P. Mäkelä, S. Akiyama, S. Yashiro, N. Thakur, CMEs during the two activity peaks in cycle 24 and their space weather consequences. Sun Geosph. **10**, 111–118 (2015b). arXiv:1509.04216

N. Gopalswamy, P. Mäkelä, S. Yashiro, N. Thakur, S. Akiyama, H. Xie, A hierarchical relationship between the fluence spectra and CME kinematics in large solar energetic particle events: a radio perspective. J. Phys. Conf. Ser. **900**(1), 012009 (2017). https://doi.org/10.1088/1742-6596/900/1/012009. arXiv:1707.00209

N. Gopalswamy, S. Akiyama, S. Yashiro, H. Xie, A new technique to provide realistic input to CME forecasting models, in *Space Weather of the Heliosphere: Processes and Forecasts* ed. by C. Foullon, O.E. Malandraki (2018a), pp. 258–262. https://doi.org/10.1017/S1743921317011048. arXiv:1709.03160

N. Gopalswamy, S. Akiyama, S. Yashiro, H. Xie, Coronal flux ropes and their interplanetary counterparts. J. Atmos. Sol. Terr. Phys. **180**, 35–45 (2018b). https://doi.org/10.1016/j.jastp.2017.06.004. arXiv:1705.08912

N. Gopalswamy, P. Mäkelä, S. Akiyama, S. Yashiro, H. Xie, N. Thakur, Sun-to-Earth propagation of the 2015 June 21 coronal mass ejection revealed by optical, EUV, and radio observations. J. Atmos. Sol. Terr. Phys. **179**, 225–238 (2018c). https://doi.org/10.1016/j.jastp.2018.07.013. arXiv:1807.10979

N. Gopalswamy, S. Yashiro, P. Mäkelä, H. Xie, S. Akiyama, C. Monstein, Extreme kinematics of the 2017 September 10 solar eruption and the spectral characteristics of the associated energetic particles. Astrophys. J. Lett. **863**, L39 (2018d). https://doi.org/10.3847/2041-8213/aad86c. arXiv:1807.09906

J. Gosling, E. Hildner, R. MacQueen, R. Munro, A. Poland, C. Ross, Speeds of coronal mass ejection events. Sol. Phys. (1976). https://doi.org/10.1007/BF00152004

J.T. Gosling, M.F. Thomsen, S.J. Bame, R.D. Zwickl, The eastward deflection of fast coronal mass ejecta in interplanetary space. J. Geophys. Res. Space Phys. **92**, 12399–12406 (1987). https://doi.org/10.1029/JA092iA11p12399

J.T. Gosling, S.J. Bame, D.J. McComas, J.L. Phillips, Coronal mass ejections and large geomagnetic storms. Geophys. Res. Lett. **17**(7), 901–904 (1990). https://doi.org/10.1029/GL017i007p00901

J.T. Gosling, R.M. Skoug, D.J. McComas, C.W. Smith, Direct evidence for magnetic reconnection in the solar wind near 1 AU. J. Geophys. Res. (Space Phys.) **110**, A01107 (2005). https://doi.org/10.1029/2004JA010809

L.M. Green, B. Kliem, T. Török, L. van Driel-Gesztelyi, G.D.R. Attrill, Transient coronal sigmoids and rotating erupting flux ropes. Sol. Phys. **246**, 365–391 (2007)

B. Gui, C. Shen, Y. Wang, P. Ye, J. Liu, S. Wang, X. Zhao, Quantitative analysis of CME deflections in the corona. Sol. Phys. (2011). https://doi.org/10.1007/s11207-011-9791-9

Y. Guo, X. Cheng, M. Ding, Origin and structures of solar eruptions II: magnetic modeling. Sci. China Earth Sci. **60**, 1408–1439 (2017). https://doi.org/10.1007/s11430-017-9081-x

D. Hassler, J.S. Newmark, S.E. Gibson, N.A. Duncan, S. Gosain, J.W. Harvey, J.P. Wuelser, T.N. Woods, The solaris solar polar mission: exploring one of the last unexplored regions of the solar system, in *AGU Fall Meeting Abstracts* (2020), pp. SH011–0003

S.G. Heinemann, M. Temmer, C.J. Farrugia, K. Dissauer, C. Kay, T. Wiegelmann, M. Dumbović, A.M. Veronig, T. Podladchikova, S.J. Hofmeister, N. Lugaz, F. Carcaboso, CME–HSS interaction and characteristics tracked from Sun to Earth. Sol. Phys. **294**, 121 (2019). https://doi.org/10.1007/s11207-019-1515-6

P. Hess, J. Zhang, Stereoscopic study of the kinematic evolution of a coronal mass ejection and its driven shock from the Sun to the Earth and the prediction of their arrival times. Astrophys. J. **792**, 49 (2014). https://doi.org/10.1088/0004-637X/792/1/49

J. Hinterreiter, T. Amerstorfer, M.A. Reiss, C. Möstl, M. Temmer, M. Bauer, U.V. Amerstorfer, R.L. Bailey, A.J. Weiss, J.A. Davies, L.A. Barnard, M.J. Owens, Why are ELEvoHI CME arrival predictions different if based on STEREO A or STEREO B heliospheric imager observations? Space Weather **19**, e02674 (2021). https://doi.org/10.1029/2020SW002674

T.A. Howard, S.J. Tappin, Three-dimensional reconstruction of two solar coronal mass ejections using the stereo spacecraft. Sol. Phys. **252**, 373–383 (2008). https://doi.org/10.1007/s11207-008-9262-0

T.A. Howard, S.J. Tappin, Interplanetary coronal mass ejections observed in the heliosphere: 1. Review of Theory. SSR **147**, 31–54 (2009). https://doi.org/10.1007/s11214-009-9542-5

R.A. Howard, D.J. Michels, N.R. Sheeley Jr., M.J. Koomen, The observation of a coronal transient directed at earth. Astrophys. J. **263**, L101–L104 (1982). https://doi.org/10.1086/183932

T.A. Howard, D.F. Webb, S.J. Tappin, D.R. Mizuno, J.C. Johnston, Tracking halo coronal mass ejections from 0–1 AU and space weather forecasting using the Solar Mass Ejection Imager (SMEI). J. Geophys. Res. (Space Phys.) **111**, A04105 (2006). https://doi.org/10.1029/2005JA011349

R.A. Howard, J.D. Moses, A. Vourlidas, J.S. Newmark, D.G. Socker, S.P. Plunkett, C.M. Korendyke, J.W. Cook, A. Hurley, J.M. Davila, W.T. Thompson, O.C. St Cyr, E. Mentzell, K. Mehalick, J.R. Lemen, J.P. Wuelser, D.W. Duncan, T.D. Tarbell, C.J. Wolfson, A. Moore, R.A. Harrison, N.R. Waltham, J. Lang, C.J. Davis, C.J. Eyles, H. Mapson-Menard, G.M. Simnett, J.P. Halain, J.M. Defise, E. Mazy, P. Rochus, R. Mercier, M.F. Ravet, F. Delmotte, F. Auchere, J.P. Delaboudiniere, V. Bothmer, W. Deutsch, D. Wang, N. Rich, S. Cooper, V. Stephens, G. Maahs, R. Baugh, D. McMullin, T. Carter, Sun Earth connection coronal and heliospheric investigation (SECCHI). Space Sci. Rev. (2008). https://doi.org/10.1007/s11214-008-9341-4

R.A. Howard, A. Vourlidas, R.C. Colaninno, C.M. Korendyke, S.P. Plunkett, M.T. Carter, D. Wang, N. Rich, S. Lynch, A. Thurn, D.G. Socker, A.F. Thernisien, D. Chua, M.G. Linton, S. Koss, S. Tun-Beltran, H. Dennison, G. Stenborg, D.R. McMullin, T. Hunt, R. Baugh, G. Clifford, D. Keller, J.R. Janesick, J. Tower, M. Grygon, R. Farkas, R. Hagood, K. Eisenhauer, A. Uhl, S. Yerushalmi, L. Smith, P.C. Liewer, M.C. Velli, J. Linker, V. Bothmer, P. Rochus, J.P. Halain, P.L. Lamy, F. Auchere, R.A. Harrison, A. Rouillard, S. Patsourakos, O.C. St Cyr, H. Gilbert, H. Maldonado, C. Mariano, J. Cerullo, The solar orbiter heliospheric imager (SoloHI). Astron. Astrophys. (2020). https://doi.org/10.1051/0004-6361/201935202

Q. Hu, J. Qiu, B. Dasgupta, A. Khare, G.M. Webb, Structures of interplanetary magnetic flux ropes and comparison with their solar sources. Astrophys. J. **793**, 53 (2014). https://doi.org/10.1088/0004-637X/793/1/53. arXiv:1408.1470

A. Hundhausen, Sizes and locations of coronal mass ejections—SMM observations from 1980 and 1984–1989. J. Geophys. Res. Atmos. (1993). https://doi.org/10.1029/93JA00157

A. Isavnin, A. Vourlidas, E.K.J. Kilpua, Three-dimensional evolution of erupted flux ropes from the Sun (2–20 R-circle dot) to 1 AU. Sol. Phys. (2013). https://doi.org/10.1007/s11207-012-0214-3

A. Isavnin, A. Vourlidas, E.K.J. Kilpua, Three-dimensional evolution of flux-rope CMEs and its relation to the local orientation of the heliospheric current sheet. Sol. Phys. (2014). https://doi.org/10.1007/s11207-013-0468-4

K. Iwai, D. Shiota, M. Tokumaru, K. Fujiki, M. Den, Y. Kubo, Validation of coronal mass ejection arrival-time forecasts by magnetohydrodynamic simulations based on interplanetary scintillation observations. Earth Planets Space **73**, 9 (2021). https://doi.org/10.1186/s40623-020-01345-5

C. Jacobs, S. Poedts, Models for coronal mass ejections. J. Atmos. Sol. Terr. Phys. **73**, 1148–1155 (2011). https://doi.org/10.1016/j.jastp.2010.12.002

M. Jin, W. Manchester, B. van der Holst, R. Oran, I. Sokolov, G. Toth, Y. Liu, X. Sun, T. Gombosi, Numerical simulations of coronal mass ejection on 2011 March 7: one-temperature and

two-temperature model comparison. Astrophys. J. **773**, 50 (2013). https://doi.org/10.1088/0004-637X/773/1/50

M. Jin, C. Schrijver, M. Cheung, M. DeRosa, N. Nitta, A. Title, A numerical study of long-range magnetic impacts during coronal mass ejections. Astrophys. J. **820**, 16 (2016). https://doi.org/10.3847/0004-637X/820/1/16

M. Jin, W.B. Manchester, B. van der Holst, I. Sokolov, G. Tóth, R.E. Mullinix, A. Taktakishvili, A. Chulaki, T.I. Gombosi, Data-constrained coronal mass ejections in a global magnetohydrodynamics model. Astrophys. J. **834**, 173 (2017a). https://doi.org/10.3847/1538-4357/834/2/173

M. Jin, W.B. Manchester, B. van der Holst, I. Sokolov, G. Tóth, A. Vourlidas, C.A. de Koning, T.I. Gombosi, Chromosphere to 1 AU simulation of the 2011 March 7th event: a comprehensive study of coronal mass ejection propagation. Astrophys. J. **834**, 172 (2017b). https://doi.org/10.3847/1538-4357/834/2/172

S.W. Kahler, N.R. Sheeley Jr., R.A. Howard, D.J. Michels, M.J. Koomen, R.E. McGuire, T.T. von Rosenvinge, D.V. Reames, Associations between coronal mass ejections and solar energetic proton events. J. Geophys. Res. Space Phys. **89**, 9683–9694 (1984). https://doi.org/10.1029/JA089iA11p09683

S.W. Kahler, S. Akiyama, N. Gopalswamy, Deflections of fast coronal mass ejections and the properties of associated solar energetic particle events. ApJ **754**, 100 (2012). https://doi.org/10.1088/0004-637X/754/2/100

M.L. Kaiser, T.A. Kucera, J.M. Davila, O.C. St. Cyr, M. Guhathakurta, E. Christian, The STEREO mission: an introduction. SSR **136**, 5–16 (2008). https://doi.org/10.1007/s11214-007-9277-0

M.B. Kallenrode, The influence of magnetic clouds on the propagation of energetic charged particles in interplanetary space, in *27th International Cosmic Ray Conference (ICRC27)*, vol. 8 (2001), p. 3273

R. Kataoka, T. Ebisuzaki, K. Kusano, D. Shiota, S. Inoue, T. Yamamoto, M. Tokumaru, Three-dimensional MHD modeling of the solar wind structures associated with 13 December 2006 coronal mass ejection. J. Geophys. Res. Space Phys. (2009). https://doi.org/10.1029/2009ja014167

C. Kay, M. Opher, R.M. Evans, Forecasting a coronal mass ejection's altered trajectory: ForeCAT. Astrophys. J. (2013). https://doi.org/10.1088/0004-637X/775/1/5

C. Kay, M. Opher, R.M. Evans, Global trends of CME deflections based on CME and solar parameters. Astrophys. J. (2015). https://doi.org/10.1088/0004-637X/805/2/168

C. Kay, M. Opher, R. Colaninno, A. Vourlidas, Using ForeCAT deflections and rotations to constrain the early evolution of CMEs. Astrophys. J. (2016). https://doi.org/10.3847/0004-637X/827/1/70

E.K.J. Kilpua, J. Pomoell, A. Vourlidas, R. Vainio, J. Luhmann, Y. Li, P. Schroeder, A.B. Galvin, K. Simunac, STEREO observations of interplanetary coronal mass ejections and prominence deflection during solar minimum period. Ann. Geophys. (2009). https://doi.org/10.5194/angeo-27-4491-2009

E.K.J. Kilpua, N. Lugaz, M.L. Mays, M. Temmer, Forecasting the structure and orientation of earthbound coronal mass ejections. Space Weather **17**, 498–526 (2019). https://doi.org/10.1029/2018SW001944

A. Kirin, B. Vršnak, M. Dumbović, B. Heber, On the interaction of galactic cosmic rays with heliospheric shocks during Forbush decreases. Sol. Phys. **295**, 28 (2020). https://doi.org/10.1007/s11207-020-1593-5. arXiv:2002.09454

B. Kliem, T. Török, W.T. Thompson, A parametric study of erupting flux rope rotation. Sol. Phys. **281**, 137–166 (2012). https://doi.org/10.1007/s11207-012-9990-z

D. Lario, R.B. Decker, S. Livi, S.M. Krimigis, E.C. Roelof, C.T. Russell, C.D. Fry, Heliospheric energetic particle observations during the October–November 2003 events. J. Geophys. Res. (Space Phys.) **110**, A09S11 (2005). https://doi.org/10.1029/2004JA010940

G. Li, G.P. Zank, Multiple CMEs and large gradual SEP events, in *29th International Cosmic Ray Conference (ICRC29)*, vol. 1 (2005), p. 173

G. Li, R. Moore, R.A. Mewaldt, L. Zhao, A.W. Labrador, A twin-CME scenario for ground level enhancement events. Space Sci. Rev. (2012). https://doi.org/10.1007/s11214-011-9823-7

X. Li, Y. Wang, R. Liu, C. Shen, Q. Zhang, S. Lyu, B. Zhuang, F. Shen, J. Liu, Y. Chi, Reconstructing solar wind inhomogeneous structures from stereoscopic observations in white light: solar wind transients in 3-D. J. Geophys. Res. (Space Phys.) (2020). https://doi.org/10.1029/2019JA027513

X. Li, Y. Wang, J. Guo, R. Liu, B. Zhuang, Radial velocity map of solar wind transients in the field of view of STEREO/HI1 on 3 and 4 April 2010. Astron. Astrophys. **649**, A58 (2021). https://doi.org/10.1051/0004-6361/202039766

P.C. Liewer, E.M. Dejong, J.R. Hall, R.A. Howard, A. Thernisien, Determination of CME trajectories by stereoscopic analysis of STEREO/SECCHI data, in Twelfth International Solar Wind Conference, AIP Conference Proceedings, vol. 1216 (2010), p. 412–415

R. Lionello, C. Downs, J. Linker, T. Török, P. Riley, Z. Mikić, Magnetohydrodynamic simulations of interplanetary coronal mass ejections. Astrophys. J. **777**, 76 (2013). https://doi.org/10.1088/0004-637X/777/1/76

K. Liou, C.C. Wu, M. Dryer, S. Wu, N. Rich, S. Plunkett, L. Simpson, G. Fry, K. Schenk, Global simulation of extremely fast coronal mass ejection on 23 July 2012. J. Atmos. Sol. Terr. Phys. (2014). https://doi.org/10.1016/j.jastp.2014.09.013

Y. Liu, J.D. Richardson, J.W. Belcher, C. Wang, Q. Hu, J.C. Kasper, Constraints on the global structure of magnetic clouds: transverse size and curvature. J. Geophys. Res. (Space Phys.) **111**, A12S03 (2006). https://doi.org/10.1029/2006JA011890. arXiv:physics/0606003

Y. Liu, A. Thernisien, J. Luhmann, A. Vourlidas, J. Davies, R. Lin, S. Bale, Reconstructing CMEs with coordinated imaging and in situ observations: global structure, kinematics, and implications for space weather forecasting. Astrophys. J. (2010). https://doi.org/10.1088/0004-637X/722/2/1762

Y.D. Liu, J.G. Luhmann, P. Kajdič, E.K.J. Kilpua, N. Lugaz, N.V. Nitta, C. Möstl, B. Lavraud, S.D. Bale, C.J. Farrugia, A.B. Galvin, Observations of an extreme storm in interplanetary space caused by successive coronal mass ejections. Nat. Commun. **5**, 3481 (2014). https://doi.org/10.1038/ncomms4481

Y.A. Liu, Y.D. Liu, H. Hu, R. Wang, X. Zhao, Multi-spacecraft observations of the rotation and nonradial motion of a CME flux rope causing an intense geomagnetic storm. Astrophys. J. **854**, 126 (2018)

Y. Liu, F. Shen, Y. Yang, Numerical simulation on the propagation and deflection of fast coronal mass ejections (CMEs) interacting with a corotating interaction region in interplanetary space. Astrophys. J. **887**, 150 (2019). https://doi.org/10.3847/1538-4357/ab543e

N. Lugaz, I.I. Roussev, Numerical modeling of interplanetary coronal mass ejections and comparison with heliospheric images. J. Atmos. Sol. Terr. Phys. **73**, 1187–1200 (2011). https://doi.org/10.1016/j.jastp.2010.08.016

N. Lugaz, W.B.I.V. Manchester, T.I. Gombosi, Numerical simulation of the interaction of two coronal mass ejections from Sun to Earth. Astrophys. J. **634**, 651–662 (2005)

N. Lugaz, A. Vourlidas, I.I. Roussev, Deriving the radial distances of wide coronal mass ejections from elongation measurements in the heliosphere—application to CME–CME interaction. Ann. Geophys. **27**, 3479–3488 (2009). https://doi.org/10.5194/angeo-27-3479-2009

N. Lugaz, J.N. Hernandez-Charpak, I.I. Roussev, C.J. Davis, A. Vourlidas, J.A. Davies, Determining the azimuthal properties of coronal mass ejections from multi-spacecraft remote-sensing observations with STEREO SECCHI. Astrophys. J. **715**, 493–499 (2010). https://doi.org/10.1088/0004-637x/715/1/493

N. Lugaz, P. Kintner, C. Möstl, L.K. Jian, C.J. Davis, C.J. Farrugia, Heliospheric observations of STEREO-directed coronal mass ejections in 2008–2010: Lessons for future observations of earth-directed CMEs. Sol. Phys. **279**(2), 497–515 (2012a). https://doi.org/10.1007/10.1007/s11207-012-0007-8

N. Lugaz, C.J. Farrugia, J.A. Davies, C. Möstl, C.J. Davis, I.I. Roussev, M. Temmer, The deflection of the two interacting coronal mass ejections of 2010 May 23–24 as revealed by combined in situ measurements and heliospheric imaging. Astrophys. J. **759**(1), 68 (2012b). https://doi.org/10.1088/0004-637X/759/1/68

N. Lugaz, C. Farrugia, W. Manchester, N. Schwadron, The Interaction of Two Coronal Mass Ejections: Influence of Relative Orientation. Astrophys. J. **778**(1), 20 (2013). https://doi.org/10.1088/0004-637X/778/1/20

N. Lugaz, C.J. Farrugia, C. Huang, H.E. Spence, Extreme geomagnetic disturbances due to shocks within CMEs. Geophys. Res. Lett. **42**(12), 4694–4701 (2015a)

N. Lugaz, C.J. Farrugia, C.W. Smith, K. Paulson, Shocks inside CMEs: a survey of properties from 1997 to 2006. J. Geophys. Res. Space Phys. **120**(4), 2409–2427 (2015b). https://doi.org/10.1002/2014JA020848

N. Lugaz, M. Temmer, Y. Wang, C.J. Farrugia, The interaction of successive coronal mass ejections: a review. Sol. Phys. **292**, 64 (2017). https://doi.org/10.1007/s11207-017-1091-6

J.G. Luhmann, N. Gopalswamy, L.K. Jian, N. Lugaz, ICME evolution in the inner heliosphere. Sol. Phys. **295**, 61 (2020). https://doi.org/10.1007/s11207-020-01624-0

B.J. Lynch, S.K. Antiochos, Y. Li, J.G. Luhmann, C.R. DeVore, Rotation of coronal mass ejections during eruption. Astrophys. J. **697**, 1918–1927 (2009). https://doi.org/10.1088/0004-637X/697/2/1918

R. MacQueen, J. Eddy, J. Gosling, E. Hildner, R. Munro, G. Newkirk, A. Poland, C. Ross, Outer solar corona as observed from Skylab—preliminary results. Astrophys. J. (1974). https://doi.org/10.1086/181402

R.M. MacQueen, A. Csoeke-Poeckh, E. Hildner, L. House, R. Reynolds, A. Stanger, H. Tepoel, W. Wagner, The high altitude observatory coronagraph/polarimeter on the solar maximum mission. Sol. Phys. **65**, 91–107 (1980)

P. Mäkelä, N. Gopalswamy, S. Yashiro, H. Xie, M.J. Reiner, White-light and radio observations of CME interaction during the 2013 May 22 solar energetic particle event, in *Solar Heliospheric and INterplanetary Environment (SHINE 2015)* (2015), p. 96

P. Mäkelä, N. Gopalswamy, S. Yashiro, The radial speed-expansion speed relation for Earth-directed CMEs. Space Weather **14**, 368–378 (2016). https://doi.org/10.1002/2015SW001335

O.E. Malandraki, D. Lario, L.J. Lanzerotti, E.T. Sarris, A. Geranios, G. Tsiropoula, October/November 2003 interplanetary coronal mass ejections: ACE/EPAM solar energetic particle observations. J. Geophys. Res. (Space Phys.) **110**, A09S06 (2005). https://doi.org/10.1029/2004JA010926

S.A. Maloney, P.T. Gallagher, R. Mcateer, Reconstructing the 3-D trajectories of CMEs in the inner heliosphere. Sol. Phys. **256**, 149–166 (2009). https://doi.org/10.1007/s11207-009-9364-3

W.B. Manchester, T.I. Gombosi, I. Roussev, D.L. De Zeeuw, I.V. Sokolov, K.G. Powell, G. Tóth, M. Opher, Three-dimensional MHD simulation of a flux rope driven CME. J. Geophys. Res. **109**, A01104 (2004a). https://doi.org/10.1029/2002JA009672

W.B. Manchester, T.I. Gombosi, I. Roussev, A. Ridley, D.L. De Zeeuw, I.V. Sokolov, K.G. Powell, G. Tóth, Modeling a space weather event from the sun to the earth: CME generation and interplanetary propagation. J. Geophys. Res. **109**, A02107 (2004b). https://doi.org/10.1029/2003JA010150

W. Manchester, E.K. Kilpua, Y.D. Liu, N. Lugaz, P. Riley, T. Török, B. Vršnak, The physical processes of CME/ICME evolution. Space Sci. Rev. **212**, 1159–1219 (2017). https://doi.org/10.1007/s11214-017-0394-0

P.K. Manoharan, Evolution of coronal mass ejections in the inner heliosphere: a study using white-light and scintillation images. Sol. Phys. (2006). https://doi.org/10.1007/s11207-006-0100-y

K. Marubashi, S. Akiyama, S. Yashiro, N. Gopalswamy, K.S. Cho, Y.D. Park, Geometrical relationship between interplanetary flux ropes and their solar sources. Sol. Phys. **290**, 1371–1397 (2015). https://doi.org/10.1007/s11207-015-0681-4

G. Michalek, N. Gopalswamy, S. Yashiro, New method for estimating widths, velocities, and source location of halo coronal mass ejections. Astrophys. J. (2003). https://doi.org/10.1086/345526

G. Michalek, N. Gopalswamy, A. Lara, P. Manoharan, Arrival time of halo coronal mass ejections in the vicinity of the Earth. Astron. Astrophys. (2004). https://doi.org/10.1051/0004-6361:20047184

W. Mishra, N. Srivastava, J.A. Davies, A comparison of reconstruction methods for the estimation of coronal mass ejections kinematics based on SECCHI/HI observations. Astrophys. J. **784**, 135 (2014). https://doi.org/10.1088/0004-637X/784/2/135

W. Mishra, N. Srivastava, D. Chakrabarty, Evolution and consequences of interacting CMEs of 9–10 November 2012 using STEREO/SECCHI and in situ observations. Sol. Phys. **290**, 527–552 (2015a). https://doi.org/10.1007/s11207-014-0625-4

W. Mishra, N. Srivastava, T. Singh, Kinematics of interacting CMEs of 25 and 28 September 2012. J. Geophys. Res. Space Phys. **120**, 10–221 (2015b)

Y. Moon, G. Choe, H. Wang, Y. Park, N. Gopalswamy, G. Yang, S. Yashiro, A statistical study of two classes of coronal mass ejections. Astrophys. J. (2002). https://doi.org/10.1086/344088

C. Möstl, J.A. Davies, Speeds and arrival times of solar transients approximated by self-similar expanding circular fronts. Sol. Phys. (2013). https://doi.org/10.1007/s11207-012-9978-8

C. Möstl, K. Amla, J.R. Hall, P.C. Liewer, E.M. De Jong, R.C. Colaninno, A.M. Veronig, T. Rollett, M. Temmer, V. Peinhart, J.A. Davies, N. Lugaz, Y.D. Liu, C.J. Farrugia, J.G. Luhmann, B. Vršnak, R.A. Harrison, A.B. Galvin, Connecting speeds, directions and arrival times of 22 coronal mass ejections from the Sun to 1 AU. Astrophys. J. **787**, 119 (2014). https://doi.org/10.1088/0004-637X/787/2/119. arXiv:1404.3579

C. Möstl, T. Rollett, R.A. Frahm, Y.D. Liu, D.M. Long, R.C. Colaninno, M.A. Reiss, M. Temmer, C.J. Farrugia, A. Posner, M. Dumbović, M. Janvier, P. Démoulin, P. Boakes, A. Devos, E. Kraaikamp, M.L. Mays, B. Vršnak, Strong coronal channelling and interplanetary evolution of a solar storm up to Earth and Mars. Nat. Commun. **6**, 7135 (2015). https://doi.org/10.1038/ncomms8135. arXiv:1506.02842

T. Nieves-Chinchilla, A. Vourlidas, G. Stenborg, N.P. Savani, A. Koval, A. Szabo, L.K. Jian, Inner heliospheric evolution of a "Stealth'' CME derived from multi-view imaging and multipoint in situ

observations. I. Propagation to 1 Au. Astrophys. J. **779**, 55 (2013). https://doi.org/10.1088/0004-637x/779/1/55

N.V. Nitta, Y. Liu, M.L. DeRosa, R.W. Nightingale, What are special about ground-level events?. Flares, CMEs, active regions and magnetic field connection. Space Sci. Rev. **171**, 61–83 (2012). https://doi.org/10.1007/s11214-012-9877-1. arXiv:1203.5777

D. Odstrcil, M. Dryer, Z. Smith, Propagation of an interplanetary shock along the heliospheric plasma sheet. J. Geophys. Res. **101**, 19973–19986 (1996). https://doi.org/10.1029/96JA00479

D. Odstrcil, V.J. Pizzo, J.A. Linker, P. Riley, R. Lionello, Z. Mikic, Initial coupling of coronal and heliospheric numerical magnetohydrodynamic codes. J. Atmos. Sol. Terr. Phys. **66**, 1311–1320 (2004a). https://doi.org/10.1016/j.jastp.2004.04.007

D. Odstrcil, P. Riley, X. Zhao, W. Hansen, Numerical simulation of the 12 May 1997 interplanetary CME event. J. Geophys. Res. (2004b). https://doi.org/10.1029/2003JA010135

D. Odstrcil, V. Pizzo, C. Arge, Propagation of the 12 May 1997 interplanetary coronal mass ejection in evolving solar wind structures. J. Geophys. Res. (2005). https://doi.org/10.1029/2004JA010745

O. Olmedo, A. Vourlidas, J. Zhang, X. Cheng, Secondary Waves and/or the "Reflection" from and "Transmission" through a coronal hole of an extreme ultraviolet wave associated with the 2011 February 15 X2.2 flare observed with SDO/AIA and STEREO/EUVI. Astrophys. J. **756**, 143 (2012). https://doi.org/10.1088/0004-637X/756/2/143. arXiv:1206.6137

O. Olmedo, N. Gopalswamy, H. Xie, S. Yashiro, P.A. Makela, S. Akiyama, O.C. St Cyr, A. Vourlidas, Forward fitting of a coronal shock front to a spheroid, in *AGU Fall Meeting Abstracts* (2013), pp. SH13A–2033

R. Oran, B. van der Holst, E. Landi, M. Jin, I. Sokolov, T. Gombosi, A global wave-driven magnetohydrodynamic solar model with a unified treatment of open and closed magnetic field topologies. Astrophys. J. **778**, 176 (2013). https://doi.org/10.1088/0004-637X/778/2/176

M.J. Owens, Combining remote and in situ observations of coronal mass ejections to better constrain magnetic cloud reconstruction. J. Geophys. Res. Space Phys. (2008). https://doi.org/10.1029/2008JA013589

M.J. Owens, V.G. Merkin, P. Riley, A kinematically distorted flux rope model for magnetic clouds. J. Geophys. Res. (Space Phys.) **111**, A03104 (2006). https://doi.org/10.1029/2005JA011460

E. Palmerio, C. Scolini, D. Barnes, J. Magdalenic, M. West, A. Zhukov, L. Rodriguez, M. Mierla, S. Good, D. Morosan, E. Kilpua, J. Pomoell, S. Poedts, Multipoint study of successive coronal mass ejections driving moderate disturbances at 1 AU. Astrophys. J. **878**, 37 (2019). https://doi.org/10.3847/1538-4357/ab1850

E. Paouris, H. Mavromichalaki, Effective acceleration model for the arrival time of interplanetary shocks driven by coronal mass ejections. Sol. Phys. **292**, 180 (2017). https://doi.org/10.1007/s11207-017-1212-2

E. Paouris, J. Čalogović, M. Dumbović, M.L. Mays, A. Vourlidas, A. Papaioannou, A. Anastasiadis, G. Balasis, Propagating conditions and the time of ICME arrival: a comparison of the effective acceleration model with ENLIL and DBEM models. Sol. Phys. **296**, 12 (2021). https://doi.org/10.1007/s11207-020-01747-4

S. Patsourakos, A. Vourlidas, B. Kliem, Toward understanding the early stages of an impulsively accelerated coronal mass ejection. SECCHI observations. Astron. Astrophys. **522**, A100 (2010a). https://doi.org/10.1051/0004-6361/200913599. arXiv:1008.1171

S. Patsourakos, A. Vourlidas, G. Stenborg, The genesis of an impulsive coronal mass ejection observed at ultra-high cadence by AIA on SDO. Astrophys. J. **724**, L188–L193 (2010b)

J. Pomoell, S. Poedts, EUHFORIA: European heliospheric forecasting information asset. J. Space Weather Space Clim. **8**, A35 (2018). https://doi.org/10.1051/swsc/2018020

W. Poomvises, J. Zhang, O. Olmedo, Coronal mass ejection propagation and expansion in three-dimensional space in the heliosphere based on STEREO/SECCHI observations. Astrophys. J. Lett. **717**, L159 (2010). https://doi.org/10.1088/2041-8205/717/2/L159

J. Qiu, Q. Hu, T.A. Howard, V.B. Yurchyshyn, On the magnetic flux budget in low-corona magnetic reconnection and interplanetary coronal mass ejections. Astrophys. J. **659**, 758–772 (2007). https://doi.org/10.1086/512060

A.N. Raghav, A. Kule, The first in situ observation of torsional Alfvén waves during the interaction of large-scale magnetic clouds. Mon. Not. R. Astron. Soc. Lett. **476**, L6–L9 (2018). https://doi.org/10.1093/mnrasl/sly020. arXiv:1710.05755

D.V. Reames, The two sources of solar energetic particles. Space Sci. Rev. **175**, 53–92 (2013). https://doi.org/10.1007/s11214-013-9958-9. arXiv:1306.3608

I. Richardson, Using energetic particles to probe the magnetic topology of ejecta. Am. Geophys. Union (AGU) (1997). https://doi.org/10.1029/GM099p0189

I.G. Richardson, H.V. Cane, Near-Earth interplanetary coronal mass ejections during solar cycle 23 (1996–2009): Catalog and summary of properties. Solar Phys. **264**, 189–237 (2010). https://doi.org/10.1007/s11207-010-9568-6

P. Riley, M. Ben-Nun, On the sources and sizes of uncertainty in predicting the arrival time of interplanetary coronal mass ejections using global MHD models. Space Weather **19**, e02775 (2021). https://doi.org/10.1029/2021SW002775

P. Riley, N.U. Crooker, Kinematic treatment of coronal mass ejection evolution in the solar wind. Astrophys. J. **600**, 1035–1042 (2004). https://doi.org/10.1086/379974

P. Riley, M.L. Mays, J. Andries, T. Amerstorfer, D. Biesecker, V. Delouille, M. Dumbović, X. Feng, E. Henley, J.A. Linker, C. Möstl, M. Nuñez, V. Pizzo, M. Temmer, W.K. Tobiska, C. Verbeke, M.J. West, X. Zhao, Forecasting the arrival time of coronal mass ejections: analysis of the CCMC CME scoreboard. Space Weather **16**, 1245–1260 (2018). https://doi.org/10.1029/2018SW001962

T. Rollett, C. Möstl, A. Isavnin, J.A. Davies, M. Kubicka, U.V. Amerstorfer, R.A. Harrison, ElEvoHI: a novel CME prediction tool for heliospheric imaging combining an elliptical front with drag-based model fitting. Astrophys. J. **824**, 131 (2016). https://doi.org/10.3847/0004-637X/824/2/131. arXiv:1605.00510

A.P. Rouillard, Relating white light and in situ observations of coronal mass ejections: a review. J. Atmos. Sol. Terr. Phys. **73**, 1201–1213 (2011). https://doi.org/10.1016/j.jastp.2010.08.015

I.I. Roussev, T.I. Gombosi, I.V. Sokolov, M. Velli, W. Manchester IV., D.L. DeZeeuw, P. Liewer, G. Tóth, J. Luhmann, A three-dimensional model of the solar wind incorporating solar magnetogram observations. Astrophys. J. Lett. **595**, L57–L61 (2003). https://doi.org/10.1086/378878

A. Ruffenach, B. Lavraud, M.J. Owens, J.A. Sauvaud, N.P. Savani, A.P. Rouillard, P. Démoulin, C. Foullon, A. Opitz, A. Fedorov, C.J. Jacquey, V. Génot, P. Louarn, J.G. Luhmann, C.T. Russell, C.J. Farrugia, A.B. Galvin, Multispacecraft observation of magnetic cloud erosion by magnetic reconnection during propagation. J. Geophys. Res. (Space Phys.) **117**, A09101 (2012). https://doi.org/10.1029/2012JA017624

A. Ruffenach, B. Lavraud, C.J. Farrugia, P. Démoulin, S. Dasso, M.J. Owens, J.A. Sauvaud, A.P. Rouillard, A. Lynnyk, C. Foullon, N.P. Savani, J.G. Luhmann, A.B. Galvin, Statistical study of magnetic cloud erosion by magnetic reconnection. J. Geophys. Res. (Space Phys.) **120**, 43–60 (2015). https://doi.org/10.1002/2014JA020628

N. Sachdeva, P. Subramanian, R. Colaninno, A. Vourlidas, CME propagation: where does solar wind drag take over? Astrophys. J. (2015). https://doi.org/10.1088/0004-637X/809/2/158

N.P. Savani, M.J. Owens, A.P. Rouillard, R.J. Forsyth, K. Kusano, D. Shiota, R. Kataoka, Evolution of coronal mass ejection morphology with increasing heliocentric distance. I. Geometrical analysis. Astrophys. J. **731**, 109 (2011). https://doi.org/10.1088/0004-637X/731/2/109

R. Schwenn, A. dal Lago, E. Huttunen, W.D. Gonzalez, The association of coronal mass ejections with their effects near the Earth. Ann. Geophys. **23**, 1033–1059 (2005). https://doi.org/10.5194/angeo-23-1033-2005

R. Schwenn, J.C. Raymond, D. Alexander, A. Ciaravella, N. Gopalswamy, R. Howard, H. Hudson, P. Kaufmann, A. Klassen, D. Maia, G. Munoz-Martinez, M. Pick, M. Reiner, N. Srivastava, D. Tripathi, A. Vourlidas, Y.M. Wang, J. Zhang, Coronal observations of CMEs. Report of Working Group A. Space Sci. Rev. (2006). https://doi.org/10.1007/s11214-006-9016-y

C. Scolini, C. Verbeke, S. Poedts, E. Chané, J. Pomoell, F. Zuccarello, Effect of the initial shape of coronal mass ejections on 3-d MHD simulations and geoeffectiveness predictions. Space Weather (2018). https://doi.org/10.1029/2018SW001806

C. Scolini, L. Rodriguez, M. Mierla, J. Pomoell, S. Poedts, Observation-based modelling of magnetised coronal mass ejections with EUHFORIA. Astron. Astrophys. (2019). https://doi.org/10.1051/0004-6361/201935053

C. Scolini, E. Chané, M. Temmer, E. Kilpua, K. Dissauer, A. Veronig, E. Palmerio, J. Pomoell, M. Dumbovic, J. Guo, L. Rodriguez, S. Poedts, CME–CME interactions as sources of CME geoeffectiveness: the formation of the complex ejecta and intense geomagnetic storm in 2017 early September. Astrophys. J. Suppl. Ser. **247**, 21 (2020). https://doi.org/10.3847/1538-4365/ab6216

A. Shanmugaraju, B. Vršnak, Transit time of coronal mass ejections under different ambient solar wind conditions. Sol. Phys. **289**, 339–349 (2014). https://doi.org/10.1007/s11207-013-0322-8

N. Sheeley, D. Michels, R. Howard, M. Koomen, Initial observations with the SOLWIND coronagraph. Astrophys. J. (1980). https://doi.org/10.1086/183243

N.R. Sheeley, J.H. Walters, Y.M. Wang, R.A. Howard, Continuous tracking of coronal outflows: two kinds of coronal mass ejections. J. Geophys. Res. (1999). https://doi.org/10.1029/1999JA900308

C. Shen, Y. Wang, P. Ye, S. Wang, Enhancement of solar energetic particles during a shock—magnetic cloud interacting complex structure. Sol. Phys. **252**, 409–418 (2008). https://doi.org/10.1007/s11207-008-9268-7

C. Shen, Y. Wang, B. Gui, P. Ye, S. Wang, Kinematic evolution of a slow CME in corona viewed by STEREO-B on 8 October 2007. Sol. Phys. (2011a). https://doi.org/10.1007/s11207-011-9715-8

F. Shen, X. Feng, Y. Wang, S. Wu, W. Song, J. Guo, Y. Zhou, Three-dimensional MHD simulation of two coronal mass ejections' propagation and interaction using a successive magnetized plasma blobs model. J. Geophys. Res. (2011b). https://doi.org/10.1029/2011JA016584

F. Shen, X. Feng, S. Wu, C. Xiang, W.B. Song, Three-dimensional MHD simulation of the evolution of the April 2000 CME event and its induced shocks using a magnetized plasma blob model. J. Geophys. Res. (2011c). https://doi.org/10.1029/2010JA015809

C. Shen, Y. Wang, S. Wang, Y. Liu, R. Liu, A. Vourlidas, B. Miao, P. Ye, J. Liu, Z. Zhou, Super-elastic collision of large-scale magnetized plasmoids in the heliosphere. Nat. Phys. **8**, 923–928 (2012a)

F. Shen, S.T. Wu, X. Feng, C.C. Wu, Acceleration and deceleration of coronal mass ejections during propagation and interaction. J. Geophys. Res. (Space Phys.) **117**, A11101 (2012b). https://doi.org/10.1029/2012JA017776

C. Shen, G. Li, X. Kong, J. Hu, X.D. Sun, L. Ding, Y. Chen, Y. Wang, L. Xia, Compound twin coronal mass ejections in the 2012 May 17 GLE event. Astrophys. J. **763**, 114 (2013a)

F. Shen, C. Shen, Y. Wang, X. Feng, C. Xiang, Could the collision of CMEs in the heliosphere be super-elastic? Validation through three-dimensional simulations. Geophys. Res. Lett. **40**, 1457–1461 (2013b). https://doi.org/10.1002/grl.50336

F. Shen, C. Shen, J. Zhang, P. Hess, Y. Wang, X. Feng, H. Cheng, Y. Yang, Evolution of the 2012 July 12 CME from the Sun to the Earth: data-constrained three-dimensional MHD simulations. J. Geophys. Res. Space Phys. (2014). https://doi.org/10.1002/2014JA020365

F. Shen, Y. Wang, C. Shen, X. Feng, Turn on the super-elastic collision nature of coronal mass ejections through low approaching speed. Sci. Rep. (2016). https://doi.org/10.1038/srep19576

C. Shen, Y. Chi, Y. Wang, M. Xu, S. Wang, Statistical comparison of the ICME's geoeffectiveness of different types and different solar phases from 1995 to 2014. J. Geophys. Res. Space Phys. (2017a). https://doi.org/10.1002/2016JA023768

F. Shen, Y. Wang, C. Shen, X. Feng, On the collision nature of two coronal mass ejections: a review. Sol. Phys. **292**, 104 (2017b). https://doi.org/10.1007/s11207-017-1129-9

C. Shen, M. Xu, Y. Wang, Y. Chi, B. Luo, Why the shock-ICME complex structure is important: learning from the early 2017 September CMEs. Astrophys. J. **861**, 28 (2018a)

F. Shen, Z. Yang, J. Zhang, W. Wei, X. Feng, Three-dimensional MHD simulation of solar wind using a new boundary treatment: comparison with in situ data at Earth. Astrophys. J. **866**, 18 (2018b). https://doi.org/10.3847/1538-4357/aad806

F. Shen, Y. Liu, Y. Yang, Numerical research on the effect of the initial parameters of a CME flux-rope model on simulation results. ApJS **253**, 12 (2021a). https://doi.org/10.3847/1538-4365/abd4d2

F. Shen, Y. Liu, Y. Yang, Numerical research on the effect of the initial parameters of a CME flux-rope model on simulation results. II. Different locations of observers. ApJ **915**, 30 (2021b). https://doi.org/10.3847/1538-4357/ac004e

D. Shiota, R. Kataoka, Magnetohydrodynamic simulation of interplanetary propagation of multiple coronal mass ejections with internal magnetic flux rope (SUSANOO-CME). Space Weather (2016). https://doi.org/10.1002/2015SW001308

T. Singh, T.K. Kim, N.V. Pogorelov, C.N. Arge, Application of a modified spheromak model to simulations of coronal mass ejection in the inner heliosphere. Space Weather **18**, e02405 (2020). https://doi.org/10.1029/2019SW002405

N. Srivastava, W. Mishra, D. Chakrabarty, Interplanetary and geomagnetic consequences of interacting CMEs of 13–14 June 2012. Solar Phys. **293**, 5. https://doi.org/10.1007/s11207-017-1227-8

O. St Cyr, J. Burkepile, A. Hundhausen, A. Lecinski, A comparison of ground-based and spacecraft observations of coronal mass ejections from 1980–1989. J. Geophys. Res. Space Phys. (1999). https://doi.org/10.1029/1999JA900045

A. Taktakishvili, A. Pulkkinen, P. MacNeice, M. Kuznetsova, M. Hesse, D. Odstrcil, Modeling of coronal mass ejections that caused particularly large geomagnetic storms using ENLIL heliosphere cone model. Space Weather **9**(6), 06002 (2011). https://doi.org/10.1029/2010SW000642

M. Temmer, Space weather: the solar perspective. Living Rev. Sol. Phys. **18**, 4 (2021). https://doi.org/10.1007/s41116-021-00030-3. arXiv:2104.04261

M. Temmer, S. Preiss, A.M. Veronig, CME projection effects studied with STEREO/COR and SOHO/LASCO. Sol. Phys. **256**, 183–199 (2009). https://doi.org/10.1007/s11207-009-9336-7

M. Temmer, T. Rollett, C. Möstl, A.M. Veronig, B. Vršnak, D. Odstrčil, Influence of the ambient solar wind flow on the propagation behavior of interplanetary coronal mass ejections. Astrophys. J. **743**(2), 101 (2011). https://doi.org/10.1088/0004-637x/743/2/101

M. Temmer, B. Vršnak, T. Rollett, B. Bein, C.A. de Koning, Y. Liu, E. Bosman, J.A. Davies, C. Möstl, T. Zic, A.M. Veronig, V. Bothmer, R. Harrison, N. Nitta, M. Bisi, O. Flor, J. Eastwood, D. Odstrcil, R. Forsyth, Characteristics of kinematics of a coronal mass ejection during the 2010 August 1 CME–CME interaction event. Astrophys. J. **749**, 57 (2012)

M. Temmer, A.M. Veronig, V. Peinhart, B. Vršnak, Asymmetry in the CME–CME interaction process for the events from 2011 February 14–15. Astrophys. J. **785**, 85 (2014). https://doi.org/10.1088/0004-637X/785/2/85

M. Temmer, L. Holzknecht, M. Dumbović, B. Vršnak, N. Sachdeva, S.G. Heinemann, K. Dissauer, C. Scolini, E. Asvestari, A.M. Veronig, S.J. Hofmeister, Deriving CME density from remote sensing data and comparison to in situ measurements. J. Geophys. Res. (Space Phys.) **126**, e28380 (2021). https://doi.org/10.1029/2020JA028380. arXiv:2011.06880

A. Thernisien, R. Howard, A. Vourlidas, Modeling of flux rope coronal mass ejections. Astrophys. J. **652**, 763 (2006). https://doi.org/10.1086/508254

A. Thernisien, A. Vourlidas, R. Howard, Forward modeling of coronal mass ejections using STEREO/SECCHI data. Sol. Phys. **256**, 111–130 (2009). https://doi.org/10.1007/s11207-009-9346-5

W.T. Thompson, B. Kliem, T. Trk, 3D reconstruction of a rotating erupting prominence. Sol. Phys. **276**, 241–259 (2012)

H. Tian, S. Yao, Q. Zong, J. He, Y. Qi, Signatures of magnetic reconnection at boundaries of interplanetary small-scale magnetic flux ropes. Astrophys. J. **720**, 454–464 (2010). https://doi.org/10.1088/0004-637X/720/1/454. arXiv:1007.2247

V. Titov, T. Török, Z. Mikic, J. Linker, A method for embedding circular force-free flux ropes in potential magnetic fields. Astrophys. J. **790**, 163 (2014). https://doi.org/10.1088/0004-637X/790/2/163

S. Toriumi, H. Wang, Flare-productive active regions. Living Rev. Sol. Phys. **16**, 3 (2019). https://doi.org/10.1007/s41116-019-0019-7

T. Török, B. Kliem, The evolution of twisting coronal magnetic flux tubes. Astron. Astrophys. **406**, 1043–1059 (2003). https://doi.org/10.1051/0004-6361:20030692

T. Török, B. Kliem, Numerical simulations of fast and slow coronal mass ejections. Astron. Nachr. (2007). https://doi.org/10.1002/asna.200710795

T. Török, C. Downs, J. Linker, R. Lionello, V. Titov, Z. Mikić, P. Riley, R. Caplan, J. Wijaya, Sun-to-Earth MHD simulation of the 14 July 2000 "bastille day'' eruption. Astrophys. J. (2018). https://doi.org/10.3847/1538-4357/aab36d

R. Tousey (1973) The solar corona, in Rycroft MJ, Runcorn SK (eds) Space Research XIII, Proceedings of Open Meetings of Working Groups on Physical Sciences of the 15th Plenary Meeting of COSPAR, Madrid, Spain, 1024 May, 1972, vol 2. Akademie-Verlag, Berlin, pp 713–730. http://adsabs.harvard.edu/abs/1973spre.conf..713T

A.J. Tylka, C. Cohen, W.F. Dietrich, M.A. Lee, C.G. Maclennan, R.A. Mewaldt, C.K. Ng, D.V. Reames, Shock geometry, seed populations, and the origin of variable elemental composition at high energies in large gradual solar particle events. Astrophys. J. **625**, 474–495 (2005)

B. van der Holst, I. Sokolov, X. Meng, M. Jin, W. Manchester IV., G. Tóth, T. Gombosi, Alfvén wave solar model (AWSoM): coronal heating. Astrophys. J. **782**, 81 (2014). https://doi.org/10.1088/0004-637X/782/2/81

C. Verbeke, M.L. Mays, M. Temmer, S. Bingham, R. Steenburgh, M. Dumbović, M. Núñez, L.K. Jian, P. Hess, C. Wiegand, A. Taktakishvili, J. Andries, Benchmarking CME arrival time and impact: progress on metadata, metrics, and events. Space Weather **17**, 6–26 (2019a). https://doi.org/10.1029/2018SW002046

C. Verbeke, J. Pomoell, S. Poedts, The evolution of coronal mass ejections in the inner heliosphere: implementing the spheromak model with EUHFORIA. Astron. Astrophys. (2019b). https://doi.org/10.1051/0004-6361/201834702

A. Veronig, T. Podladchikova, K. Dissauer, M. Temmer, D.B. Seaton, D. Long, J. Guo, B. Vršnak, L.K. Harra, B. Kliem, Genesis and impulsive evolution of the fast CME associated with the X8.2 flare on 2017 September 10, in *AGU Fall Meeting Abstracts* (2019), pp. SH13A–02

A. Vourlidas, D. Buzasi, R.A. Howard, E. Esfandiari, Mass and energy properties of LASCO CMEs, in Wilson, A. (ed.) Solar Variability: From Core to Outer Frontiers. ESA Special Publication SP-506, ESA, Noordwijk, 91 (2002)

A. Vourlidas, R. Colaninno, T. Nieves-Chinchilla, G. Stenborg, The first observation of a rapidly rotating coronal mass ejection in the middle corona. Astrophys. J. Lett. **733**, L23 (2011). https://doi.org/10.1088/2041-8205/733/2/L23

A. Vourlidas, R.A. Howard, S.P. Plunkett, C.M. Korendyke, A.F.R. Thernisien, D. Wang, N. Rich, M.T. Carter, D.H. Chua, D.G. Socker, M.G. Linton, J.S. Morrill, S. Lynch, A. Thurn, P. Van Duyne, R. Hagood, G. Clifford, P.J. Grey, M. Velli, P.C. Liewer, J.R. Hall, E.M. DeJong, Z. Mikic, P. Rochus, E. Mazy, V. Bothmer, J. Rodmann, The wide-field imager for solar probe plus (WISPR). Space Sci. Rev. (2016). https://doi.org/10.1007/s11214-014-0114-y

A. Vourlidas, S. Patsourakos, N.P. Savani, Predicting the geoeffective properties of coronal mass ejections: current status, open issues and path forward. Philos. Trans. R. Soc. Lond. Ser. A **377**, 20180096 (2019). https://doi.org/10.1098/rsta.2018.0096

B. Vršnak, N. Gopalswamy, Influence of the aerodynamic drag on the motion of interplanetary ejecta. J. Geophys. Res. Space Phys. (2002). https://doi.org/10.1029/2001JA000120

B. Vršnak, T. Zic, Transit times of interplanetary coronal mass ejections and the solar wind speed. Astron. Astrophys. (2007). https://doi.org/10.1051/0004-6361/20077499

B. Vršnak, D. Sudar, D. Ruzdjak, The CME-flare relationship: are there really two types of CMEs? Astron. Astrophys. (2005). https://doi.org/10.1051/0004-6361:20042166

B. Vršnak, D. Maricic, A.L. Stanger, A.M. Veronig, M. Temmer, D. Rosa, Acceleration phase of coronal mass ejections: I. Temporal and spatial scales. Sol. Phys. (2007). https://doi.org/10.1007/s11207-006-0290-3

B. Vršnak, T. Zic, T.V. Falkenberg, C. Moestl, S. Vennerstrom, D. Vrbanec, The role of aerodynamic drag in propagation of interplanetary coronal mass ejections. Astron. Astrophys. (2010). https://doi.org/10.1051/0004-6361/200913482

B. Vršnak, T. Zic, D. Vrbanec, M. Temmer, T. Rollett, C. Moestl, A. Veronig, J. Calogovic, M. Dumbovic, S. Lulic, Y.J. Moon, A. Shanmugaraju, Propagation of interplanetary coronal mass ejections: the drag-based model. Sol. Phys. (2013). https://doi.org/10.1007/s11207-012-0035-4

B. Vršnak, T. Amerstorfer, M. Dumbović, M. Leitner, A.M. Veronig, M. Temmer, C. Möstl, U.V. Amerstorfer, C.J. Farrugia, A.B. Galvin, Heliospheric evolution of magnetic clouds. Astrophys. J. **877**, 77 (2019). https://doi.org/10.3847/1538-4357/ab190a. arXiv:1904.08266

Y. Wang, P. Ye, S. Wang, G. Zhou, J. Wang, A statistical study on the geoeffectiveness of Earth-directed coronal mass ejections from March 1997 to December 2000. J. Geophys. Res. Space Phys. (2002). https://doi.org/10.1029/2002JA009244

Y.M. Wang, P.Z. Ye, S. Wang, Multiple magnetic clouds: several examples during March–April 2001. J. Geophys. Res. Space Phys. **108**, 1370 (2003a). https://doi.org/10.1029/2003JA009850

Y.M. Wang, P.Z. Ye, S. Wang, X.H. Xue, An interplanetary cause of large geomagnetic storms: fast forward shock overtaking preceding magnetic cloud. Geophys. Res. Lett. **30**, 31–33 (2003b). https://doi.org/10.1029/2002GL016861

Y. Wang, C. Shen, S. Wang, P. Ye, Deflection of coronal mass ejection in the interplanetary medium. Sol. Phys. (2004). https://doi.org/10.1023/B:SOLA.0000043576.21942.aa

Y. Wang, P. Ye, G. Zhou, S. Wang, S. Wang, Y. Yan, J. Wang, The interplanetary responses to the great solar activities in late October 2003. Sol. Phys. **226**, 337–357 (2005a)

Y. Wang, H. Zheng, S. Wang, P. Ye, MHD simulation of the formation and propagation of multiple magnetic clouds in the heliosphere. Astron. Astrophys. **434**, 309–316 (2005b)

Y. Wang, C. Chen, B. Gui, C. Shen, P. Ye, S. Wang, Statistical study of CME source locations: I. Understanding CMEs viewed in coronagraphs. J. Geophys. Res. (Space Phys.) (2011). https://doi.org/10.1029/2010JA016101

Y. Wang, B. Wang, C. Shen, F. Shen, N. Lugaz, Deflected propagation of a coronal mass ejection from the corona to interplanetary space. J. Geophys. Res. (Space Phys.) **119**, 5117–5132 (2014). https://doi.org/10.1002/2013JA019537

Y. Wang, Z. Zhou, C. Shen, R. Liu, S. Wang, Investigating plasma motion of magnetic clouds at 1 AU through a velocity-modified cylindrical force-free flux rope model. J. Geophys. Res. (Space Phys.) **120**, 1543–1565 (2015). https://doi.org/10.1002/2014JA020494

Y. Wang, C. Shen, R. Liu, J. Liu, J. Guo, X. Li, M. Xu, Q. Hu, L.Z. Tielong, Understanding the twist distribution inside magnetic flux ropes by anatomizing an interplanetary magnetic cloud. J. Geophys. Res. Space Phys. **123**(5), 3238–3261 (2018). https://doi.org/10.1002/2017JA024971

Y. Wang, H. Ji, Y. Wang, L. Xia, C. Shen, J. Guo, Q. Zhang, Z. Huang, K. Liu, X. Li, Concept of the solar ring mission: overview. Sci. China Technol. Sci. **63**, 1699–1713 (2020). https://doi.org/10.1007/s11431-020-1603-2

D.F. Webb, T.A. Howard, Coronal mass ejections: observations. Living Rev. Sol. Phys. **9**, 3 (2012). https://doi.org/10.12942/lrsp-2012-3

D. Webb, C. Möstl, B. Jackson, M. Bisi, T. Howard, T. Mulligan, E. Jensen, L. Jian, J. Davies, C. de Koning, Y. Liu, M. Temmer, J. Clover, C. Farrugia, R. Harrison, N. Nitta, D. Odstrcil, S. Tappin, H.S. Yu, Heliospheric imaging of 3d density structures during the multiple coronal mass ejections of late July to early August 2010. Sol. Phys. (2013). https://doi.org/10.1007/s11207-013-0260-5

A.L.E. Werner, E. Yordanova, A. Dimmock, M. Temmer, Modeling the multiple CME interaction event on 6–9 September 2017 with WSA-ENLIL+Cone. Space Weather (2019). https://doi.org/10.1029/2018SW001993

B.E. Wood, R.A. Howard, A. Thernisien, S.P. Plunkett, D.G. Socker, Reconstructing the 3D morphology of the 17 May 2008 CME. Sol. Phys. **259**, 163–178 (2009). https://doi.org/10.1007/s11207-009-9391-0

B. Wood, C.C. Wu, A. Rouillard, R. Howard, D. Socker, A coronal hole's effects on CME shock morphology in the inner heliosphere. Astrophys. J. (2012a). https://doi.org/10.1088/0004-637X/755/1/43

B.E. Wood, C.C. Wu, A.P. Rouillard, R.A. Howard, D.G. Socker, A coronal hole's effects on coronal mass ejection shock morphology in the inner heliosphere. Astrophys. J. **755**, 43 (2012b). https://doi.org/10.1088/0004-637X/755/1/43. arXiv:1206.3584

B.E. Wood, C.C. Wu, R.P. Lepping, T. Nieves-Chinchilla, R.A. Howard, M.G. Linton, D.G. Socker, A STEREO survey of magnetic cloud coronal mass ejections observed at Earth in 2008–2012. Astrophys. J. Suppl. Ser. **229**, 29 (2017). https://doi.org/10.3847/1538-4365/229/2/29. arXiv:1701.01682

C.C. Wu, M. Dryer, S. Wu, B. Wood, G. Fry, K. Liou, S. Plunkett, Global three-dimensional simulation of the interplanetary evolution of the observed geoeffective CME during the epoch August 1–4, 2010. J. Geophys. Res. **116**, A12103 (2011). https://doi.org/10.1029/2011JA016947

S. Wu, Y. Zhou, C. Jiang, X. Feng, C.C. Wu, Q. Hu, A data-constrained three-dimensional magnetohydrodynamic simulation model for a coronal mass ejection (CME) initiation. J. Geophys. Res. Space Phys. (2016). https://doi.org/10.1002/2015JA021615

C.C. Wu, K. Liou, R. Lepping, A. Vourlidas, S. Plunkett, D. Socker, S. Wu, Observation of an extremely large-density heliospheric plasma sheet compressed by an interplanetary shock at 1 AU. Sol. Phys. (2017). https://doi.org/10.1007/s11207-017-1114-3

H. Xie, L. Ofman, G. Lawrence, Cone model for halo CMEs: application to space weather forecasting. J. Geophys. Res. Space Phys. (2004). https://doi.org/10.1029/2003JA010226

H. Xie, P. Mäkelä, O.C. St. Cyr, N. Gopalswamy, Comparison of the coronal mass ejection shock acceleration of three widespread SEP events during solar cycle 24. J. Geophys. Res. (Space Phys.) **122**, 7021–7041 (2017). https://doi.org/10.1002/2017JA024218

M. Xiong, H. Zheng, Y. Wang, S. Wang, S.T. Wu, Magnetohydrodynamic simulation of the interaction between interplanetary strong shock and magnetic cloud and its consequent geoeffectiveness: 2. Oblique collision. J. Geophys. Res. **111**, 11102 (2006)

M. Xiong, H. Zheng, S.T. Wu, Y. Wang, S. Wang, Magnetohydrodynamic simulation of the interaction between two interplanetary magnetic clouds and its consequent geoeffectiveness. J. Geophys. Res. **112**, 11103 (2007)

M. Xiong, H. Zheng, S. Wang, Magnetohydrodynamic simulation of the interaction between two interplanetary magnetic clouds and its consequent geoeffectiveness: 2. Oblique collision. J. Geophys. Res. **114**, 11101 (2009)

X. Xu, F. Wei, X. Feng, Observations of reconnection exhausts associated with large-scale current sheets within a complex ICME at 1 AU. J. Geophys. Res. (Space Phys.) **116**, A05105 (2011). https://doi.org/10.1029/2010JA016159

M. Xu, C. Shen, Y. Chi, Y. Wang, Q. Hu, G. Li, Z. Zhong, J. Liu, The enhancement of the energetic particle intensities in ICMEs. Astrophys. J. (2019a). https://doi.org/10.3847/1538-4357/ab4596

M. Xu, C. Shen, Y. Wang, B. Luo, Y. Chi, Importance of shock compression in enhancing ICME's geoeffectiveness. Astrophys. J. Lett. (2019b). https://doi.org/10.3847/2041-8213/ab4717

M. Xu, C. Shen, Q. Hu, Y. Wang, Y. Chi, Whether small flux ropes and magnetic clouds have the same origin: a statistical study of small flux ropes in different types of solar wind. Astrophys. J. **904**, 122 (2020). https://doi.org/10.3847/1538-4357/abbe21

X.H. Xue, C.B. Wang, X.K. Dou, An ice-cream cone model for coronal mass ejections. J. Geophys. Res. (Space Phys.) **110**, A08103 (2005a). https://doi.org/10.1029/2004JA010698

X.H. Xue, Y. Wang, P.Z. Ye, S. Wang, M. Xiong, Analysis on the interplanetary causes of the great magnetic storms in solar maximum (2000–2001). Planet. Space Sci. **53**, 443–457 (2005b)

J. Yang, Y. Jiang, R. Zheng, Y. Bi, J. Hong, B. Yang, Sympathetic filament eruptions from a bipolar helmet streamer in the Sun. ApJ **745**, 9 (2012). https://doi.org/10.1088/0004-637X/745/1/9

S. Yashiro, N. Gopalswamy, G. Michalek, O.C. St Cyr, S.P. Plunkett, N.B. Rich, R.A. Howard, A catalog of white light coronal mass ejections observed by the SOHO spacecraft. J. Geophys. Res. **109**, 7105 (2004)

V. Yurchyshyn, S. Yashiro, V. Abramenko, H. Wang, N. Gopalswamy, Statistical distributions of speeds of coronal mass ejections. Astrophys. J. (2005). https://doi.org/10.1086/426129

V. Yurchyshyn, Q. Hu, R. Lepping, B. Lynch, J. Krall, Orientations of LASCO Halo CMEs and their connection to the flux rope structure of interplanetary CMEs. Adv. Space Res. **40**, 1821–1826 (2007). https://www.sciencedirect.com/science/article/pii/S0273117707000737. https://doi.org/10.1016/j.asr.2007.01.059

J. Zhang, A study on the acceleration of coronal mass ejections. Proc. Int. Astron. Union **2004**, 65–70 (2004)

J. Zhang, K. Dere, R. Howard, M. Kundu, S. White, On the temporal relationship between coronal mass ejections and flares. Astrophys. J. (2001). https://doi.org/10.1086/322405

J. Zhang, I.G. Richardson, D.F. Webb, N. Gopalswamy, E. Huttunen, J. Kasper, N.V. Nitta, W. Poomvises, B.J. Thompson, C.C. Wu, S. Yashiro, A.N. Zhukov, Correction to "Solar and interplanetary sources of major geomagnetic storms (Dst 100 nT) during 1996–2005". J. Geophys. Res. **112**, A12103 (2007a)

J. Zhang, I.G. Richardson, D.F. Webb, N. Gopalswamy, E. Huttunen, J.C. Kasper, N.V. Nitta, W. Poomvises, B.J. Thompson, C.C. Wu, S. Yashiro, A.N. Zhukov, Solar and interplanetary sources of major geomagnetic storms (Dst 100 nT) during 1996–2005. J. Geophys. Res. **112**, A10102 (2007b)

J. Zhang, M. Temmer, N. Gopalswamy, O. Malandraki, N.V. Nitta, S. Patsourakos, F. Shen, B. Vršnak, Y. Wang, D. Webb, M.I. Desai, K. Dissauer, N. Dresing, M. Dumbović, X. Feng, S.G. Heinemann, M. Laurenza, N. Lugaz, B. Zhuang, Earth-affecting solar transients: a review of progresses in solar cycle 24. Prog. Earth Planet. Sci. **8**, 56 (2021). https://doi.org/10.1186/s40645-021-00426-7. arXiv:2012.06116

X. Zhao, M. Dryer, Current status of CME/shock arrival time prediction. Space Weather **12**, 448–469 (2014). https://doi.org/10.1002/2014SW001060

X.H. Zhao, X.S. Feng, Shock propagation model version 2 and its application in predicting the arrivals at Earth of interplanetary shocks during solar cycle 23. J. Geophys. Res. (Space Phys.) **119**, 1–10 (2014). https://doi.org/10.1002/2012JA018503

X. Zhao, S. Plunkett, W. Liu, Determination of geometrical and kinematical properties of halo coronal mass ejections using the cone model. J. Geophys. Res. Space Phys. (2002). https://doi.org/10.1029/2001JA009143

X. Zhao, X. Feng, C.C. Wu, Influence of solar flare's location and heliospheric current sheet on the associated shock's arrival at Earth. J. Geophys. Res. (Space Phys.) **112**, A06107 (2007). https://doi.org/10.1029/2006JA012205

Y.F. Zhou, X.S. Feng, MHD numerical study of the latitudinal deflection of coronal mass ejection. J. Geophys. Res. (Space Phys.) **118**, 6007–6018 (2013). https://doi.org/10.1002/2013JA018976

Y. Zhou, X. Feng, Numerical study of the propagation characteristics of coronal mass ejections in a structured ambient solar wind: the study on the propagation characteristics of CMEs. J. Geophys. Res. Space Phys. (2017). https://doi.org/10.1002/2016JA023053

Y. Zhou, X. Feng, S. Wu, D. Du, F. Shen, C. Xiang, Using a 3-D spherical plasmoid to interpret the Sun-to-Earth propagation of the 4 November 1997 coronal mass ejection event. J. Geophys. Res. (Space Phys.) **117**, 1102 (2012). https://doi.org/10.1029/2010JA016380

Y. Zhou, X. Feng, X. Zhao, Using a 3-D MHD simulation to interpret propagation and evolution of a coronal mass ejection observed by multiple spacecraft: the 3 April 2010 event. J. Geophys. Res. Space Phys. (2014). https://doi.org/10.1002/2014JA020347

B. Zhuang, Y. Wang, C. Shen, S. Liu, J. Wang, Z. Pan, H. Li, R. Liu, The significance of the influence of the CME deflection in interplanetary space on the CME arrival at Earth. Astrophys. J. (2017). https://doi.org/10.3847/1538-4357/aa7fc0

B. Zhuang, Y. Wang, Y. Hu, C. Shen, R. Liu, T. Gou, Q. Zhang, X. Li, Numerical simulations on the deflection of coronal mass ejections in the interplanetary space. Astrophys. J. **876**, 73 (2019). https://doi.org/10.3847/1538-4357/ab139e

B. Zhuang, N. Lugaz, T. Gou, L. Ding, Y. Wang, The role of successive and interacting CMEs in the acceleration and release of solar energetic particles: multi-viewpoint observations. Astrophys. J. **901**, 45 (2020). https://doi.org/10.3847/1538-4357/abaef9

T. Žic, B. Vršnak, M. Temmer, Heliospheric propagation of coronal mass ejections: drag-based model fitting. ApJS **218**, 32 (2015). https://doi.org/10.1088/0067-0049/218/2/32

F.P. Zuccarello, A. Bemporad, C. Jacobs, M. Mierla, S. Poedts, F. Zuccarello, The role of streamers in the deflection of coronal mass ejections: comparison between STEREO three-dimensional reconstructions and numerical simulations. ApJ **744**, 66 (2012). https://doi.org/10.1088/0004-637X/744/1/66

T.H. Zurbuchen, I.G. Richardson, In-situ solar wind and magnetic field signatures of interplanetary coronal mass ejections. Space Sci. Rev. **123**, 31–43 (2006). https://doi.org/10.1007/s11214-006-9010-4

Authors and Affiliations

Fang Shen[1,2] **· Chenglong Shen**[3] **· Mengjiao Xu**[3] **· Yousheng Liu**[1,2] **· Xueshang Feng**[1] **· Yuming Wang**[3]

[1] SIGMA Weather Group, State Key Laboratory of Space Weather, National Space Science Center, Chinese Academy of Sciences, Beijing 100190, China

[2] College of Earth and Planetary Sciences, University of Chinese Academy of Sciences, Beijing 100049, China

[3] CAS Key Laboratory of Geospace Environment, Department of Geophysics and Planetary Sciences, University of Science and Technology of China, Hefei 230026, Anhui, China